

INVESTIGATING THE OPTIMAL INTEGRATION OF AIRBORNE, SHIP-BORNE, SATELLITE AND
TERRESTRIAL GRAVITY DATA FOR USE IN GEOID DETERMINATION

BY

Rachelle Lee Winefield

A thesis

submitted to the Victoria University of Wellington

in fulfilment of the requirements for the degree of

Master of Science Geophysics

School of Geography, Environmental and Earth Science

Victoria University of Wellington

2016

“Gravity is a habit that is hard to shake off.”

- Terry Pratchett

Abstract

Each gravity observation technique has different parameters and contributes to different pieces of the gravity spectrum. This means that no one gravity dataset is able to model the Earth's gravity field completely and the best gravity map is one derived from many sources. Therefore, one of the challenges in gravity field modelling is combining multiple types of heterogeneous gravity datasets.

The aim of this study is to determine the optimal method to produce a single gravity map of the Canterbury case study area, for the purposes of use in geoid modelling.

This objective is realised through the identification and application of a four-step integration process: purpose, data, combination and assessment. This includes the evaluation of three integration methods: natural neighbour, ordinary kriging and least squares collocation.

As geoid modelling requires the combination of gravity datasets collected at various altitudes, it is beneficial to be able to combine the dataset using an integration method which operates in a three-dimensional space. Of the three integration methods assessed, least squares collocation is the only integration method which is able to perform this type of reduction.

The resulting product is a Bouguer anomaly map of the Canterbury case study area, which combines satellite altimetry, terrestrial, ship-borne, airborne, and satellite gravimetry using least squares collocation.

Acknowledgements

I would like to extend my gratitude to my supervisor Prof Euan Smith. I have been amazingly fortunate to have a supervisor with such a positive outlook and the ability to keep things in perspective. I am deeply appreciative for the long discussions that helped me better understand the peculiarities of New Zealand's gravitational landscape.

I am grateful to my co-supervisor, Dr Matt Amos for this support and encouragement. His insightful comments and constructive criticisms at different stages of my research were thought-provoking and continually extended my thinking.

I am indebted to my student colleague Jack McCubbine for his support and Matlab training.

I am extremely thankful for the support of my employer, Land Information New Zealand, who provided me the opportunity to undertake this research. I would like to acknowledge the National Geodetic Office and the wider Location Information teams for their ongoing encouragement throughout my studies.

Finally, I must express my very profound gratitude to my parents for providing me with unfailing support and continuous encouragement throughout my years of study and through the process of researching and writing this thesis.

Thank you.

Table of Contents

Abstract.....	i
Acknowledgements.....	ii
List of Figures	vi
List of Tables	ix
List of Abbreviations	x
List of Symbols	xii
1. INTRODUCTION.....	1
1.1. Background	1
1.2. Motivation.....	1
1.3. Significance of Study	3
1.4. Objectives of Study	4
1.5. Outline of Thesis	4
2. GRAVITY	5
2.1. Introduction	5
2.2. Gravity Instruments	6
2.2.1. Absolute Gravity Meters	6
2.2.2. Relative Gravity Meters	8
2.2.3. Dynamic Gravity Meters	10
2.2.4. Satellite Gravimetry	11
2.3. Data Collection Methods	13
2.3.1. Terrestrial Gravimetry.....	13
2.3.2. Ship-borne Gravimetry.....	15
2.3.3. Airborne Gravimetry	17
2.3.4. Satellite Altimetry	19
2.3.5. Global Geopotential Models.....	21
2.4. Gravity Anomalies and Reductions	23
2.4.1. Relative Gravity Observations.....	24
2.4.2. Normal Gravity Model	24
2.4.3. Free-Air Model	25
2.4.4. Bouguer Slab Model.....	25
2.4.5. Terrain Models	27
2.4.6. Complete Bouguer Model.....	32
2.5. Combination Considerations.....	33

2.5.1.	Combination Data Type	33
2.5.2.	Downward Continuation.....	35
2.6.	Summary	40
3.	INTEGRATION.....	41
3.1.	Introduction	41
3.2.	Step One: Purpose	41
3.3.	Step Two: Data.....	42
3.4.	Step Three: Combination	43
3.4.1.	Simple Gridding.....	43
3.4.2.	Kriging	48
3.4.3.	Least Squares	50
3.5.	Step Four: Assessment.....	52
3.6.	Summary	53
4.	CASE STUDY: Canterbury, New Zealand	54
4.1.	Introduction	54
4.2.	The Canterbury Test Area	54
4.3.	Integration Step One: Purpose	55
4.4.	Integration Step Two: Data.....	56
4.4.1.	Terrestrial Gravity	56
4.4.2.	Ship-borne Gravity	63
4.4.3.	Airborne Gravity.....	64
4.4.4.	Satellite Altimetry	70
4.4.5.	Global Gravity Model	72
4.5.	Integration Step Three: Combination	73
4.5.1.	Test One – Combines Multiple Datasets.....	74
4.5.2.	Test Two – Uses <i>a priori</i> Weights.....	76
4.5.3.	Test Three – Is an Exact Interpolation Method.....	79
4.5.4.	Test Four – Supports Three-Dimensional Interpolation	81
4.6.	Step Four: Assessment.....	88
4.6.1.	Comparison of Models.....	88
4.6.2.	Test of Fit.....	90
4.7.	Summary	90
5.	SUMMARY, CONCLUSIONS AND RECOMMENDATIONS	93
5.1.	Project Summary.....	93

5.1.1.	Purpose	93
5.1.2.	Data	93
5.1.3.	Combination.....	94
5.1.4.	Assessment	95
5.2.	Conclusions and Recommendations	95
5.3.	Future Work.....	95
References	97
A.	Appendix	107
A.1.	Gravity Datasets.....	107

List of Figures

Figure 2.1: Schematic diagram of a LaCoste and Romberg zero-length spring (LaCoste & Romberg, 1998)	8
Figure 2.2: Diagram of the basic operation of a superconducting gravity meter (Harms, 2015)	9
Figure 2.3: Photo of Lacoste and Romberg model "S" air-sea dynamic gravity meter (LaCoste & Romberg, 1998)	10
Figure 2.4: Concept of satellite-to-satellite tracking in high-low mode (Albertella <i>et al</i> , 2002)	11
Figure 2.5: Concept of satellite-to-satellite tracking in low-low mode, combined with SST-hl mode (Albertella <i>et al</i> , 2002)	12
Figure 2.6: Concept of satellite gradiometry combined with SST-hl mode (Albertella <i>et al</i> , 2002)	13
Figure 2.7: Observations from the New Zealand terrestrial gravity database (Amos, 2007)	14
Figure 2.8: Ship-track observations from the New Zealand ship-borne gravity database	16
Figure 2.9: Recorded acceleration from a gravity flight (McCubbine, 2016).....	18
Figure 2.10: Recovered gravity signal	18
Figure 2.11: Satellite altimetry principle (NOAA, 2010)	19
Figure 2.12: Illustration of the Bouguer slab model (McCubbine, 2016)	26
Figure 2.13: Illustration of the Bouguer spherical cap model.....	27
Figure 2.14: List of Hammer zones (left) and geometry of zones (right; Amos, 2007).....	29
Figure 2.15: Illustration of the Nagy prism method (Nagy, 1966)	30
Figure 2.16: Illustration of the Hammer prism method (McCubbine, 2016).....	32
Figure 2.17: Gravity observations	34
Figure 2.18: Free-air gravity anomaly	34
Figure 2.19: Bouguer gravity anomaly	34
Figure 2.20: Diagram of gravity anomaly profile of a buried sphere (McCubbine, 2016)	35
Figure 2.21: Diagram of data prior to remove-restore process.....	36
Figure 2.22: Diagram of data after the remove-restore process.....	37
Figure 2.23: Original sample data	38
Figure 2.24: Downward continued sample data.....	38
Figure 3.1: A demonstration of the simple gridding technique.....	44
Figure 3.2: Example of GMT 'surface' interpolation method	45
Figure 3.3: Example of GMT nearest neighbour 'nearneighbor' interpolation method	45
Figure 3.4: Illustration of multiple datasets combined using the natural neighbour method	46
Figure 3.5: Examples of Matlab interpolation methods:	47
Figure 3.6: Illustration describing the components of the semi-variogram	48
Figure 3.7: Conceptual diagram of the ordinary kriging process.....	50
Figure 3.8: Illustration of the semi-variogram (kriging) and covariance (least squares) models	50
Figure 3.9: Graphical representation of the least squares collocation method (Ilie, 2014).....	52
Figure 4.1: Location of the Canterbury test area, New Zealand.....	54
Figure 4.2: Location of terrestrial gravity stations within the Canterbury test area	57
Figure 4.3: Visualisation of the coordinates for the terrestrial gravity mark: Station 39/Sheet 21	58
Figure 4.4: CDF plot of differences between terrestrial database and DEM heights	60
Figure 4.5: Terrestrial gravity stations identified within the 95% confidence interval (2508)	61
Figure 4.6: Terrestrial gravity stations identified beyond the 95% confidence interval (66)	61
Figure 4.7: Plot showing the locations of the resulting three irregularities	62
Figure 4.8: Location plot of the Canterbury test area ship-borne data tracks	63

Figure 4.9: Extent of Canterbury airborne gravity survey, April 2012.....	64
Figure 4.10: Comparison of north-south calibration lines.....	65
Figure 4.11: Cessna 402B, used in airborne gravity survey.....	65
Figure 4.12: Aircraft rotations.....	66
Figure 4.13: Flight altitude is constantly above the topography.....	67
Figure 4.14: Example of a dipole in the airborne gravity signal.....	67
Figure 4.15: Airborne Bouguer anomaly map, with dipole event present.....	68
Figure 4.16: Airborne Bouguer anomaly map, flight-line with dipole event removed.....	69
Figure 4.17: Sandwell & Smith satellite altimetry model, Version 23.1.....	70
Figure 4.18: Bathymetry of the Canterbury test area.....	71
Figure 4.19: Expected errors from Sandwell & Smith satellite altimetry model v23.1.....	71
Figure 4.20: Location of Sandwell & Smith v23.1 satellite altimetry data points within the Canterbury test area (5487).....	72
Figure 4.21: Global geoid height difference between EGM2008 and DIR-R5 (Brunisma <i>et al</i> , 2014)..	73
Figure 4.22: Natural neighbour method - displaying terrestrial, airborne and ship-borne gravity datasets.....	75
Figure 4.23: Ordinary kriging method: displaying - terrestrial, airborne and ship-borne gravity datasets.....	75
Figure 4.24: Least squares collocation method - displaying terrestrial, airborne and ship-borne gravity datasets.....	75
Figure 4.25: Ordinary kriging method, terrestrial dataset additional weight set to 'zero'.....	77
Figure 4.26: Ordinary kriging method, terrestrial dataset additional weight set to 'three'.....	77
Figure 4.27: Least squares collocation method, terrestrial dataset additional weight set to 'zero'....	78
Figure 4.28: Least squares collocation method, terrestrial dataset additional weight set to 'three'..	78
Figure 4.29: Location of terrestrial gravity data points used in Test Three.....	79
Figure 4.30: Natural neighbour method - CDF plot difference of terrestrial gravity values before and after integration.....	80
Figure 4.31: Ordinary kriging method - CDF plot difference of terrestrial gravity values before and after integration.....	80
Figure 4.32: Least squares collocation method - CDF plot difference of terrestrial gravity values before and after integration.....	80
Figure 4.33: Natural neighbour method - combination of airborne and terrestrial datasets.....	82
Figure 4.34: Ordinary kriging method - combination of airborne and terrestrial datasets.....	82
Figure 4.35: Least squares collocation method - combination of airborne and terrestrial datasets...	82
Figure 4.36: Combination of airborne and terrestrial datasets, difference between least squares collocation and natural neighbour methods.....	83
Figure 4.37: Combination of airborne and terrestrial datasets, difference between least squares collocation and ordinary kriging methods.....	83
Figure 4.38: Combination of airborne and terrestrial datasets, difference between ordinary kriging and natural neighbour methods.....	83
Figure 4.39: Natural neighbour method, difference map of integration result, without and with downward continued airborne data.....	85
Figure 4.40: Natural neighbour method - combination of terrestrial and downward continued airborne datasets.....	85

Figure 4.41: Ordinary kriging method, combination of terrestrial and downward continued airborne datasets.....	86
Figure 4.42: Ordinary kriging method, difference map of integration result, without and with downward continued airborne data.....	86
Figure 4.43: Least squares collocation method, difference map of integration result, without and with downward continued airborne data.....	87
Figure 4.44: Least squares collocation method, combination of terrestrial and downward continued airborne datasets.....	87
Figure 4.45: Case study Bouguer anomaly map.....	89
Figure 4.46: EGM2008 derived Bouguer anomaly map of the Canterbury test area.....	89
Figure 4.47: Differences map between the case study and EGM2008 Bouguer anomalies.....	89
Figure 4.48: Final Bouguer anomaly map of the Canterbury case study region (Enlargement of Figure 4.45).....	92
Figure A.1: Canterbury test area terrestrial gravity dataset.....	107
Figure A.2: Canterbury test area ship-borne gravity dataset.....	108
Figure A.3: Canterbury test area airborne gravity dataset.....	108
Figure A.4: Canterbury test area satellite altimetry dataset.....	109
Figure A.5: Canterbury test area satellite gravity data, GGM DIR_5.....	109

List of Tables

Table 2.1: Expected accuracy of Lacoste and Romberg D- and G-model gravity meters	14
Table 2.2: The prevalence of height types in the New Zealand terrestrial gravity database	15
Table 2.3: Common sources of error in ship-borne gravity surveys (Wessel & Watts, 1988)	17
Table 2.4: Comparison of selected satellite only GGMs and EGM2008	22
Table 2.5: Constants used in GRS80 gravity reductions.....	25
Table 2.6: Summary of gravity dataset limitations	40
Table 3.1: Comparison of Kriging methods.....	49
Table 3.2: Summary of integration techniques	53
Table 4.1: Extent of the Canterbury Test Area	54
Table 4.2: Metadata for terrestrial gravity database, as supplied (Stagpoole, 2012)	57
Table 4.3: Parameters of ellipsoids most commonly used in New Zealand	58
Table 4.4: Metadata for terrestrial gravity database, corrected	59
Table 4.5: Terrestrial gravity database height determination methods.....	59
Table 4.6: List of the resulting three irregularities	62
Table 4.7: Cross-validation result (mGal).....	90

List of Abbreviations

AHD	Australian Height Datum
CAA	Civil Aviation Authority
CDF	Cumulative Distribution Function
CGVD2013	Canadian Geodetic Vertical Datum 2013
CHAMP	CHALLENGING Mini-satellite Payload
CORS	Continuously Operating Reference Stations
DEM	Digital Elevation Model
DGPS	Differential Global Positioning System
DSM	Digital Surface Model
DTM	Digital Terrain Model
DIR	Direct approach
DIR_05	GO_CONS_GCF_2_DIR_R5
EGM2008	Earth Gravitational Model 2008
Envisat	Environmental Satellite
ESA	European Space Agency
FFT	fast Fourier Transformation method
GEOS-3	Geodynamics Experimental Ocean Satellite 3
GeoSat	GEOdetic SATellite
GIS	Geographic Information Systems
GGM	Global Geopotential Model
GMT	Generic Mapping Tools
GNSS	Global Navigation Satellite System
GOCE	Gravity field and steady-state Ocean Circulation Explorer
GPS	Global Positioning System
GRS67	Geodetic Reference System 1967
GRS80	Geodetic Reference System 1980
GRACE	Gravity Recovery And Climate Experiment
ITRF	International Terrestrial Reference Frame
LAGEO	Laser Geodynamic satellite
LINZ	Land Information New Zealand
LVD	Local Vertical Datum
MDT	Mean Dynamic Topography
MSS	Mean Sea Surface
NaN	Not a Number
NGA	National Geospatial-Intelligence Agency
NZMG	New Zealand Map Grid
NZGD1949	New Zealand Geodetic Datum 1949
NZGD2000	New Zealand Geodetic Datum 2000
NZGeoid2009	New Zealand quasi-geoid 2009
NZTM2000	New Zealand Transverse Mercator 2000
NZVD2009	New Zealand Vertical Datum 2009
MHW	Mean High Water
MSL	Mean Sea Level
RMS	Root Mean Squared
RTK	Real Time Kinematic
SI	International System of units
SLR	Satellite Laser Ranging
SPW	Space Wise approach
SRTM	Shuttle Radar Topographic Mission
SSH	Sea Surface Height

SST-hI	Satellite-to-satellite tracking in high-low mode
SST-II	Satellite-to-satellite tracking in low-low mode
TIM	Time Wise approach
WGS84	World Geodetic System 1984

List of Symbols

d	falling distance
d_r	gravity meter dial reading
e^2	square of the first eccentricity
$ \mathbf{f} $	Fourier wave-vector
f	Fourier wave-number
g	local gravity acceleration on the Earth's Surface
g_B	complete Bouguer model
g_d	Instrument drift
g_F	Free air model
g_{obs}	observed gravity
g_{SC}	Bouguer spherical cap model
g_{SLAB}	Bouguer slab model
g_{TC}	terrain correction
g_ϕ	normal gravity (or latitude) model
h	height above the ellipsoid
h_s	observed distance from the satellite to the geoid
h_s^*	modelled distance from the satellite to the geoid
k	calibration factor
k_{SPRING}	the spring constant
l	length of spring
m	known mass
n	degree
r	average Earth's radius
r_i	inner raids of Hammer zone
s	estimated signal
t	time elapsed
v	ground velocity
x	observations
AT	local gravity
AT'	residual gravity
AT^s	satellite gravity
$A\delta V^H$	topographic and atmospheric effects
$B\hat{T}$	restored gravity signal
$B\hat{T}'$	restored residual gravity
$B\hat{T}^s$	restored satellite gravity
$B\delta V^H$	restored topographic and atmospheric effects
C_0	nugget
C_1	partial sill
C_{sx}	covariance matrix of signal and observations
C_{xx}	covariance matrix of the observations
D	range
$F(\Delta g)$	gravity anomalies at altitude
G	gravitational constant
H	elevation above the geoid
K	normal gravity constant
L	pendulum length
M	mass of the Earth
N	gravity anomaly
N_{DATA}	number of data points

N_{co}	covariance matrix of the observation noise
O	observations
P	observation point
R	radius of the earth, from centre to station height
R_0	outer radius of Hammer zone
T	period of time to complete a pendulum observation
T_c	terrain correction
Z_i	known values
Z_p	predicted value of P

α	heading
δ	resolution of DEM
ε	Eötvös correction
η	east vertical deflections
λ	wavelength
λ_i	weights of Z_i
ξ	north vertical deflections
μ	dimensionless coefficient (LaFehr, 1991)
ρ	density of mass
ϕ	latitude
Λ	dimensionless coefficient (LaFehr, 1991)
γ_a	normal gravity at the equator

1. INTRODUCTION

1.1. Background

Within the Earth sciences, the problem of having to combine complementary heterogeneous datasets in order to derive a seamless model is not uncommon. For example, the International Terrestrial Reference Frame (ITRF) is primarily determined using five observation techniques (Wang *et al*, 2009), while natural hazard monitoring benefits from combining observation methods from multiple disciplines (examples such as: Custodio *et al*, 2007 and Serra *et al*, 2013).

In geoid modelling the requirement to combine disparate datasets occurs at the gravity field mapping stage. Each gravity observation technique has different parameters, and contributes to different pieces of the gravity signal spectrum. This means that no one gravity dataset is able to adequately represent the gravity field at the national scale, cover the full gravity signal spectrum and provide the spatial resolution required for geoid modelling. Therefore, the best gravity map is one that is derived using datasets from multiple sources.

During the time of the computation of the current New Zealand geoid (NZGeoid2009; LINZ, 2009), the gravity datasets observed on the Earth's surface were artificially separated, abutting at the natural barrier of the coastlines (Claessens *et al*, 2009). This was a reasonable approach, as there were no data available from an observation technique which traversed this boundary at a suitable scale.

In 2012 a trial airborne gravity dataset was collected over the Canterbury region (Winefield *et al*, 2014). This technique is unique as it is the only method which is able to seamlessly capture observations across the transition between land and sea, at a resolution for geoid modelling (Forsberg *et al*, 2000). This means that the approach of combining datasets by using the coastline to delineate a dataset's zone of influence is no longer valid.

It is the intention of this study to combine the 2012 airborne gravity dataset with existing satellite altimetry, terrestrial, ship-borne and satellite gravimetry datasets, to form a single gravity map over the Canterbury region.

Consideration will be given to ensuring how the spectral characteristics of each gravity dataset can be integrated. Finally, an optimal integration method for the combination of multiple gravity datasets will be recommended.

1.2. Motivation

Within geodesy the collection and interpretation of gravity data is of particular importance to height determination.

Unlike horizontal coordinates (latitude and longitude), which are generally understood by the layperson, the concept of '*height*' can be significantly more complex. It is generally accepted that '*elevation*' is the distance from a point to a reference surface, while that the term '*height*' is used exclusively to describe the distance between the top and bottom of an entity (Warf, 2006). However,

the Geodetic Glossary (NGS, 1986) defines '*height*' as: *the distance, measured along a perpendicular, between a point and a reference surface*. Therefore, within this text two terms are used interchangeably. The only exception to this when referencing flights, were '*altitude*' is the distance between the aircraft and the geoid, and '*height*' is the distance between the aircraft and ground level (Warf, 2006).

A vertical datum is the reference surface defined for precise height measurements. Vertical datums are required in areas such as surveying, civil works, construction, hydrology, agriculture and land management, to ensure consistency when comparing and exchanging elevation information.

However, heights are also able to be expressed in less formal, and often more ambiguous terms when precision is not critical. Some examples of these arbitrary reference surfaces are: the height of a balloon above the ground, or snow fall to a height above sea level.

Traditionally, heights in New Zealand have been determined in terms of an averaged sea level reading at a local tide gauge. This has resulted in at least 13 Local Vertical Datums (LVD) determined across the country. These local heights were then transferred via linear networks of benchmarks, using methods such as precise and trig levelling. While often referred to as orthometric heights, gravity observations were not measured as part of the survey. Rather, the levelling observations were reduced using the Geodetic Reference System 1967 (GRS67) normal-orthometric correction (DoSLI, 1989). Therefore, the LVD heights in New Zealand are normal-orthometric.

The twentieth century has seen an increasing prevalence in the use of GNSS (Global Navigation Satellite System) observations. However, GNSS observations are provided as ellipsoidal heights i.e. in terms of an idealised geometric shape, rather than as traditional orthometric or normal-orthometric heights, which are related to sea level. While ellipsoidal heights have practical uses, such as monitoring long term changes, they are less intuitive than gravity based heights. Most notably, as ellipsoidal heights are not based on gravity, they are unsuitable for use in predicting fluid flow for local engineering purposes.

On the other hand, deformation and other geophysical phenomena such as changes in sea level, make the continued use of the 13 LVD and other datums based on tide gauges inconvenient and costly.

The contemporary solution for this situation is for a country to provide a national geoid. This allows the transformation of ellipsoidal heights to orthometric heights, in terms of a national datum. This can currently be seen in New Zealand with New Zealand Vertical Datum 2009 (NZVD2009; LINZ, 2009) and in Canada with Canadian Geodetic Vertical Datum 2013 (CGVD2013; NRCan, 2014).

The geoid is an equipotential surface which would coincide with mean sea level, if the sea was allowed to extend through the continents. While global geoid models exist, they are tailored to provide a global fit of the data and their maximum resolution is restricted to that of the regions with the sparsest gravity coverage (Huang & Véronneau, 2015). These grids are often too coarse for use in surveying or engineering applications. For this reason a number of countries are finding that a national geoid will soon become a necessity (for example: Wonnacott & Merry, 2011 and Othman *et al*, 2014). The local geoid model is computed by augmenting a global model with locally collected gravity data, providing a higher resolution model, with a better fit across the area of interest.

NZGeoid2009 was computed using data available at the time, namely the Earth Gravitational Model 2008 (EGM2008), which was regionally enhanced with terrestrial gravity, altimetry-derived marine gravity anomalies and a digital elevation model (Claessens *et al*, 2009). However, much of these regional datasets are historic, and are heavily spatially biased, resulting in greater distribution in areas of scientific or economic interest. Rather than being collected for the purposes of national-scale geoid modelling, for which well distributed and uniform sampling is required. For example the terrestrial methods of gravity data collection tend to limit observations to easy-to-access areas, such as along roadways and coastlines, and few in areas which are difficult to access or with steep terrain (Amos & Featherstone, 2004). This can result in aliasing as the sample points are restricted to areas of like features.

In early 2011 Land Information New Zealand (LINZ) began investigating methods to improve the vertical datum. The favoured approach was to improve the national geoid by incorporating a national airborne gravity dataset in the geoid computations. One of the major advantages of the airborne gravity technique is its uniform data collection method (LINZ, 2011).

In 2012 LINZ completed a trial airborne gravity survey over Canterbury (Winefield *et al*, 2014). This provided the opportunity to improve the regional gravity data maps in Canterbury, and provide recommendations as to the optimal process for the integration of airborne gravity data with existing gravity datasets.

1.3. Significance of Study

Combining more than two gravity datasets, collected over different spectral ranges, using multiple technologies and with individual error characteristics has been identified as one of the challenges in gravity field modelling (Kern *et al*, 2003). As their different error characteristics and the integration method chosen impact on the final solution. Each of the data types must be combined in a way that the datasets yet to be integrated will not be biased by the effects of previous integrations. Sjöberg (2011) continues this line of research providing a theoretical study combining satellite, airborne and terrestrial gravity, confirming that such multispectral integration is best achieved by a weighted approach.

Previously in New Zealand the coastline has been exploited during the gravity integration process, as it provides a natural buffer between the land and sea datasets (Amos, 2007; Claessens *et al*, 2009). In the case where two sea-based datasets were considered, the ship-borne observations were first integrated with the satellite altimetry derived datasets to form a single *sea-gravity* dataset, prior to combination with the *land-gravity* dataset.

The significance of this study is that the final data integration approach may be required to deviate from the approaches of Amos (2007) and Claessens *et al* (2009). This is primarily because the airborne gravity dataset traverses the gap between the land and sea, precluding the use of the coastline as a division.

This study will use gravity data collected from the Canterbury region of New Zealand to determine an optimal integration process, using physical datasets.

1.4. Objectives of Study

The principal aim of this research is to identify the best method for the combination of satellite altimetry, airborne, ship-borne, terrestrial and satellite gravity collected in Canterbury, to form a single dataset for use in geoid determination.

There are four sub-objectives:

- To determine the characteristics of each of the gravity datasets available over the Canterbury region, their limitations and contributions to defining the gravity field.
- To identify data integration techniques that can be used when combining more than two gravity datasets.
- To evaluate each of the integration techniques on its ability to best preserve the strengths of each gravity dataset.
- To recommend an optimal integration process, and create a gravity map of the Canterbury region using this process.

1.5. Outline of Thesis

This thesis is divided in to five chapters. Chapter One is an introductory section which provides a brief description of the relevance of this project and its outcomes. This chapter introduces the difficulties associated with the integrating of more than two datasets and provides an overview as to the role of gravity in the geoid determination process.

Chapter Two is an introduction to gravity. This chapter includes brief descriptions of the gravity data collection methods and the considerations and corrections applied during the reduction process.

Chapter Three describes the four steps of the Integration Process: understanding the purpose of the model, the data being used, and the integration methods available, combining the data and finally assessing the model to ensure that the requirements have been met.

Chapter Four is a case study, where the Canterbury test area is defined and gravity datasets which cover the Canterbury region are identified and critiqued. The four-step integration process is applied and an optimal gravity map of the Canterbury test area is presented.

Chapter Five is the conclusion and provides a summary of this research. This includes recommendations and findings which could be applied to future research.

2. GRAVITY

2.1. Introduction

Gravity is the universal force of attraction between all objects which have mass. The Earth's gravity keeps the Moon in orbit and the Sun's gravity keeps the Earth in orbit. In short, gravity is the force that causes everything on the surface of the Earth to either fall to the ground or remain in place.

While commonly misunderstood by the layperson, acceleration due to gravity is not constant across the entire Earth's surface (i.e. $g \approx 9.81 \text{ ms}^{-2}$). This over-simplification can be attributed to, and is perpetuated by, commonly using the Earth's average radius ($r = 6,371 \text{ km}$) in Equation 2.1, when solving for gravity acceleration (g) on the surface of the Earth.

$$g = G \frac{M}{r^2}$$

Equation 2.1

where:

G is the gravitational constant ($6.67408 \times 10^{-11} \text{ m}^3 \text{ kg}^{-1} \text{ s}^{-2}$),
 M is the mass of the Earth ($5.98 \times 10^{24} \text{ kg}$), and
 r is the distance from the Earth's centre.

However, it is important to note that the Earth is not a perfect sphere, for example it bulges at the equator (equatorial radius $\sim 6,378 \text{ km}$) and flattens at the poles (polar radius $\sim 6,357 \text{ km}$; Tarbuck *et al*, 2002).

In fact, the value of g varies with respect to latitude, distance from the centre of the Earth and the irregular distribution of mass within the Earth. It is also subject to temporal changes which are able to redistribute mass through processes such as precipitation, ice formation, tides and ocean currents/temperature.

Because of the units reported by the gravity meters providing the raw data, throughout this study gravity units will be represented in Gals (also referred to as a Galileo) using the CGS (centimetre–gram–second) system of units for acceleration. A Gal is defined as 1 centimetre per second squared or in SI (International System) units $1 \text{ Gal} = 0.01 \text{ m/s}^2$ (Cardarelli, 2006). However, differences in g , which can be attributed to variations within the Earth's crust, including the effects of the solid Earth tide, are typically represented in milliGals (mGal). Where $1 \text{ mGal} = 0.001 \text{ Gal} = 10^{-5} \text{ m/s}^2$.

When mapping the Earth's gravity field reference is made to the term 'wavelength' in the case of geoid modelling long wave-length (low-degree) variations signify global-scale anomalies, while conversely short wave-length (high-degree) variations signify local-scale mass anomalies (Matsuo & Otsubo, 2013).

This Chapter reviews the two basic types of gravity meter and describes the various methods which are commonly used to collect gravity observations or determine the Earth's gravity field. Including a

discussion on two of the complexities faced when combining gravity data: which stage of the data reduction process the observations should be combined at, and the problem of downward continuation. This chapter concludes with a reduction, demonstrating how raw gravity observations are reduced to provide gravity anomalies.

2.2. Gravity Instruments

Gravity is measured using an instrument known as a gravity meter, or gravimeter. More specifically they are a type of accelerometer that observes the constant downward acceleration of gravity.

The types of gravity meter used on the surface of the Earth can be divided into two basic categories based on how the gravity field is being measured: absolute meters measure the gravity field directly. In contrast, relative meters observe the difference in gravity between points (Niebauer, 2007).

Most types of gravity meter are designed to remain static. Either providing long term continuous observations at a single station, or are able to be moved to a place for a time (Herring, 2007). However, certain gravity meters have been designed to operate from a moving platform, such as a ship or airplane. In this study these types of movable meters will be referred to as 'dynamic gravity meters'.

Space-borne gravity missions use a different approach in order to determine the Earth's gravity field. They use either satellite-to-satellite tracking or satellite gravity gradiometry to determine the satellite's orbit, and then second derivatives of the gravity potential are used to approximate the gravity field (Rummel, 1986).

2.2.1. Absolute Gravity Meters

Absolute gravity meters directly determine the value of the gravity field. They are ideally suited for use in establishing and monitoring a reference gravity network, or as control points to monitor long term changes in gravitational mass, such as Earth Tides (Herring, 2007).

There are two main absolute gravity observation methods:

- the pendulum method, which is no longer in use (Niebauer, 2007), but remains of interest to this study as this was the method used to provide the first control for the New Zealand terrestrial gravity network (Robertson & Garrick, 1960), and
- the free-fall method, also known as interferometry.

2.2.1.1. The Pendulum method

The pendulum method is based on the measurement of the period and length of a freely swinging pendulum. The concept behind the pendulum method is expressed by Equation 2.2.

$$T = 2\pi \sqrt{\frac{L}{g}}$$

where:

T is the time period to complete an observation,
 L is the length of the pendulum, and
 g is the local gravity acceleration

The pendulum gravimeter was the principal method of observing absolute gravity from 1818, starting with the development of the Kater pendulum (Kater, 1818). The expected accuracy of the various pendulum methods are between 2-40 mGal (Marson, 2012). For all practical purposes free-fall meters have superseded the use of pendulum devices since the 1950s (Torge & Müller, 2012).

The first absolute gravity observations conducted in New Zealand were made in Auckland, in 1882, using the Kater three-pendulum method. However, it was not until 1947 that a framework of 19 absolute gravity reference stations was established across the country (Robertson & Garrick, 1960), using the Cambridge Pendulum Apparatus. This is a method which uses two pendulums swung in anti-phase (Jackson, 1961).

2.2.1.2. Free-fall method

The free-fall method determines g by dropping a known mass, over a known distance, in a vacuum chamber. A laser interferometer is used to determine the position of the mass, as a function of time during its fall. This concept is based on the motion of a body falling freely from rest, Equation 2.3

$$d = \frac{g t^2}{2}$$

where:

d is the falling distance, and
 t is the time to fall under gravity

The most accurate commercially available absolute gravity meter is the Micro-g LaCoste FG5 (Micro-g Solutions, 1999). At a quiet site, a single FG5 is able to observe a repeatability of 3 μ Gal, while different machines at the same site are able to agree to within 1-2 μ Gal (Niebauer *et al*, 1995). In 2015, the New Zealand absolute gravity reference network was re-established using an FG5, observing three South Island and five North Island gravity stations (Stagpoole *et al*, 2015).

While not yet commercially available, recent advancements in absolute gravity have seen the introduction of cold atom gravimeters, including the development of a portable device (Merlet *et al*, 2010). Cold atom gravimeters use atomic interferometry, a method much the same as laser interferometry, as it involves the measurement of a free-falling mass. However, in this case the test masses are atoms, which have been cooled to micro-kelvin temperatures before being released. It is the free-fall time of these frozen atoms which is being measured. A 24 hour occupation from this portable meter is able to provide an accuracy of a few μ Gal (Merlet *et al*, 2010).

2.2.2. Relative Gravity Meters

Rather than observing the gravity field (g) directly, relative gravity meters observe the difference in gravity between two locations. This means that the change in gravity between stations A and B can be determined by Equation 2.4

$$g_B - g_A = k(d_{rB} - d_{rA})$$

Equation 2.4

where:

k is the calibration factor of the gravimeter, and
 d_r is the dial reading at the station.

By observing a station with an absolute gravity value as part of the observation network, the absolute gravity value can then be transferred relatively, to the connecting sites. Often relative gravity meters are portable and readings can usually be determined within a matter of minutes. Therefore a network of relative gravity observations can be observed in a day.

2.2.2.1. Spring-based method

The most common relative gravity meters are spring based. They work on the principle of monitoring the changes in spring length, such as the LaCoste and Romberg zero-length spring shown schematically in Figure 2.1. The changes in gravity are measured by suspending a known mass from a spring. The spring will then stretch and contract as the gravity field varies.

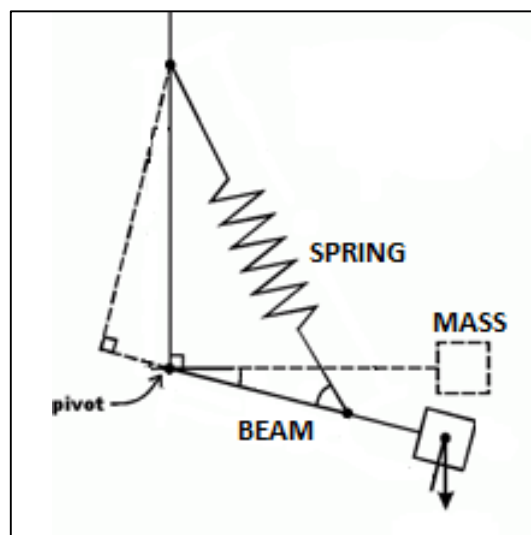


Figure 2.1: Schematic diagram of a LaCoste and Romberg zero-length spring (LaCoste & Romberg, 1998)

In practice, the spring moves to restore the beam to an optimally sensitive position for each site. The change in the gravity field can be determined by measuring the elongation of the spring and by applying the concept shown in Equation 2.5.

$$mg - k_{SPRING}(l_B - l_A) = 0$$

Equation 2.5

where:

m is the known mass at the end of the spring,
 k_{SPRING} is the spring constant, and
 l is the length of the spring

Portable relative gravity meters such as the North American AGI (Hunt, 1970), Worden (Reynolds, 2011) and LaCoste and Romberg G-meter (Seigel, 1995), have observation resolutions in the order of 0.01 mGal.

2.2.2.2. Superconducting method

The superconducting gravity meter is a type of spring type gravimeter. However, in this case the superconducting magnetic field produces a non-mechanical spring, which is used to suspend the mass (Goodkind, 1999). The operational mechanism is made up of three main parts: the mass, the field coils and magnetic plates, as illustrated by the diagram in Figure 2.2. The position of the suspended sphere moves relative to the coils in response to variations in the gravity field (Goodkind, 1999). The superconducting gravity meter is able to monitor the Earth tides at the level of 1 nanoGal (Hinderer *et al*, 2007).

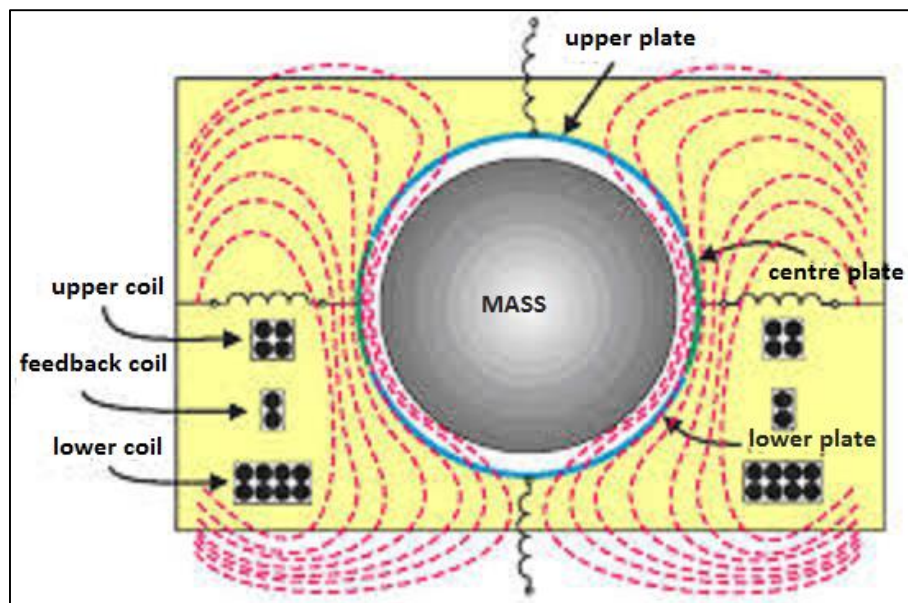


Figure 2.2: Diagram of the basic operation of a superconducting gravity meter (Harms, 2015)

The entire instrument is cooled to 4 kelvin using liquid helium, producing a uniform gravity field which could not otherwise be maintained at room temperature (Niebauer, 2007).

Superconducting gravity meters are best suited as continuous observation stations, as they are prone to large tares in the observations if moved. As such they are used in tidal modelling, seismic studies and monitoring atmospheric effects (Goodkind, 1999).

However, portable superconducting gravity meters do exist (Wilson *et al*, 2012), such as the iGrav: developed by GWR Instruments in 2011 (<http://www.gwrinstruments.com/index.html>).

2.2.3. Dynamic Gravity Meters

Certain models of relative gravity meters are considered to be 'dynamic'. That is to say that they are able to make observations on a moving platform, such as a ship or airplane. Sea and airborne gravimetry generally employs a type of modified land gravity meter, such as the Lacoste and Romberg model "S" meter, shown in Figure 2.3.

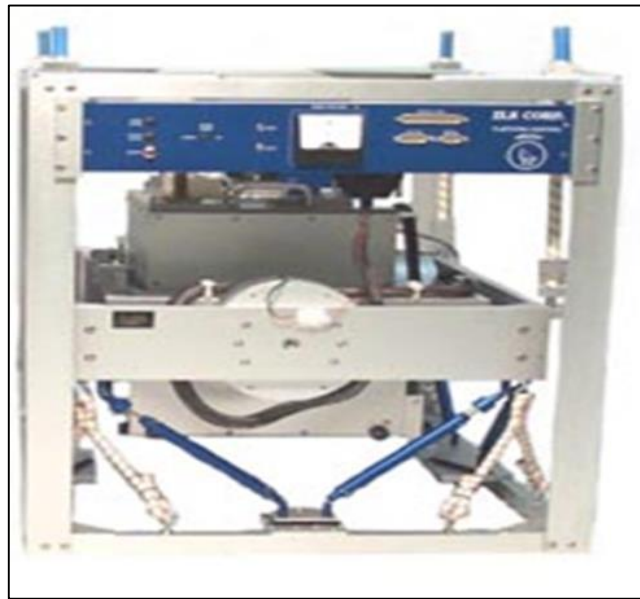


Figure 2.3: Photo of Lacoste and Romberg model "S" air-sea dynamic gravity meter (LaCoste & Romberg, 1998)

Observing gravity in a dynamic environment introduces additional complexities such as vibrations, and kinematic (non-gravity) accelerations caused by the movement of the vehicle, contaminating the gravity signal. For this reason, the meter consists of a highly damped, spring type gravity sensor mounted on a mechanically stabilised frame, eliminating (as far as possible) the effect of tilt, pitch and roll by using gyros and accelerometers in a feedback loop (Alberts, 2009).

When observing from a moving platform the Eötvös Effect must also be considered. The Eötvös Effect occurs due to the vertical component of the Coriolis Effect. It is observed through a decrease in gravity when moving from west to east, and likewise, an increase when moving east to west (Allaby & Allaby, 2008). The Coriolis Effect is dependent on latitude: it is zero at the poles and increases with distance towards the equator.

The Eötvös (ϵ) correction (Equation 2.6) restores the free-air gravity measurements to what they would have been, had the platform not been moving at the time the observations were made (Dehlinger, 1978).

$$\epsilon = 14.585v \cos\phi \sin\alpha + 0.01569v^2 \text{ mGal}$$

Equation 2.6

where:

- ϕ is the latitude
- α is the heading, and
- v is the ground velocity in m/s

2.2.4. Satellite Gravimetry

In essence a satellite in orbit can be considered as a test mass, it is in free fall in the Earth's gravitation field. Therefore, through the motion of the satellite the Earth's gravity field can be deduced (Rummel *et al*, 2002). However, this theory is limited by two factors: the ability for the satellite to be continuously tracked (in all three dimensions), and the effects of non-gravitational forces on the satellite's orbit.

As such, recent space-based gravity missions have relied on satellite-to-satellite tracking, where the gravity satellite is monitored to cm-level precision through uninterrupted GNSS observations (Rummel *et al*, 2002). While, the measurement or compensation for the effect of non-gravitation forces has been determined via one of three techniques:

- a) **Satellite-to-Satellite tracking in high-low mode (SST-hl):** Shown conceptually in Figure 2.4, a low Earth orbiter is tracked by the higher orbiting GNSS satellites (Rummel *et al*, 2002). The non-gravitational forces on the orbiter are measured by a three-axis accelerometer placed at the orbiter's centre of mass (Schwintzer *et al*, 2000).

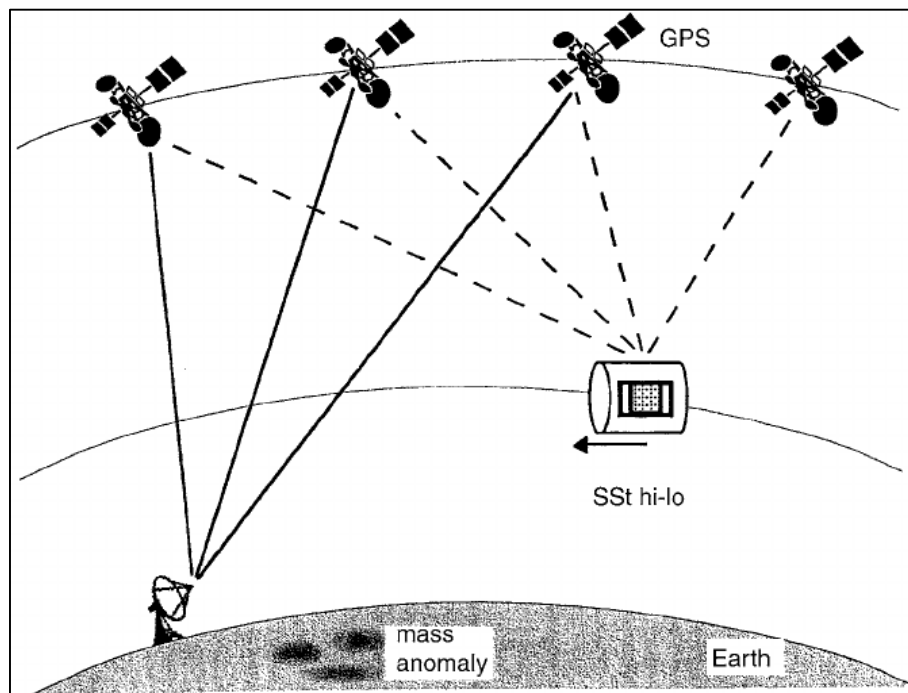


Figure 2.4: Concept of satellite-to-satellite tracking in high-low mode (Albertella *et al*, 2002)

The SST-hl method was first used by the German mission CHALLENGING Mini-satellite Payload (CHAMP). Launched 15 July, 2000, this was a small satellite mission for geo-scientific and atmospheric research. The CHAMP mission included collecting observations for the recovery of the global long-to medium-wavelength, static and temporal gravity field of the Earth (Reigber *et al*, 2002).

- b) **Satellite-to-Satellite tracking in low-low mode (SST-II) combined with SST-hl mode:** Shown conceptually in Figure 2.5, two low orbiters are set-up following each other on the same orbit, but a few hundred kilometres apart. In addition, both satellites are connected to SST-hl mode. While the relative motion, acceleration and altitude data, between the two satellites is measured by a high precision inter-satellite link (Rummel *et al*, 2002).

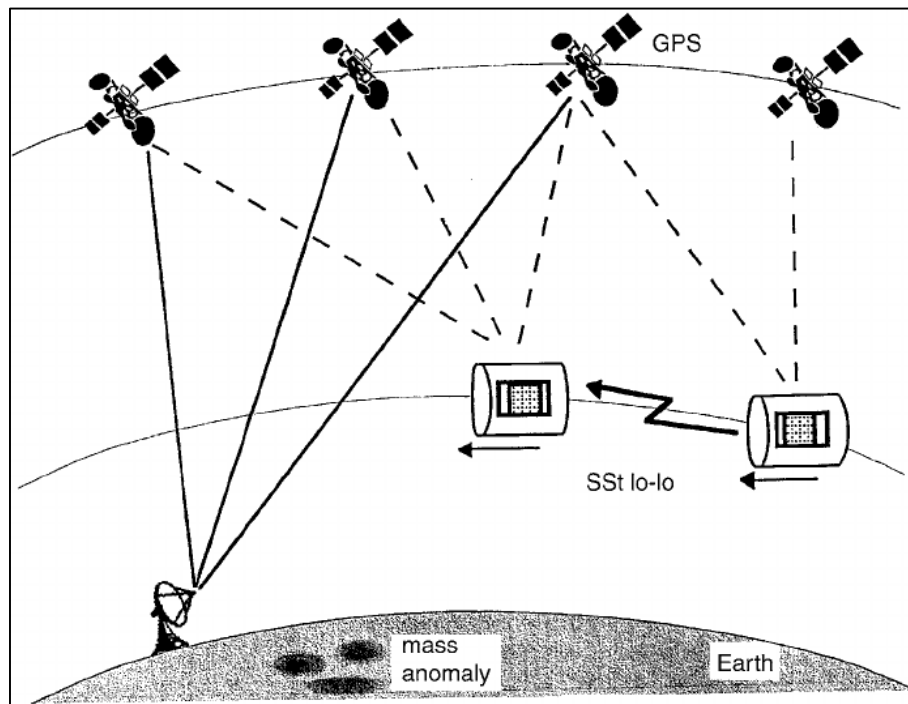


Figure 2.5: Concept of satellite-to-satellite tracking in low-low mode, combined with SST-hl mode (Albertella *et al*, 2002)

The first experiment to use the SST-II method was the US-German mission the Gravity Recovery And Climate Experiment (GRACE). Launched 17 March 2002 (and still in orbit today), GRACE provides global coverage of the Earth's gravity field every 30 days, allowing the study of the time variable gravity effects (Tapley *et al*, 2004).

The GRACE mission consists of twin satellites, separated by 240 km along track. As the lead satellite detects a variation in the Earth's gravity field, such as an increase in gravitational pull, it will 'speed-up', increasing the distance from the trailing satellite. The distance between the satellites is determined by the time a microwave pulse takes to travel from one satellite to the other and back (GRACE, 1998).

- c) **Satellite gradiometry combined with SST-hl mode:** Shown conceptually in Figure 2.6, satellite gradiometry is the measurement of acceleration in all three spatial directions, from a collection of accelerometers inside a single satellite. The measured signal corresponds to the second derivation of the gravitation potential and the non-gravitational accelerations drop out when taking the differences (Rummel *et al*, 2002).

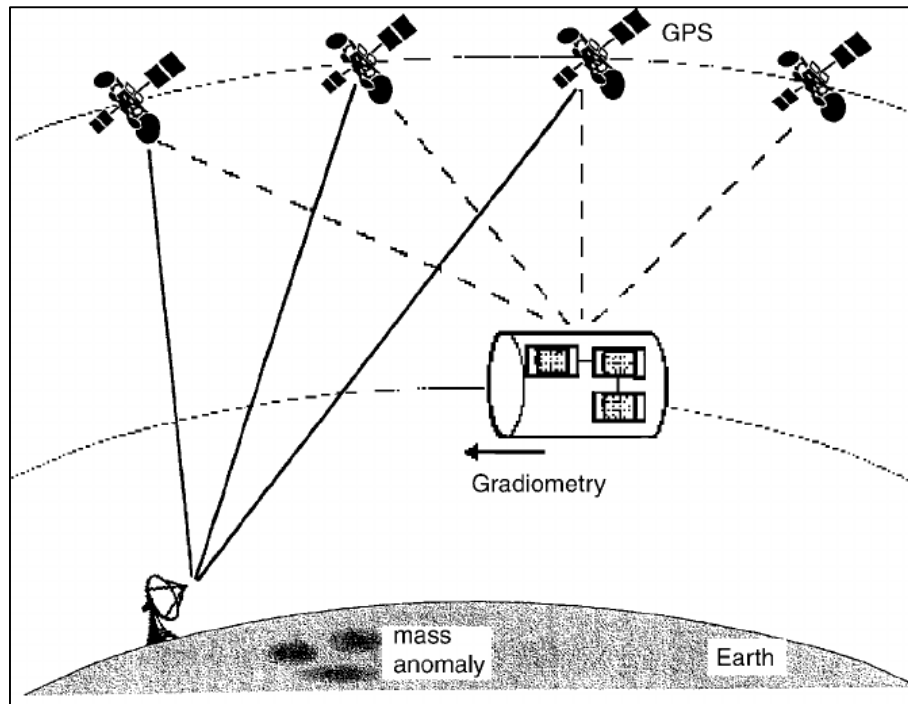


Figure 2.6: Concept of satellite gradiometry combined with SST-hl mode (Albertella *et al*, 2002)

The satellite gradiometry method was first used by the European Space Agency (ESA) on the Gravity field and steady-state Ocean Circulation Explorer (GOCE) mission. Launched 17 March 2009, the purpose of the GOCE mission was to provide gravity information to support steady-state ocean circulation and physics of Earth's interior (Drinkwater *et al*, 2003).

2.3. Data Collection Methods

The various methods of gravity observation are usually identified by their observing environment or platform. For example, this study considers: terrestrial, ship-borne, airborne, and satellite observation methods. Each dataset provides solutions to different parts of the gravity spectrum, each having individual strengths and limitations.

Notably, each dataset is observing a different part of the spectral range. Long wavelength features (greater than 110 km) can only be recovered from satellite gravity datasets. Medium wavelength features (110 - 25 km) are recovered from satellite altimetry and airborne datasets. While the short wavelength features (shorter than 25 km) are recovered from terrestrial and ship-borne datasets (Szűcs *et al*, 2014).

This section provides additional detail on each of the gravity dataset collection methods and their features.

2.3.1. Terrestrial Gravimetry

The New Zealand terrestrial gravity database (maintained by GNS Science: www.gns.cri.nz) contains 40,667 records of terrestrial gravity data within mainland New Zealand, and 70 within the Chatham Islands group. The locations of these observations are shown in Figure 2.7.

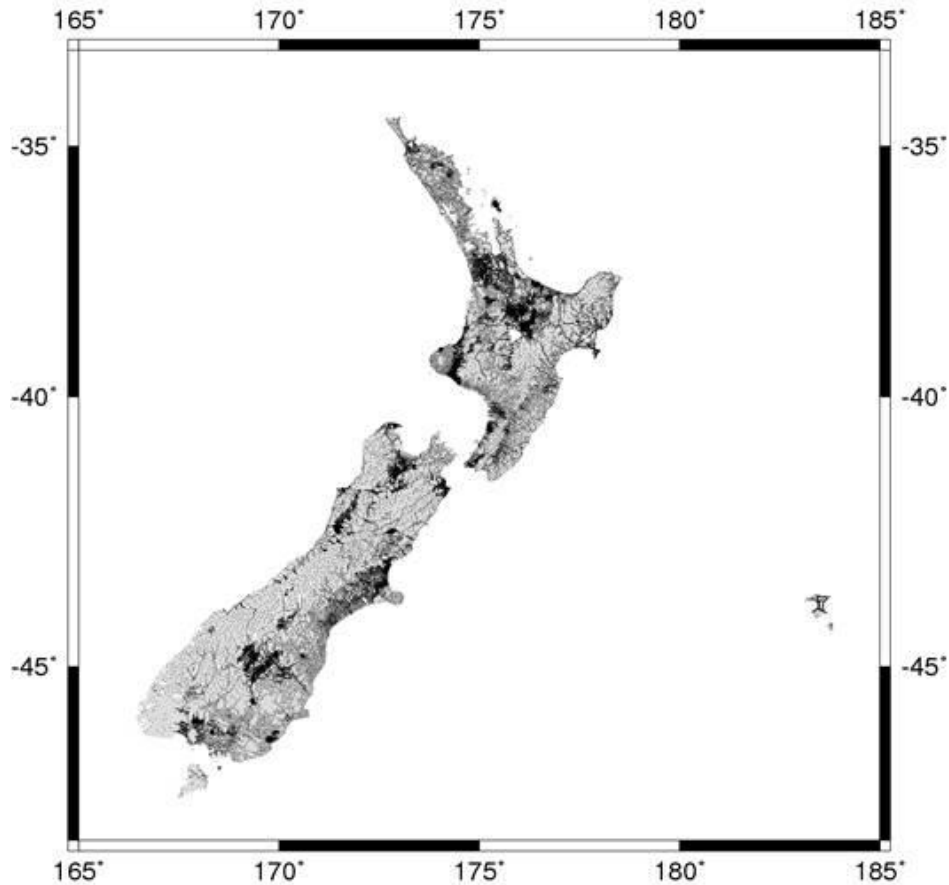


Figure 2.7: Observations from the New Zealand terrestrial gravity database (Amos, 2007) where each observation is represented by a black dot, the darker the shading the higher the density of observations

The primary purpose for the collection of the New Zealand terrestrial gravity network was to support regional geological mapping. To enable geological features in excess of 20 km to be resolvable, the gravity observations are required to be at a spacing of 5-10 km (Seigel, 1995).

The average spacing of terrestrial gravity marks across New Zealand is in the order of 7.5 km. However, their distribution favours roadways and areas of scientific interest, with gaps in regions where access is difficult. This has resulted in unknown uncertainties when interpolating terrestrial gravity data over areas which contain rough terrain and steep slopes (Dumrongchai *et al*, 2012).

Most of the data are observations by the Geophysics Division, the Department of Scientific and Industrial Research, (now GNS Science) using Lacoste and Romberg D- and G-model relative gravity meters. The majority of the observations are collected between 1949 and 1991. The expected accuracy of the readings from these types of meters is shown in Table 2.1.

Model	Resolution mGal	Range mGal	Accuracy mGal
Lacoste and Romberg G-meter	0.01	7,000	0.015
Lacoste and Romberg D-meter	0.001	200	0.005

Table 2.1: Expected accuracy of Lacoste and Romberg D- and G-model gravity meters

The associated uncertainties of these measurements depend on how the observations were positioned. Reilly (1972), states that the expected accuracy of the anomalies in the New Zealand terrestrial gravity database is in the order of 1-2 mGal, though may reach 5-10 mGal in mountainous areas. However, Stagpoole (2012) advises that there are significant discrepancies in the database. In general, the associated uncertainties are directly dependant on how the observations were positioned.

The accuracy of the resulting gravity anomalies is dependent on both the north-south co-ordinate and the elevation of an observation. For example, a positional uncertainty of ± 5 m in the north-south direction results in an uncertainty of ± 0.004 mGal at the mid-latitudes, and less elsewhere. Given that the majority of the horizontal coordinates have been scaled off 1:63,000 (mile) regional geological maps. We should expect that in these cases the positional uncertainties will approach ± 100 m, or ± 0.4 mGal at mid-latitudes.

More significantly, ± 1 m of uncertainty in the elevation results in an uncertainty of ± 0.3 mGal in the gravity anomalies. The method of obtaining heights for gravity surveys has changed significantly over the last two decades. Since the late 1990s GNSS heights with an uncertainty of ± 10 cm (± 0.03 mGal), have been able to be obtained in any location with open sky (and visibility of more than four satellites). However, prior to the advent of GNSS, elevations were determined using either:

- a) Spirit levelling (from the tide gauge to the observation point), with an uncertainty of ± 2 cm (± 0.006 mGal). This method is expensive, and limited to areas easy to access, or
- b) Barometric levelling, which in rough terrain has an uncertainty of ± 10 m at best (± 2 mGal), when weather patterns remain stable (Amos, 2007).

Table 2.2 provides a summary as to the prevalence of each height type in the New Zealand terrestrial gravity dataset. As seen in this table the majority of heights have been determined using barometric levelling. Therefore, the determination of elevation is expected to be the limiting factor as to the reliability of the gravity anomaly values produced from this dataset.

Height Type	Number of Observations	Percentage
Benchmark, Survey point, DGPS	6,519	16%
Spot height, GPS	5,277	13%
Estimated from barometric levelling	2,8871	71%

Table 2.2: The prevalence of height types in the New Zealand terrestrial gravity database

2.3.2. Ship-borne Gravimetry

Ship-borne gravimetry provides the most direct approach of measuring marine gravity.

Unfortunately, ship-borne gravity data does not provide uniform global coverage. This is particularly problematic in the Southern Hemisphere where ship-borne gravity data is predicted to have half the density of that collected in the Northern Hemisphere (Wessel & Chandler, 2011).

Satellite altimetry observations (c.f. Chapter 2.3.4) are unable to be collected in the shallow waters near the coast, and cannot be used to resolve short wavelength features < 25 km. Therefore, ship-borne gravity observations still serve a practical purpose in geoid modelling, especially through the

contribution of wavelengths of >200 m and observations in ports, harbours and the near coast (Sandwell *et al*, 2001).

The New Zealand ship-borne gravity database contains over 3 million observations, equating to at least 900,000 line kilometres of ship-tracks. Figure 2.8 shows the survey lines contained in the New Zealand ship-borne gravity database, illustrating the non-uniform and variable density, nature of the dataset.

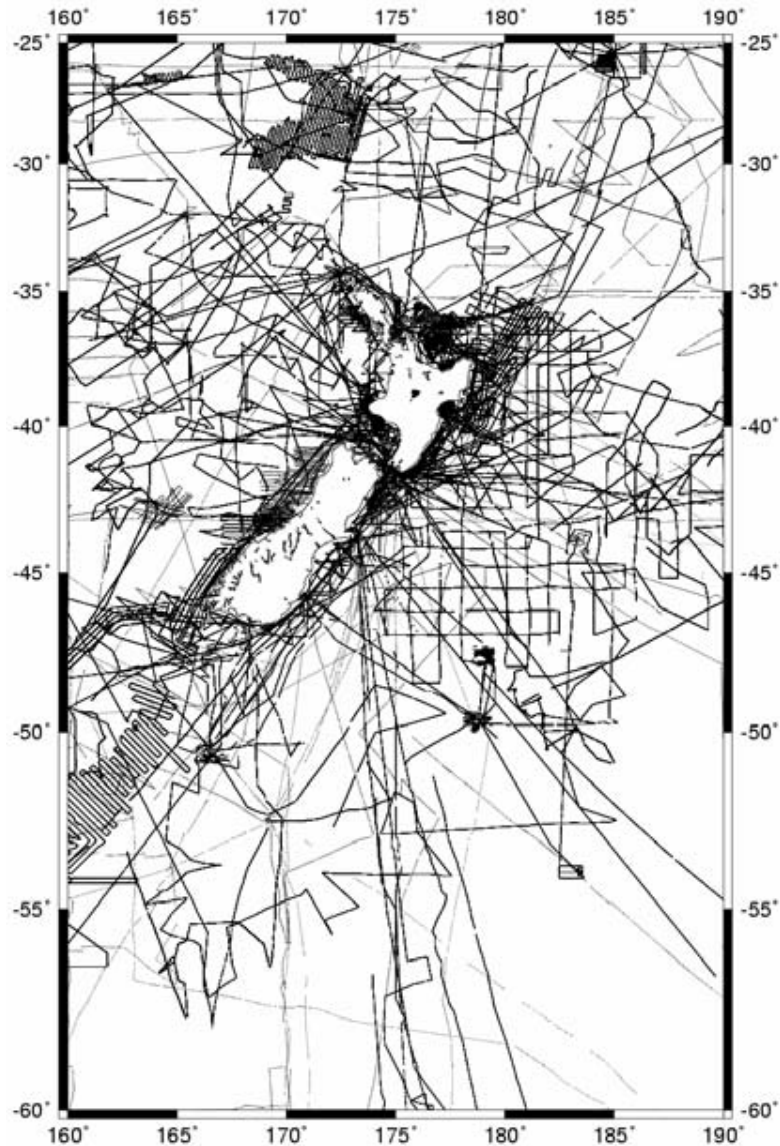


Figure 2.8: Ship-track observations from the New Zealand ship-borne gravity database

The New Zealand ship-borne gravity database is made up of numerous ship-borne surveys, which have taken place since the 1960s. The observations have been collected by various agencies, for various purposes and over varying time periods (Amos *et al*, 2005). As reported by Wessel & Watts (1988) and Yale *et al* (1998), the database is expected to be of a varying quality. The common sources of error in ship-track surveys are shown in Table 2.3.

Navigation	<ul style="list-style-type: none"> ○ Uncertainties in Position ○ Incorrect Eötvös calculations
Instrument	<ul style="list-style-type: none"> ○ Cross-coupling ○ Off Levelling ○ Instrument drift
Other	<ul style="list-style-type: none"> ○ Inconsistent use of gravity formula ○ Inconsistent datum ○ Sea conditions ○ Control ties

Table 2.3: Common sources of error in ship-borne gravity surveys (Wessel & Watts, 1988)

However, the most significant contributions to uncertainties in the database are due to two sources: inter-cruise offsets, and navigational positioning error (Brett, 2004). Therefore only these two methods will be discussed below.

As ship-borne observations are made using a dynamic gravity meter (c.f. Chapter 2.2.3), the meter should be calibrated at a known site immediately prior and following a campaign. However, in some cases this has not occurred or has not been recorded. This leads to uncertainties when comparing data between campaigns, and limits the opportunity to identify tares (jumps) in the data (Brett, 2004).

The largest single source of error in the ship-borne gravity database is due to uncertainties in the positioning of the observations, particularly the latitude component. Latitude impacts the gravity derivations twice, as the radius of the earth changes with latitude and the Eötvös corrections are dependent on the distance from the equator.

Continuing improvements of gravity instrumentation and ship navigational accuracy suggests that the quality of ship-track gravity measurements should improve over time (Wessel & Watts, 1988). For example observations improve when positioned using GNSS and for newer surveys the expected gravity values are accurate to 1 mGal (LaCoste & Romberg, 1998).

However, much of the database was collected prior to GNSS positioning and ship-borne gravity data collected using celestial navigation or other methods can be of a highly variable accuracy (Wessel & Watts, 1988). For example, comparisons between the New Zealand ship-track database and satellite altimetry would show significant variations, such as standard deviations of approximately 2 mGal between two campaigns (Amos *et al*, 2005).

In order to improve the consistency of the ship-borne gravity data, the dataset was crossover-adjusted in 2003 (Brent, 2004). During this exercise the more recent observations were assumed to be correct, and the values of earlier observations adjusted to reflect the expected value at their recorded position. This resulted in a final standard deviation of 0.3 mGal, between the New Zealand ship-track database and satellite altimetry observations (Amos *et al*, 2005).

2.3.3. Airborne Gravimetry

The concept of observing gravity from an airborne platform is not new. For example, both Hannah (2001) and Thompson & LaCoste (1960) refer to airborne geophysical exploration activities which

occurred in the 1960s and one of the first large-scale airborne gravity surveys took place over Greenland 1991-92 (Brozena, 1992).

However, until the availability of GNSS observations, the practical application of this approach has been limited by the ability to model the non-gravitational noise signal from the airborne platform. As seen in Figure 2.9, the total acceleration signal observed from an airborne platform is many times ($\times 10^4$) the accelerations as a result of variations in the gravity field. The recovered gravity signal is shown in Figure 2.10.

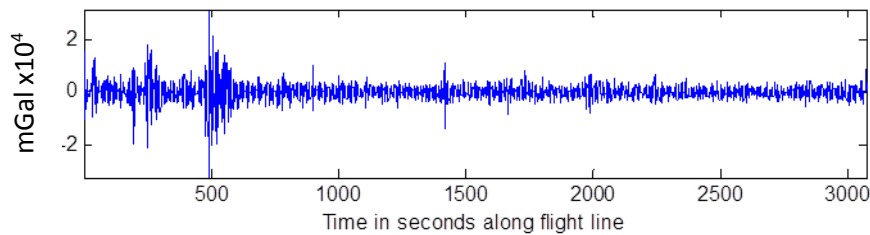


Figure 2.9: Recorded acceleration from a gravity flight (McCubbine, 2016)

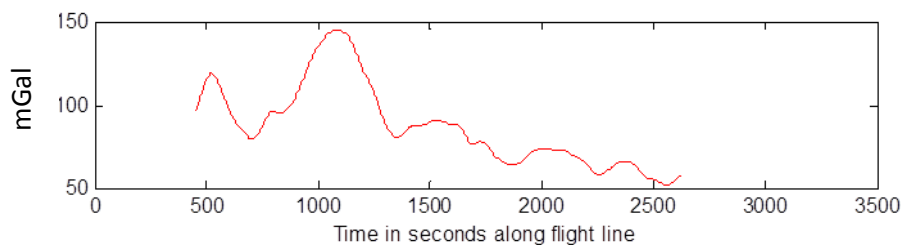


Figure 2.10: Recovered gravity signal
Same flight as shown in Figure 2.9 (McCubbine, 2016)

For localised surveys, aircraft positions were able to be observed via radio signals, the lengths of flight lines being restricted to areas within direct radio contact (Jekeli & Kwon, 1999). However, the time/economic advantage of airborne surveying is gained from the ability to survey large regions in a uniform manner. Without an accurate method of determining the kinematic acceleration of the aircraft throughout the flight, the ability to extract the recovered gravity signal has been limited.

Not until the advent of GNSS, namely the 24 hour availability of GPS (Global Positioning System), has the concept of an airborne gravity survey at a national or regional scale become feasible, as the accelerations of the aircraft are now able to be obtained throughout the flight, allowing the gravity signals to be readily separated from the kinematic acceleration signals (Olesen, 2002). The process to separate the aircraft accelerations from the gravity signal is described in McCubbine (2016) Section 6.3 Gravity Reduction.

The benefits of airborne gravity are that it is fast, economic and provides a uniform and seamless coverage of the survey areas. This includes any high/inaccessible mountains, where existing data are typically sparse (Hwang *et al*, 2014). It is also the only technique that can fill the transition between land & sea (Alberts, 2009), including the littoral and shallow coastal zones.

In addition, by being flown at altitude, airborne gravity is the only method that fills the spectral gap between land and space-based approaches (Abbasi *et al*, 2007), observing wavelengths shorter than 100 km.

2.3.4. Satellite Altimetry

In contrast to the gravity observation methods discussed in the sections above, satellite altimetry does not directly measure gravity, but uses a satellite-borne radar altimeter (altitude meter) to directly measure the height and slope of the sea surface. The principle of satellite altimetry is shown in Figure 2.11.

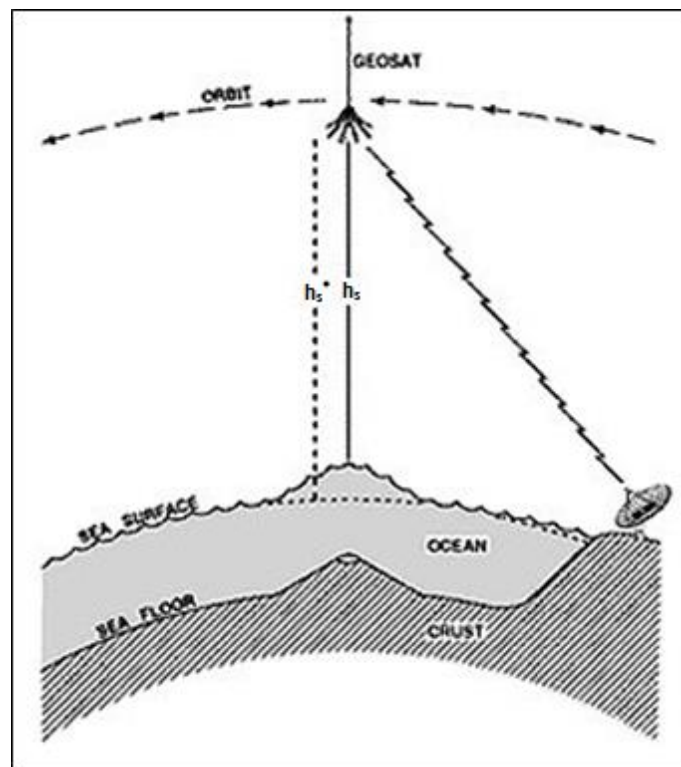


Figure 2.11: Satellite altimetry principle (NOAA, 2010)

The altimeter transmits pulses in the vertical direction towards the ocean surface and measures the time interval for the radar pulse to be reflected off the sea surface and travel back to the satellite (Deng *et al*, 2002). The time taken is then converted to a height above the instantaneous sea surface and the anomaly value (N) is approximated by (Equation 2.7).

$$N = h_s^* - h_s$$

Equation 2.7

where:

h_s^* is the expected distance from the satellite to the geoid, and
 h_s is the observed distance from the sea surface to the satellite.

Also seen in Figure 2.11, is the icon of a radio antenna, referring to the Ground Control segment. The satellite's three-dimensional position is determined by control, such as GNSS or retro-reflectors for use with Satellite Laser Ranging (SLR). Newer satellites are also capable of determining their orbit using satellite-to-satellite tracking.

Incidentally, the height of the ocean surface is a first approximation of the gravitational potential at that point. Gravity anomalies are the vertical derivative of gravitational potential and potential values can be recovered through Laplace's equation (Garcia *et al*, 2014).

To enable the satellite altimetry data to be combined with other gravity datasets, the height and/or sea slope observations need to be converted to a gravity anomaly. In order to do this transformation a grid of east η and north ξ vertical deflections should be constructed from a dense network of satellite altimetry measurements. The grid is Fourier transformed (see Sandwell *et al*, 2013) and then Equation 2.8 (Haxby *et al*, 1983) is used to compute the gravity anomaly.

$$\Delta g(\mathbf{f}) = \frac{ig}{|\mathbf{f}|} [f_x \eta(\mathbf{f}) + f_y \xi(\mathbf{f})]$$

Equation 2.8

where:

the Fourier wave-vector is define as: $|\mathbf{f}| = \sqrt{f_x^2 + f_y^2}$ and $\mathbf{f} = (f_x, f_y)$, and

with wave numbers (λ is wavelength, in radians) $f_x = 2\pi/\lambda_x$ and $f_y = 2\pi/\lambda_y$

The observations from satellite altimetry datasets are able to provide medium wavelengths (50-100 km; Andersen *et al*, 2005) for use in geoid determination. Satellite altimeter derived gravity is about two times more accurate than ship-track data at medium wavelengths, over the open ocean, but degrades closer to the coast.

Satellite altimetry has been monitoring the open ocean for several decades. Data from the original missions such as GEOS-3 (Geodynamics Experimental Ocean Satellite 3), and GeoSat (GEOdetic SATellite), suffered significant degradation close to the coast (Andersen *et al*, 2010), when compared with the newer missions such as CryoSat-2, Envisat (Environmental Satellite) and Jason-1.

This improvement has been achieved through the introduction of various measurement modes. For example CryoSat-2 has three measurement modes. These switch automatically as the satellite moves though a 'mode mask' (Wingham *et al*, 2006), such as the transition between land and sea or sea and ice. However, Anderson *et al* (2005) demonstrate that the accuracy of the altimetry-derived gravity field close to the coast is still half that of the open ocean. Coastal observations continue to be a major source of error in satellite altimetry observations.

There are many different mean surface models, derived for different purposes or areas of interest (Andersen & Knudsen, 2009). High-resolution Mean Sea Surface (MSS) models are derived by merging several years of repeated observations across multiple satellite altimetry campaigns (Andersen & Knudsen, 2009). This means that all modern gravity fields are comparably accurate over the open oceans between 82°N and 82°S (Andersen *et al*, 2010).

One important point of difference is that MSS models provide the average height of the Oceans. In contrast, Mean Dynamic Topography (MDT) models provide the temporal mean of the oceans' dynamic topography i.e. these are models related to a specific time period (Kundsen *et al*, 2011).

The determination of Sea Surface Height (SSH) is approaching the goal of 1 mGal accuracy across the global marine gravity field. However, Sandwell *et al* (2013) identify four features that influence the accuracy of the gravity field:

- a) spatial track density,
- b) altimeter range precision,
- c) track orientation, and
- d) accuracy of coastal models.

The high latitude areas (beyond 82°N and 82°S) are the most difficult regions to model due to fewer satellites covering this area (Andersen & Knudsen, 2009). This means that quality, spatial and temporal coverage of these areas decreases. In addition, these regions are subject to seasonal ice coverage requiring different observational modes during different times of the year.

In regards to satellite orientation, errors in the east-west component can be up to 3.5 times as large as the errors in the north-south component, as missions tend to run north-south. In addition, adjacent slope estimates are less accurate than along track estimates, as the environmental and orbit errors are not entirely corrected with crossover adjustments (Sandwell *et al*, 2001).

The coastal regions have noisier returns (Deng *et al*, 2002) due to coastal sea states (waves) and footprint returns from land. This often prevents information from coastal regions being included in the satellite altimetry models. Shum *et al* (1997) states it was common practice to exclude all SSH data in water shallower than 200 m, while Deng *et al* (2002) hypothesizes that the SSH range should be interpreted with some caution for distances less than 22 km from the coast and should be discarded completely for distances less than 4 km. More recent studies such as Tseng (2014), use re-tracking and trimming of the footprint size to extend the reliability of data coverage to 1-7 km offshore.

2.3.5. Global Geopotential Models

A Global Geopotential Model (GGM) comprises a set of spherical harmonic coefficients that describe the long-wavelength characteristics of the Earth's gravity field. Numerous GGM models exist and have been computed by various organisations around the world. A list of models can be found on the International Centre for Global Earth Models website: <http://icgem.gfz-potsdam.de/ICGEM/>

GGMs which are created using only satellite data are known as *Satellite Only GGMs*. While GGMs which use additional gravity data, such as terrestrial or ship-borne, in their realisation are referred to as *Combined GGMs* (Featherstone, 2010). Because of the attenuation of signal with altitude, satellite only GGMs are always only long wavelength models.

A GGM is used to describe the Earth's gravity potential (geopotential) in terms of an infinite series of spherical harmonics, outside of the Earth's attracting masses. The geopotential is given as a truncated set of harmonic coefficients (Omar *et al*, 2005), up to a specified degree and order. As

shown in Equation 2.9, minimum wavelength (λ) is approximately half the planet's circumference, divided by the degree (n). This means that the higher the value of the degree, the better the spatial resolution and finer the results (Ellmann, 2011).

$$\lambda = \left(2\pi \frac{r}{n}\right) \cos\phi$$

Equation 2.9

where:

r is the mean Earth radius (i.e. 6,371 km), and
 ϕ is the latitude.

EGM2008 is a GGM released by the National Geospatial-Intelligence Agency (NGA; Pavlis, 2012). EGM2008 is a combined geopotential model, based on a GRACE derived dataset, augmented with terrestrial gravity data (Andersen *et al*, 2008). EGM2008 was computed from a global 5 arc-minute grid of gravity anomalies developed up to degree/order 2160 (c.f. table 2.3), with some additional terms up to degree/order 2190 (Pavlis *et al*, 2012). EGM2008 does not incorporate any GPS/Levelling. Over areas covered with high quality gravity data, the discrepancies between EGM2008 geoid undulations and independent GPS/Levelling values are on the order of ± 5 to ± 10 cm (Pavlis *et al*, 2012).

In regions with insufficient terrestrial data (for example where data are protected by military or commercial purposes), the shorter wavelengths were reconstructed using Shuttle Radar Topographic Mission (SRTM) Bouguer anomalies (Featherstone, 2010).

SRTM was an 11 day 2004 mission, using a single-pass radar interferometer to produce a Digital Elevation Model (DEM) of the Earth's land surface between 60°N and 56°S (Farr & Kobrick, 2000).

Table 2.4 shows the approximate spatial wavelengths for each of the gravity satellite missions (discussed in Chapter 2.2.4) at a latitude of 45°, for their maximum degree and order (n_{MAX}). An example satellite only GGM is provided for each mission, along with its Root Mean Squared (RMS) when compared to the 40,667 GPS/Levelling marks across New Zealand (McCubbine, 2016). This is then compared to the combined GGM EGM2008.

Mission <i>Example model</i>	Degree and Order (n_{max})	Wavelength (km) $\phi = 45^\circ$	RMS (metres) (Comparison with GPS/Levelling)
CHAMP <i>EIGEN-CHAMP05S</i>	120	175.2	29.4
GRACE <i>Tongji-GRACE01</i>	160	131.4	38.9
GOCE <i>JYY GOCE04S</i>	240	87.6	38.0
EGM2008	2160	9.7	17.9

Table 2.4: Comparison of selected satellite only GGMs and EGM2008

For GGMs which use GOCE data, there are three different approaches which may be applied, the Direct approach (DIR), Time Wise approach (TIM) and Space Wise approach (SPW).

There are two distinguishing differences between these three methods. First, the DIR and TIM approaches are solved using normal equation systems. However, while DIR starts with an *a priori* gravity field model and adds GOCE information to improve it, the TIM approach is based solely on GOCE data. In contrast SPW works predominately in the space domain, applying Least Squares Collocation and extrapolating the spatial correlation of the gravity field (Pail *et al*, 2011).

Secondly, all three methods have different models for the stochastic behaviour of the gradiometer. DIR uses a moving average method (Klees *et al*, 2003) within the measurement bandwidth (5 and 100 mHz). TIM also uses a moving average method, but over the entire observation spectrum. Again SPW uses a collocation approach (Pail *et al*, 2011).

Pail *et al* (2011), Knudsen *et al* (2011) and McCubbine (2016) test these three approaches. All three authors find that the DIR outperforms the TIM and SPW approaches. Knudsen *et al* (2011) stated that the DIR approach yields the largest resolution with the least noise. This is expected to be due to the direct approach using a combined gravity field as background and *a priori* model.

2.4. Gravity Anomalies and Reductions

A gravity anomaly is the difference between the gravity fields observed and the value predicted by a model. Models are susceptible to over simplification, presenting a featureless Earth's surface which is more uniform than it is in reality (Lyatsky & Pana, 2003).

Gravity measurements provide information about mass distribution within the earth. A deviation from a global model can be the result of a physical change in the distribution of mass. For example the mass of a large mountain range may provide a positive gravity anomaly. In contrast an ocean trench, an area where the expected mass is missing, will cause a negative gravity anomaly. Observations which differ from the theoretical value can be investigated, refined and finally combined with additional geodetic and geophysical data to make inferences about the earth's true structure. Gravity reductions are always made with heights in terms of the geoid (Hackney & Featherstone, 2003).

Gravity anomalies play an important role in both geophysics and geodesy. However, the application can differ slightly between the disciplines. For example, in geodesy gravity anomalies are to be preserved as they are used to define the geoid and derive heights. However, in geophysics gravity anomalies are removed, in order to infer variation in sub-surface structure which would have otherwise been masked by the effects of the anomalies (Hackney & Featherstone, 2003).

The global gravity formulas (discussed later in this section) are theoretically straightforward, largely based on the magnitude of the Earth's mass and the distances from it. However, things soon become more complex as we find that the Earth is not a perfect sphere, nor can it be perfectly modelled by any other geometric shape such as an ellipsoid. This is because the Earth's masses are not uniformly distributed, its surface is undulating, and the mass distribution is not static.

Sharma (1997) describes the process for reducing raw gravity measurements to interpretable anomalies as follows: Latitude correction; which accounts for Earth's elliptical shape and rotation, Free-air correction; which accounts for gravity variations caused by elevation, Bouguer slab correction; which accounts for excess mass about the observation station and Terrain correction; which accounts for detailed variations in the terrain about the observation station. The application of all these corrections results in a Bouguer anomaly. This section describes these corrections by modelling the differences.

2.4.1. Relative Gravity Observations

Observed gravity (g_{obs}) values are the reduced gravity readings (on the topographic surface), corrected for earth tides (Longman, 1959) and instrument drift (Reynolds, 2011).

First, most relative gravity instruments are sensitive enough to observe the effects caused by the positions of the sun and the moon (a range of ± 0.3 mGal). These variations are dependent on latitude and time. Corrections can be calculated by making repeat measurements at known stations (over short time intervals), or using computer software which computes global earth tide models.

Second, the measurements recorded by a stationary gravity meter changes (drifts) over time. Initially, the instrument will drift as it comes to temperature and therefore should be allowed to stabilise prior to survey. However, all meters will drift as the internal spring, or other inner workings fatigue. Fatigue drift is assumed to be linear, smooth, slow and independent of location. Frequent readings at a calibration point, along with readings at the same point at the start and end of the survey will allow the drift pattern to be characterised. Drift can be correct for through the use of Equation 2.10.

$$g_{obs} = g - (g_d \times t)$$

Equation 2.10

where:

- g is the raw gravity reading,
- g_d is the instrument drift rate, and
- t is the time elapsed.

If the meter is jarred, a tare in the record may occur. This is a systematic error which needs to be identified and removed. However, usually a tare in a terrestrial gravity dataset will require a resurvey of the section of measurements in question.

2.4.2. Normal Gravity Model

The normal gravity (or latitude) model (g_ϕ) provides values that would be observed if the Earth was a perfect ellipsoid, with a regularly distributed mass. The normal gravity model applied through the use of Somigliana's closed formula (Moritz, 1980) is shown by Equation 2.11

$$g_{\phi} = \gamma_a \frac{1 + K \sin^2 \phi}{\sqrt{1 - e^2 \sin^2 \phi}}$$

Equation 2.11

where:

the Geodetic Reference System 1980 (GRS80) constants from Moritz (1980) are shown in Table 2.5.

Constant	Description	Value
K	Normal gravity constant	0.001 931 851353
γ_a	Normal gravity at the equator	9.780 326 771 5 m s ⁻²
e^2	Square of the first eccentricity	0.006 694 380 022 90
ϕ	Geodetic latitude	Observed Latitude

Table 2.5: Constants used in GRS80 gravity reductions

2.4.3. Free-Air Model

The free-air model (g_F), shown in Equation 2.12, is used to account for gravity variations caused by elevation at the observation location (Heiskanen & Moritz, 1981). It is analogous to taking a measurement while in flight, hence the term free-air (Reynolds, 2011).

$$g_F = g_{\phi} - 0.3086H$$

Equation 2.12

where:

H is the elevation (in metres above the geoid).

The constant (0.3086 mGal/m) is the approximate rate of the change in gravity for elevation, excluding the effects of density or topography.

2.4.4. Bouguer Slab Model

The Bouguer slab model, Equation 2.13, accounts for the effect of mass exerted by the rock slab between the observation station and the geoid.

$$g_{SLAB} = g_{\phi} - 0.3086H + 2 \pi G \rho H$$

Equation 2.13

where:

G is the gravitational constant

($6.67 \times 10^{-11} \text{ Nm}^2/\text{kg}^2$ and therefore $2\pi G \approx 4.191 \times 10^{-5} \text{ mGal m}^2 \text{ kg}^{-1}$),

H is the elevation (in metres above the geoid), and

ρ is the average density (g/cm^{-3}) between the observation station and the geoid.

An average rock density of 2.67 g/cm^{-3} is generally assumed for the density (ρ) of the included mass in regional gravity survey (Hinze, 2003).

This model assumes flat topography. As shown in Figure 2.12 undulations in the terrain are completely ignored in the slab model, resulting in areas of over and under corrected terrain (Hammer, 1939). It is effectively an infinite slab with a continuous thickness (H), the distance from geoid to the gravity station (A).

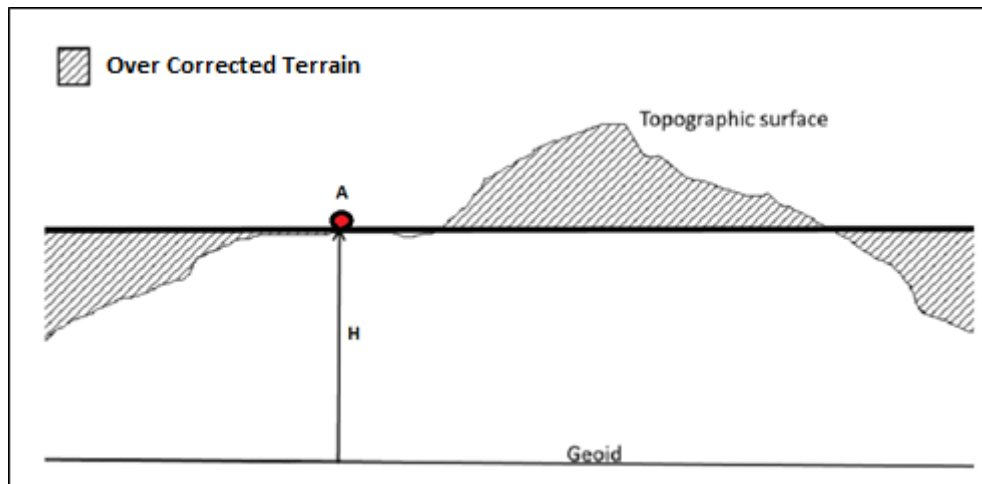


Figure 2.12: Illustration of the Bouguer slab model (McCubbine, 2016) where H is the distance from the geoid to the gravity station A

However, there are alternative approaches to this model, such as the Bouguer spherical cap model, shown in Equation 2.14. The Bouguer spherical cap model uses the height (h) modelling a simple mass from the ellipsoid to the station height (Holm & Oldow, 2007).

$$g_{SC} = 2\pi G\rho(\mu h - \Lambda R)$$

Equation 2.14

where:

μ and Λ are dimensionless coefficients (LaFehr, 1991),

h is the height of the gravity station above the ellipsoid (km), and

R is the combined height of the gravity station and average radius of Earth (km).

As illustrated by Figure 2.13 the main difference between these models is that while the Bouguer slab model assumes a flat Earth, the Bouguer spherical cap model accounts for the curve of the earth. This means modelling a sphere of thickness h , rather than a slab of thickness H .

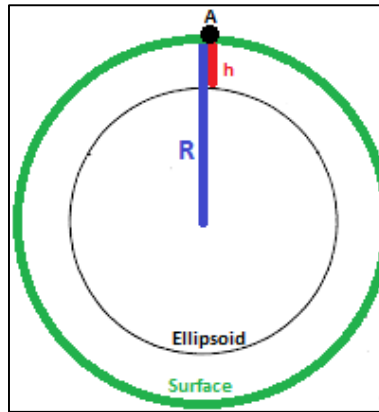


Figure 2.13: Illustration of the Bouguer spherical cap model

2.4.5. Terrain Models

A DEM is a statistical representation of the terrain (height) in a digital form (Omar *et al*, 2005). DEMs are typically employed for use in three-dimensional visualisation and are commonly used in applications such as orthorectification of satellite imagery, geoid computations and hydrological, environmental, and climate modelling. Within geodesy the DEM is used to better account for terrain effects on the gravity field.

The term DEM is often used synonymously with other terms such as Digital Terrain Model (DTM) or Digital Surface Model (DSM). However, these terms represent different products, with slight differences between them (Li *et al*, 2004). The DTM is a surface formed with respect to the bare Earth (without any objects like trees and buildings), while the DSM represents the Earth's surface and all objects on top of it. Li *et al* (2004) defines the DEM as a special case of DTM, with elevations referenced as a height above a given level.

A DEM is an auxiliary elevation model which is necessary for use in geoid determination, especially within New Zealand's rugged mountains and other difficult to access terrain (Amos & Featherstone, 2003). In fact, there is a direct relationship between the quality of a DEM and the precision of the geoid (Catalão & Sevilla, 2009). The purpose of "handling terrain" is to remove the irregularities from the dataset so that gravity anomalies are easier to reconstruct (Dahl & Forsberg, 1999).

When making gravity observations on land it is convenient to conduct them in areas which are readily accessible (Featherstone & Kirby, 2000). This results in the majority of gravity observations located on routes accessible to vehicles: along road ways (cars), on mountain tops (helicopters) and along river valleys (boats). This approach causes the observations' locations to be unrepresentative of the terrain as a whole i.e. the gravity signal has not been randomly sampled.

Featherstone & Kirby (2000) likened this to "aliasing in signal processing", when sampling a mathematical function. That is to say that if the sampling period is incorrect then the sample will not be able to replicate the entire function. While gravity samples appear to be irregular in nature, the consequence of this biased sampling method is similar: one is unable to reconstruct the entire gravity signal from a biased sample.

There are a number of benefits for using DEM heights for these transformations (Featherstone & Kirby, 2000). As the DEM was created for cartography purposes it is an independent height model which is less affected by unrepresentative sampling than gravity observations alone. The DEM is of a higher resolution than the sampled gravity data, also allowing the prediction of gravity values in voids (areas where direct observations have not been made; Forsberg & Tscherning, 1981) and creation of a uniform restored surface (Higgins *et al*, 1996). Therefore the DEM can be used to restore the terrain effects, reducing the impact of aliasing, once the gravity reductions have been completed.

Gravity is usually measured on the Earth's surface, for use in physical geology. For these uses the Bouguer reduction removes the effects of the topography from the sample observations (Featherstone & Kirby, 2000). However, in order to calculate the geoid using Stokes' formula the gravity anomaly must be transferred onto the geoid surface (Omang & Forsberg, 2000).

The Geographx (geographx.co.nz) New Zealand DEM version 2.1 covers New Zealand's North Island, South Island and Rakiura/Stewart Island. It contains 115 tiles, at a cell resolution of 8 m. The objective of developing this DEM was to support cartographic visualisation and other purposes which require low resolution terrain data (such as terrain analysis, before the acquisition of high-resolution data over an area of interest).

The model is primarily derived from LINZ 20 m contour data (at a scale of 1:50 000), supplemented with 3-second SRTM data. The spatial accuracy is nominally the same as for the LINZ source data: 90% of well-defined points are within ± 22 m horizontally and within ± 10 m vertically.

2.4.5.1. Terrain Corrections

The terrain correction accounts for the effects of variation in the elevation of the surrounding topography (mountains and valleys), removing the over approximation of the Bouguer slab model. The calculation of the terrain correction can be computed in a number of different ways, including Hammer charts, Fourier transformation and prism methods.

Hammer charts

Traditionally, terrain correction calculations are conducted in the field as part of the gravity measurement process. The estimated mean height of the surrounding topographic features are recorded and divided into specified annuli (or Hammer zones). The far field sectors are difficult to estimate by eye and so these zones may be derived using a topographic map. The accuracy of this method largely relies on how well the mean topographic height can be estimated and also the number of compartments in each Hammer zone (Nowell, 1999). Figure 2.14 provides a list of the Hammer zones; including their radii (in metres), the number of compartments in each zone and a diagram illustrating the geometry of the zones.

Zone	Inner Radius	Outer Radius	Number of Compartments
A	0.0	2.0	1
B	2.0	16.6	4
C	16.6	53.3	6
D	53.3	170.1	6
E	170.1	390.1	8
F	390.1	894.9	8
G	894.9	1530	12
H	1530	2615	12
I	2615	4469	12
J	4469	6653	16
K	6653	9903	16
L	9903	14,742	16
M	14,742	21,944	16

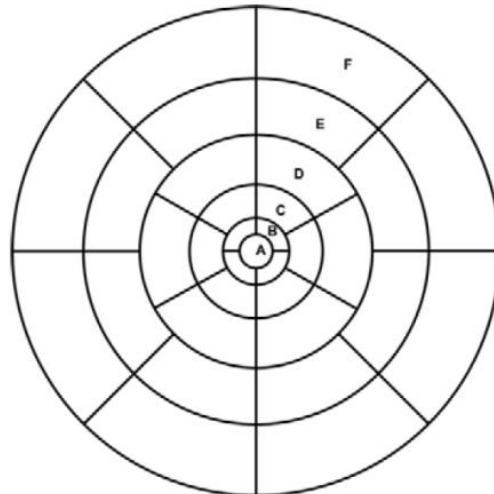


Figure 2.14: List of Hammer zones (left) and geometry of zones (right; Amos, 2007)

However, using a DEM to provide an approximation of the topography, means that topographic heights can now mostly be computed in the office. As this process does not rely on field estimates of height, the number of compartments can be increased (up to the resolution of the DEM) resulting in an improved estimate of the mean topography. The only limitations to this method are in the near zones as these sectors are affected by the DEM resolution. For example, a DEM with a resolution of 64 m will result in no topographic variability in zones A and B (out to around 32 m) and so the terrain correction for this range will be zero (McCubbine, 2016). In rough terrain this may result in errors in the near zone calculations up to several mGal (Kirby & Featherstone, 2002).

Fourier Transformation

The fastest method of terrain correction calculation (example: Sideris, 1985) is the fast Fourier transformation method (FFT), as it is able to exploit the gridded nature of a DEM to make efficiency gains. Such that a space-domain integration, given N data points would be required to perform $O(N_{\text{DATA}}^2)$ operations, whereas the FFT method only preforms $O(N_{\text{DATA}} \ln N_{\text{DATA}})$ operations. In Australia this meant reduce computation time of a set of national terrain corrections from months, to a matter of days (Kirby & Featherstone, 1999).

While use of the FFT method is preferred due to its speed, it should be employed with caution. As differences between the space domain and FFT methods are negligible in flat regions. However, in rugged terrain the differences can exceed tens of mGal. For example when terrain slopes are greater than 45° , the FFT becomes unstable, causing the series to fail to converge (Kirby & Featherstone, 2001).

In order to force the operation to converge, it is possible to smooth the DEM to small gradients. However, this requires compromise between the best representation of the topography and the application of the method (Gomez *et al*, 2013).

Prism Methods

The Nagy prism method for making terrain corrections is performed by approximating the topography of a given DEM, with rectangular prisms. Figure 2.15 illustrates the Nagy prism concept (Nagy,1966) , where topography centred at the point x_p, y_p can be approximated with a rectangular prism with an area of $\delta x \times \delta y$ and four corners in the x, y plane, (x_{p1}, y_{p1}) , (x_{p2}, y_{p1}) , (x_{p1}, y_{p2}) and (x_{p2}, y_{p2}) .

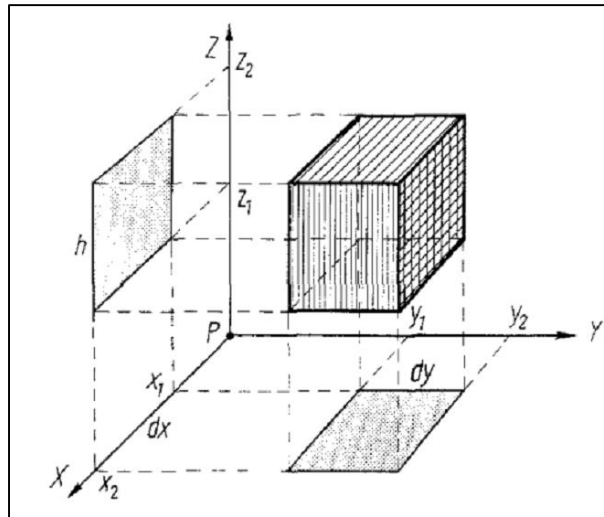


Figure 2.15: Illustration of the Nagy prism method (Nagy, 1966)

where:

$$x_{p1} = x_p - \frac{\delta x}{2} \quad x_{p2} = x_p + \frac{\delta x}{2}$$

$$y_{p1} = y_p - \frac{\delta y}{2} \quad y_{p2} = y_p + \frac{\delta y}{2}$$

Therefore, coordinates (x_p, y_p, z_p) are with respect to an observation made at the origin and Nagy's prism based terrain correction is calculated by the closed Equation 2.15. To obtain the terrain correction over some area, the g_{TC} for all x_p, y_p are summed up.

$$\begin{aligned}
g_{TC} = G\rho \left[x_{p2} \left(\ln \left(\frac{y_{p2} + \sqrt{x_{p2}^2 + y_{p2}^2}}{y_{p2} + \sqrt{x_{p2}^2 + y_{p2}^2 + z_p^2}} \right) - \ln \left(\frac{y_{p1} + \sqrt{x_{p2}^2 + y_{p1}^2}}{y_{p2} + \sqrt{x_{p2}^2 + y_{p1}^2 + z_p^2}} \right) \right) \right. \\
- x_{p1} \left(\ln \left(\frac{y_{p2} + \sqrt{x_{p1}^2 + y_{p2}^2}}{y_{p2} + \sqrt{x_{p1}^2 + y_{p2}^2 + z_p^2}} \right) - \ln \left(\frac{y_{p1} + \sqrt{x_{p1}^2 + y_{p1}^2}}{y_{p1} + \sqrt{x_{p1}^2 + y_{p1}^2 + z_p^2}} \right) \right) \\
+ y_{p2} \left(\ln \left(\frac{yx_{p2} + \sqrt{x_{p2}^2 + y_{p2}^2}}{x_{p2} + \sqrt{x_{p2}^2 + y_{p2}^2 + z_p^2}} \right) - \ln \left(\frac{x_{p1} + \sqrt{x_{p1}^2 + y_{p2}^2}}{x_{p1} + \sqrt{x_{p1}^2 + y_{p2}^2 + z_p^2}} \right) \right) \\
- y_{p1} \left(\ln \left(\frac{y_{p2} + \sqrt{x_{p1}^2 + y_{p2}^2}}{y_{p2} + \sqrt{x_{p1}^2 + y_{p2}^2 + z_p^2}} \right) - \ln \left(\frac{x_{p1} + \sqrt{x_{p1}^2 + y_{p1}^2}}{x_{p1} + \sqrt{x_{p1}^2 + y_{p1}^2 + z_p^2}} \right) \right) \\
+ z_p \left(\arcsin \left(\frac{y_{p2}^2 + h^2 + y_{p2} \sqrt{x_{p2}^2 + y_{p2}^2 + h^2}}{y_{p2} + \sqrt{x_{p2}^2 + y_{p2}^2 + h^2}} \sqrt{y_{p2}^2 + h^2} \right) \right. \\
- \arcsin \left(\frac{y_{p2}^2 + h^2 + y_{p2} \sqrt{y_{p2}^2 + h^2}}{y_{p2} + \sqrt{x_{p2}^2 + y_{p2}^2 + h^2}} \sqrt{y_{p2}^2 + h^2} \right) \\
- \arcsin \left(\frac{y_{p1}^2 + h^2 + y_{p1} \sqrt{x_{p2}^2 + y_{p1}^2 + h^2}}{y_{p1} + \sqrt{x_{p2}^2 + y_{p1}^2 + h^2}} \sqrt{y_{p1}^2 + h^2} \right) \\
\left. \left. + \arcsin \left(\frac{y_{p1}^2 + h^2 + y_{p1} \sqrt{x_{p2}^2 + y_{p1}^2 + h^2}}{y_{p1} + \sqrt{x_{p1}^2 + y_{p1}^2 + h^2}} \sqrt{y_{p1}^2 + h^2} \right) \right) \right]
\end{aligned}$$

Equation 2.15

where:

G is the gravitational constant

ρ is the density, and

$h = |z_p - z_0|$ with z_0 the height at the origin.

The equation for the prism method is compared to the Hammer prism method adapted from Hammer (1939), where the terrain correction for (x_p, y_p, h_p) is given by Equation 2.16.

$$g_{TC} = f\delta g(r_i, R_o, h, \rho)$$

Equation 2.16

where:

δ is the resolution of the DEM,

r_i is the inner radius of the Hammer zone,

h is the height above the origin.

R_o is the outer radius of the Hammer zone, and

f is a factor which corresponds to the ratio between the area of terrain and the area of the Hammer zone, shown in Equation 2.17.

$$f = \frac{\delta^2}{\pi(R_o^2 - r_i^2)}$$

Equation 2.17

The Hammer prism method concept is illustrated by Figure 2.16. Where the prism zone are approximated by the application of Hammer zones in a three dimensional space.

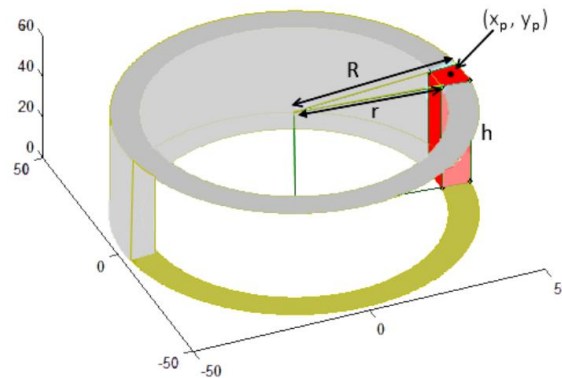


Figure 2.16: Illustration of the Hammer prism method (McCubbine, 2016)

As a consequence of its simpler formula, fewer computational steps are needed and the Hammer prism method is noted to return terrain corrections 10 times faster than the Nagy prism calculations (McCubbine, 2016). While, comparisons of the output terrain corrections show only negligible differences e.g. the difference in the near zone corrections had maximum difference of 0.014 mGal, while in the far zones the maximum difference was 0.023 mGal.

Therefore, the Hammer prism method is the preferable solution for generating the terrain corrections.

2.4.6. Complete Bouguer Model

The complete Bouguer model (g_B) is given by Equation 2.18. Assuming these corrections have accurately accounted for the variations in gravitational acceleration they are intended to account for, any remaining variations in the gravitational acceleration associated with the terrain corrected Bouguer gravity can be assumed to be caused by geologic structure.

$$g_B = g_\phi - 0.3086h + 2\pi G\rho h - g_{Tc}$$

Equation 2.18

where:

T_c is the value of the computed terrain correction.

2.5. Combination Considerations

In an effort to ensure that only similar datasets are being combined this section will address two problems. The first being at which stage of the gravity data reduction process should the datasets be combined i.e. as raw observations, free-air anomalies or complete Bouguer anomalies. The second being as to how to address the problem of downward continuation: the reduction of gravity observations observed above the Earth's surface, to the surface of the Earth.

2.5.1. Combination Data Type

Before we are able to combine the data we should consider at which stage of the gravity reduction process (Chapter 2.4) we should optimally combine the datasets. There are three practical stages where the dataset could be rationally combined: gravity observations, free-air gravity anomalies or Bouguer gravity anomalies. The three options are illustrated with the Canterbury terrestrial gravity dataset (c.f. Chapter 4.4.3) shown by Figure 2.17, Figure 2.18 and Figure 2.19.

The choice of data type to combine will be influenced by the requirement to combine the datasets on a homogenous surface.

The gravity observations are at 'observation elevation', in the case of the terrestrial data this is on the topography. However, airborne datasets flown at altitude can be several kilometres above the topography. This means that the high frequency effects of the airborne data are smoothed-out. Therefore, the terrestrial and airborne data sets do not contain the same frequency content and should not be combined at the observations level.

By definition the free-air correction adjusts the gravity observations to represent what the measurements would have been, had they been measured on the geoid. This means we are now comparing the datasets on the same surface. However, they are still under the influence of terrain. The free-air gravity anomalies contain high frequency effects of topography which can be aliased by sparse data sampling (Featherstone & Kirby, 2000).

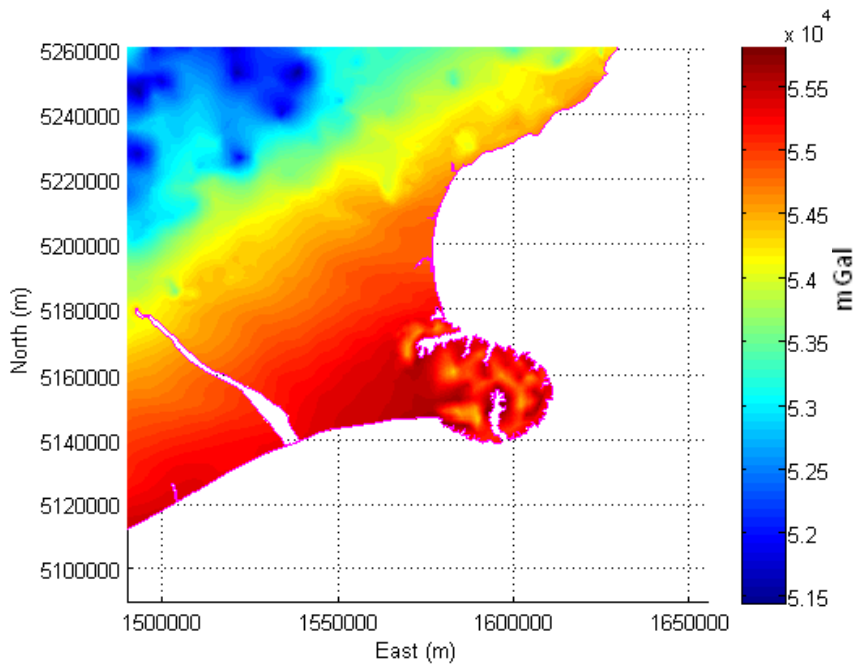


Figure 2.17: Gravity observations

Figure 2.18: Free-air gravity anomaly

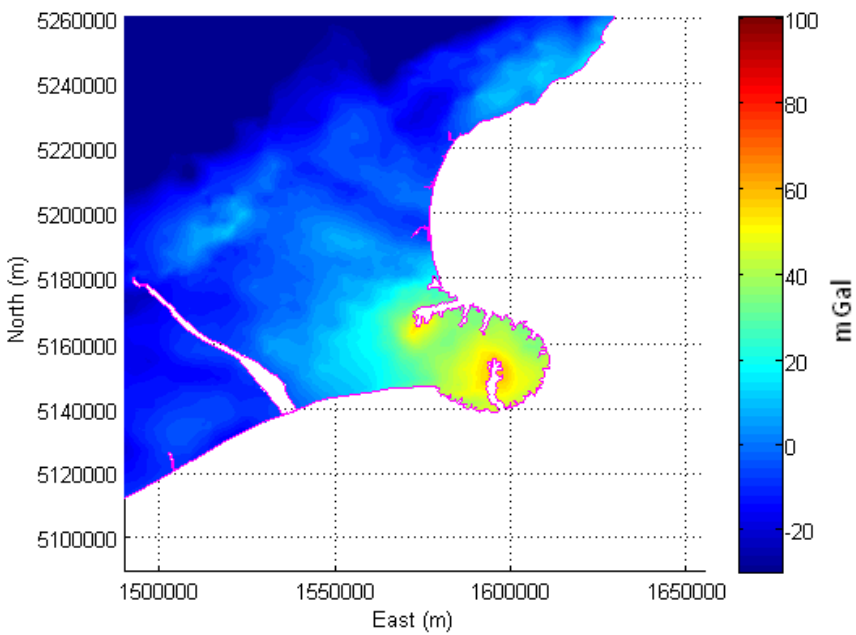
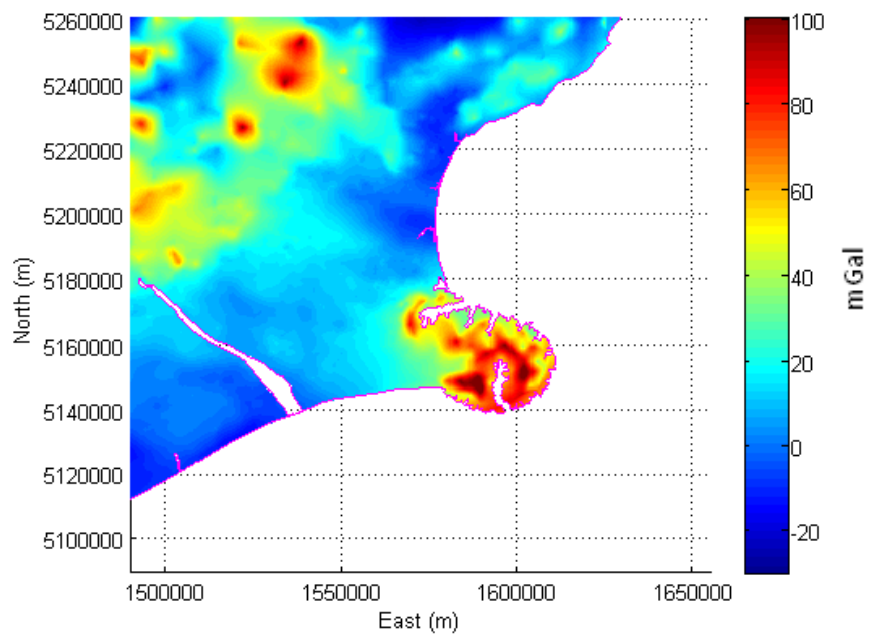


Figure 2.19: Bouguer gravity anomaly

For example, the New Zealand terrestrial gravity dataset, does not provide uniform coverage of the country, many of the observations are located along roadways, coastlines and along river valleys; the most accessible routes. However, since the topographic effect would be strongest where the topography is steepest, if only the readily accessible observations are used to compute the free-air signal, it would give the impression of significantly smoother topography. For this reason it is best to grid the Bouguer anomaly signal.

A Bouguer anomaly model has the effects of the terrain removed. This allows the integration of the data in a consistent manner. The effects of topography can easily be restored at a later stage to the gridded Bouguer anomaly using the DEM.

2.5.2. Downward Continuation

Gravity observations are effected by elevation, as the high frequency signals diminish with distance from a mass i.e. as the distance from the body increases the gravity profile flattens out. This is demonstrated by Figure 2.20, which illustrates how the gravity anomaly profile of a buried sphere varies with elevation (h).

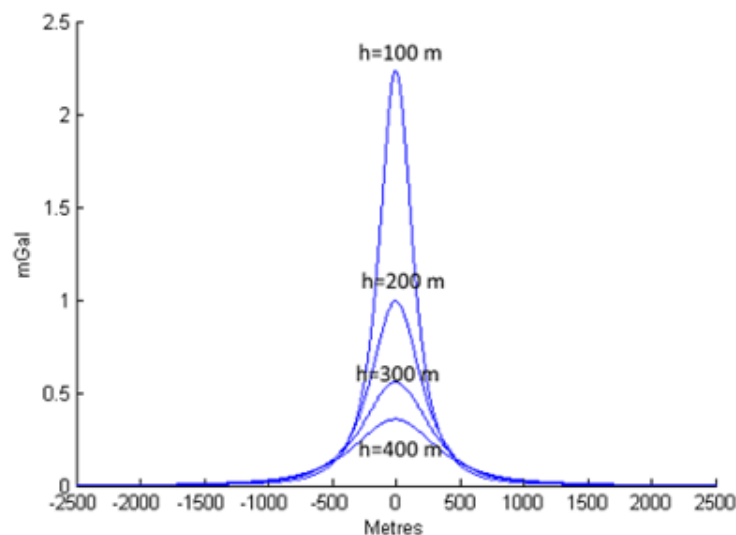


Figure 2.20: Diagram of gravity anomaly profile of a buried sphere (McCubbine, 2016)

The formulas for geoid determination require that the gravity anomalies are reduced to a common surface. Therefore, we must downward continue the airborne gravity data from flight altitude to the geoid (Wang, 1988), so that it is comparable to the other gravity datasets. Without a proper method of downward continuation data will contain false gravity signatures (Hsiao & Hwang, 2010).

However, it is well documented that downward continuation of airborne data is not a trivial task (Wang *et al*, 2013; Hwang *et al*, 2014). This section identifies three methods which have been used for the downward continuation of gravity datasets.

2.5.2.1. Remove-Restore Technique

The remove-restore technique is a proven method for combining of satellite data and a local gravity datasets (such as the terrestrial or airborne gravity data; Kern *et al*, 2003). The scenario is illustrated by Figure 2.21, where the local and satellite data are confined to their spectral range.

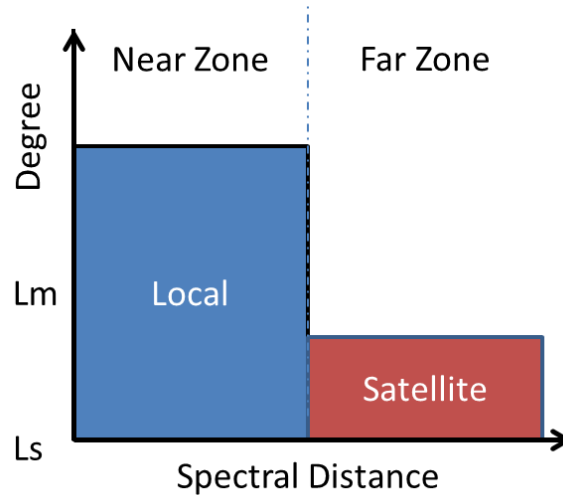


Figure 2.21: Diagram of data prior to remove-restore process

This is a three-step method documented in Rapp & Rummel (1975) and Forsberg & Tschering (1981). In the first step (Equation 2.19) the local gravity (AT) is reduced by satellite model (AT^s) and the topographic and atmospheric effects $A\delta V^H$ are removed. The result (AT') is the residual gravity.

$$AT' = AT - AT^s - A\delta V^H$$

Equation 2.19

In the second step the residual observable (AT') is mapped to the output function ($B\hat{T}'$).

Finally, as shown in Equation 2.20, the removed components are restored ($B\hat{T}$), by adding back the low frequency satellite data (BT^s) and the topographic and atmospheric effects $B\delta V^H$.

$$B\hat{T} = B\hat{T}' + BT^s + B\delta V^H$$

Equation 2.20

This last step is illustrated in Figure 2.22, where the low order terms of the local data have now been enhanced with the satellite observations.

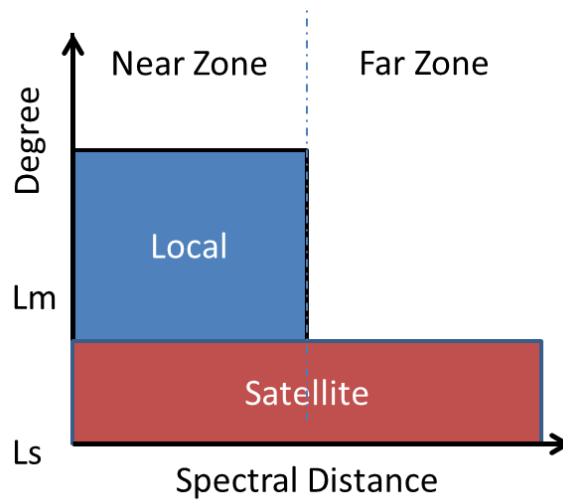


Figure 2.22: Diagram of data after the remove-restore process

However, this method has a number of limitations. Firstly, the errors from the satellite or local data tend to 'leak' across bands and into the final solution. Secondly the remove-restore technique does not provide quality indicators. However, most importantly, while this solution works well with only two datasets, with multiple local gravity datasets an over-determined situation arises and this cannot be handled directly by the remove-restore technique (Kern *et al*, 2003).

2.5.2.2. Inverse Poisson Method

The basic downward continuation method is the inverse Poisson method (Wang *et al*, 2004). The Poisson method was designed for the upward continuation of harmonic quantities, such as gravity anomalies (Forsberg *et al*, 2007), and is an unstable operation and only applies if flight altitude (h) is constant. The gravity anomalies at altitude ($F(\Delta g)$) are modelled by Equation 2.21:

$$F(\Delta g) = \Delta g(x, y) e^{-i(k_{xx} + k_{yy})} dx dy,$$

Equation 2.21

while gravity at the geoid ($F(\Delta g *)$) is modelled by Equation 2.22:

$$F(\Delta g *) = e^{kh} F(\Delta g),$$

Equation 2.22

where:

$$k = \sqrt{k_x^2 + k_y^2} \text{ and } k_x, k_y \text{ are wave numbers (E,N)}$$

Downward continuation enhances high frequencies. Therefore upward continuation, a high pass filtering operation, is require to remove the high frequency signal prior to downward continuation. For example, Figure 2.23 and Figure 2.24 represent the original dataset on the top and the downward continued dataset on the bottom.

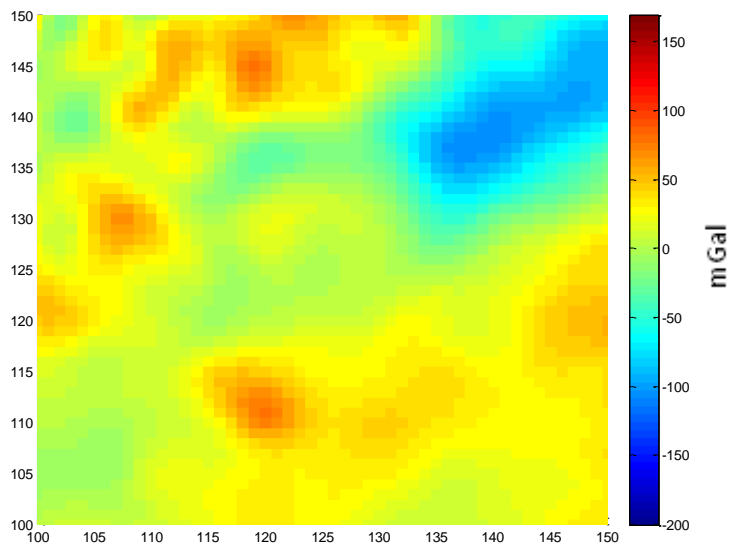


Figure 2.23: Original sample data

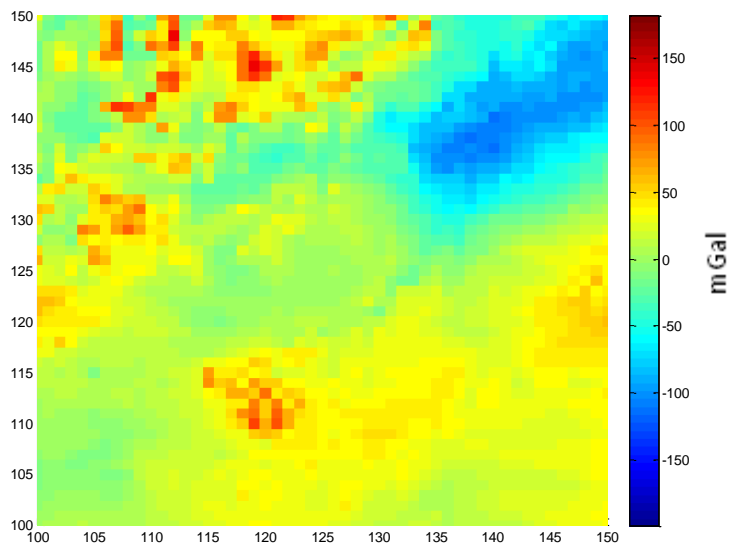


Figure 2.24: Downward continued sample data

The formula used for downward continuation is inherently unstable and requires low-pass filtering to obtain a stable solution (Kern *et al*, 2003). On the other hand, filtering can be equally as problematic as a significant part of the gravity signal is also filtered out (Bayoud & Sideris, 2003). The higher the continuation height and finer the data spacing the more severe the problem (Kern *et al*, 2003).

2.5.2.3. Least Squares Collocation

Least squares collocation is an integration method which will be considered in Chapter 3.4.3. One of the features of least squares collection is that with the correct choice of a co-variance function, it allows input variables to be estimated anywhere in a three-dimensional space and therefore is able to complete the downward continuation as part of the integration process (Barzaghi *et al*, 2009). This means that when using the least squares collocation integration method that prior downward continuation is not required.

The general procedure to downward continue the gravity data using least squares collocation is describe in McCubbine (2016), in seven steps:

1. Compute the Bouguer anomaly,
2. Calculate the long wavelength gravity anomaly for each observation,
3. Subtract the long wavelength signal from the Bouguer anomaly data,
4. Calculate the covariance of the residual gravity observations and the best fitting analytic logarithmic covariance model parameters,
5. Calculate the covariance matrix,
6. Calculate the desired signal, and
7. Restore the long wavelength gravity model.

2.6. Summary

Gravitation acceleration (g) on the surface of the Earth varies due to the non-uniform distribution of the Earth's mass. Due to the shape of the Earth, these variations are largely dependent on latitude. As one moves from the Equator to the poles the distance from the centre of the Earth decreases and accelerations due to the Coriolis Effect becomes less.

While the global gravity field is able to modelled, these models are often coarse. The variation between the observed and modelled gravity values are known as anomalies.

The gravity field can be observed by one of two basic methods: directly, using an absolute gravity meter or by using a relative meter to observe apparent changes between sites. Most absolute gravity meters use a type of interferometry, measuring acceleration with time and distance. In contrast relative meters are frequently dependant on observing the veritable length of a spring.

The gravity field observation techniques mentioned in this study are commonly referred to by their observation platform. That is terrestrial, ship-borne, airborne and satellite. These methods are summarised in Table 2.6.

	Terrestrial	Ship-Track	Airborne	Satellite
Topography:				
Land	✓		✓	
Shallow Coast			✓	
Harbours		✓	✓	
Open Ocean		✓		✓
Typical Instrumentation				
LaCoste and Romberg: <i>D</i> or <i>G</i> meter	✓			
LaCoste and Romberg: <i>S</i> meter		✓	✓	
Gradiometry				✓
Density:				
Uniform			✓	✓
Non-Uniform	✓	✓		
Elevation:				
On Topography	✓	✓		
Above Topography			✓	✓
Spectral Range:				
Long (>110 km)				✓
Medium (25-110 km)			✓	✓
Short (<25 km)	✓	✓		

Table 2.6: Summary of gravity dataset limitations

Each of the gravity observation methods observes separate parts of the Earth's gravity field at different resolutions. Ultimately, no one gravity dataset is able to provide a uniform, high resolution, mode which includes all of the wavebands alone.

In order for the datasets to be combined, they are first reduced to a complete Bouguer model. The dataset are then required to be on the same surface, this can be achieved either using downward continuation or by using a three-dimensional integration method, such as least squares collocation.

3. INTEGRATION

3.1. Introduction

It is a common goal of the Earth Sciences to map the entire Earth, seamlessly and to a high resolution (Monahan, 2008). Seamlessly means combining data using consistent vertical and horizontal datums and filling in the spaces between observed data points (interpolation).

Frequently this means integrating datasets which have a degree of disparity. For example they may have been collected at different resolutions, using different methodologies and/or over different scales or time periods. The method chosen to integrate these disparate datasets is largely dependent on the purpose of the final model and the properties of the data being combined.

A number of studies have investigated the combination of satellite, terrestrial and/or airborne gravity data (examples include: van Loon & Kusche, 2007; Tscherning *et al*, 1998; and Featherstone *et al*, 1998). However, these studies only combine two data sources. Less attention has been given to the combination of more than two measurement types.

This study identifies the integration process in four steps:

1. **Purpose:** Determining the use of the model; which properties we wish our model to display.
2. **Data:** Identify each dataset; understand the datasets characteristics, remove gross errors and estimate the remaining uncertainties.
3. **Combination:** Identify the range of combination methodologies available, including their strengths, limitations and suitability in relation to the datasets.
4. **Assessment:** ensuring that the final output model dataset has met the requirements.

This section defines each of these steps in the integration process in relation to the combination of various gravity datasets.

3.2. Step One: Purpose

The purpose of this integration is to produce a single map of the gravity field, which could be used for geoid modelling. Modern geoid determination requires a map of the gravity field which covers the full gravity field spectrum (Triarahmadhana & Heliani, 2014). This includes combining three components:

- Short Wavelength data, <25 km (DEM, terrestrial, ship-borne)
- Medium wavelength 25-110 (airborne, satellite Altimetry)
- Long wavelength, >110km (satellite gravity; GGM)

One of the challenges when combining the different spatial resolutions, accuracies and altitudes, to form a single gravity grid, is that there are more data than required to reach a unique solution (Sacerdote & Sanso, 1984). However, as the multiple observation methods provide alternative information about the same parameters, the data are generally found to be inconsistent at some level, and some parametric information may not be in agreement (Schaffrin & Iz, 2002).

For example, in geodesy it is common to combine GNSS observations with precise levelling data: The horizontal components of survey grade (~1 cm) GNSS observation vectors are at least twice as accurate as the vertical component. In contrast, levelling observations provide a highly precise vertical observation (~ 1 mm), but the horizontal position is often scaled from a topographic map (~100 m; Schaffrin & Iz, 2002). This means that when combining these datasets more weight should be applied to the GNSS horizontal positions than the precise levelling horizontal position. However, the precise levelling heights should be weighted higher than the GNSS heights.

A well-integrated gravity dataset should combine data from the entire spectral range to form a single gravity map. In doing so we encounter the over determined boundary value problem: the case where there is an over specification of data (Payne & Schaefer, 1989) i.e. when combining the different spatial resolutions, accuracies and altitudes, to form a single gravity grid, is that there is more data than required to reach a unique solution (Sacerdote & Sanso, 1984). However, as the multiple observation methods provide alternative information about the same parameters, the data are generally found to be inconsistent at some level, and so some parametric information may not be in agreement (Schaffrin & Iz, 2002).

An optimal solution is expected to minimise the inconsistencies between the datasets or otherwise address the over determined boundary value problem.

3.3. Step Two: Data

We are only able to combine datasets which are similar. Similar means having properties which are of the same feature, scale and related to the same reference surface. However, similar does not mean that we are unable to combine different types of the same data. For example it is possible to combine terrestrial distance and bearing observations with GNSS vector data as they are both types of distance measurements.

In order to do this successfully we must first ensure that the data are similar. This involves assessing the accuracy and completeness of the metadata provided, performing transformations between datasets where required.

Second, we must determine the expected accuracy of the dataset. This involves understanding how the data were collected. This allows us to determine the limitations of the equipment and methodologies used. Based on the expected accuracy, the database can be checked for outliers (gross errors). An outlier may indicate a peculiarity in the sample or may indicate a blunder. Outliers should be resolved or removed (Osborne & Overbay 2004) from the dataset as they can unduly and significantly influence surrounding data points. Once the outliers are removed we can then identify and attend to any systematic errors (Filmer *et al*, 2014).

Finally, we use the results of this error analysis to compute *a priori* weights. This included the expected errors of the dataset. However, observations within a dataset can also be weighted.

This weighting can be binary i.e. 1 if the observation is used, zero if it is to be rejected. It could be complex with every observation within the dataset being assigned a weighted value based on their

individual stochastic properties. Or it could be grouped, with observations collected using different methodologies assigned similar weightings.

For example, when assessing a database with height observations, the expected accuracy may be 1 cm. The GNSS observations could be assigned a weight of 1, while, the levelling observations may be assigned a weight such as: 10 (or a value higher than 1) reflecting that we have more certainty in the levelling height values.

3.4. Step Three: Combination

During step three of the integration process the data selection of integration methods are test and the dataset are combined. Each of the integration methods are then assessed including their strengths, limitations and suitability in relation to the datasets, as the favourable method will depend on the characteristics of the data being integrated.

The result will be a set of models, one for each integration technique, supported with dialogue as to the pros and cons of each method. Finally one method will be identified as the optimal data combination technique for the integration of heterogeneous gravity datasets. This section will identify the integration methods which will be considered for this study.

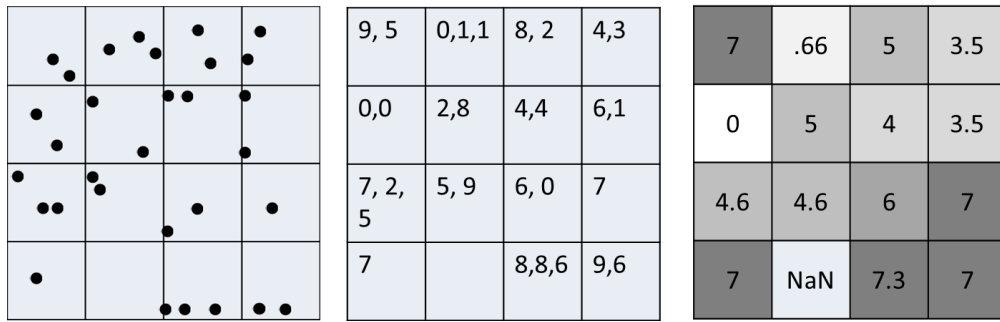
A number of integration methods have been identified in the literature (for example: Mortiz, 1978; Goovaerts, 1997; and Ligas & Kulczycki, 2010) as commonly used in the Earth Science to combine data, these are: Simple Gridding, Kriging and Least Squares.

As will be seen, there are multiple variations of the Kriging and Least Squares methods and many software that are suited to these interpolation methods. Therefore, a short list of methods used by various authors is presented. However, only Ordinary Kriging and Least Squares Collocation are considered for comparison as they are the most relevant variations of these methods for use with gravity datasets. Data processing and analysis will be completed using Matlab V14.a (mathworks.com).

3.4.1. Simple Gridding

The purpose of integration is to create a continuous surface from a sample of point values. At its most basic level *simple gridding* divides the observation area into regular sized grids or 'bins'. The observations which fall within each bin are then averaged to provide a value for a grid cell.

This is demonstrated in Figure 3.1, where in Figure 3.1 a) the 31 observations are divided in to a regular 4x4 grid. The observation values for each bin are determined in Figure 3.1 b). The final grid cell mean values calculated are coloured in Figure 3.1 c).



a) Location of observations points

b) Observation values, in each bin

c) Averaged observation per bin

Figure 3.1: A demonstration of the simple gridding technique

Most GIS (Geographic Information Systems) software packages (such as ArcGIS; www.arcgis.com, and QGIS; <http://www.qgis.org/>) and other graphical tools such as GMT (Generic Mapping Tools; <http://gmt.soest.hawaii.edu/>) and Matlab (<http://au.mathworks.com/products/matlab/>), have the ability to combine multiple files and interpolate all the data on to a single grid.

Once divided, each of these programs may have several averaging techniques or interpolation methods to determine an average for the bin.

For example, in GMT (Wessel *et al*, 2013) the arbitrarily located data point's observations point are used to create a regularly gridded output file by using the block averaging tools: Where the output position is either a mean (sum of all values in the grid, divided by the number of values in the grid): '*blockmean*', median (middle value of observations in the grid): '*blockmedian*' or mode (most common value in the grid): '*blockmode*'.

These regularly populated grids can then be transformed into a surface using functions such as 'surface' and 'nearneighbor'.

- 'surface' is a global method; this means that it is able to interpolate data beyond the observation values. In this function the user is able to select modifiers such as tension and curvature to control the smoothness of the output surface. An example of the 'surface' method is shown in Figure 3.2
- 'nearneighbor' (or nearest neighbour) is a local method; this means that it is only able to interpolate values within the area of interest and only provided values for the bins were observations exist. Bin value is a weighted mean of the nearest points from inside search radius. An example of the 'nearneighbor' method is shown in Figure 3.3.

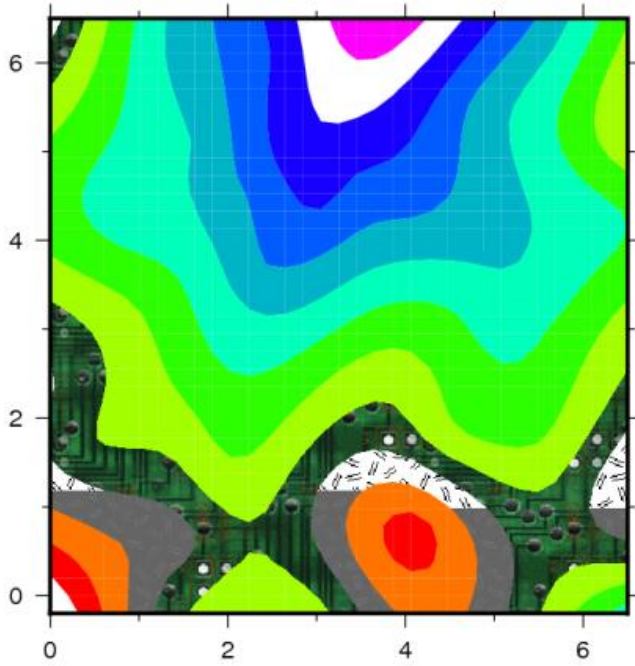


Figure 3.2: Example of GMT 'surface' interpolation method

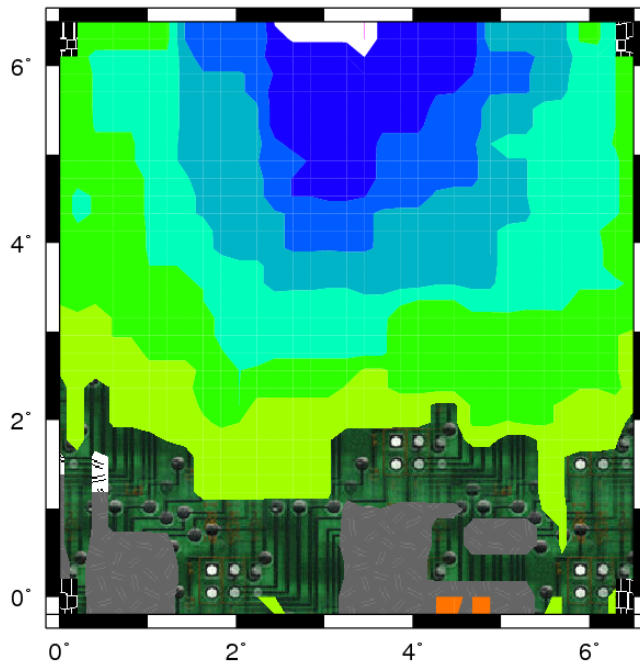


Figure 3.3: Example of GMT nearest neighbour 'nearneighbor' interpolation method

In Matlab the function *'griddata'* is used, to derive the regularly spaced bins. *'griddata'* interpolates a scattered sample of points to form a surface. The Matlab package includes five interpolations methods: Linear, Cubic interpolation, natural neighbour, nearest neighbour and bi-harmonic interpolation, where:

- Linear Interpolation ('linear'): Fits a linear polynomial between sets of three points for surfaces. See Figure 3.5 a).
- Cubic Interpolation ('cubic'): Fits a cubic polynomial between sets of three points for surfaces. This method can create extreme values along the edges of the dataset. Also, as this

method uses triangulation it is a local method, and creates null values outside of the dataset area. See Figure 3.5 b).

- Natural Neighbour Interpolation ('natural'): Sets a value based on a weighted method by a ratio of surrounding points. See Figure 3.5 c).
- Nearest Neighbour Interpolation ('nearest'): Sets the value of an interpolated point to the value of the nearest point. This method is better suited to non-continuous datasets. See Figure 3.5 d).
- Matlab (Bi-harmonic) Interpolation ('V4'): Sets the value of an interpolated point to the value of the nearest point. This is a computationally intensive method, as a full ' $N_{DATA} \times N_{DATA}$ ' matrix is created for all of the sample points. See Figure 3.5 e).

As the gravity datasets are continuous data and contain many thousands of observations over a large national/regional area. Natural neighbour is the most appropriate interpolation method for this investigation.

3.4.1.1. Natural Neighbour Gridding

The benefit of natural neighbour grids is that they are quick to determine than average value for a bin. The computation complexity is determined by the number of observations per bin and how to assign values to a bin with no observations (as seen in the bottom row of Figure 3.1 c). In Matlab these bins are assigned a NaN (Not a Number) value, which then must be defined by the user.

The limitations of the natural neighbour gridding method are that it does not take in to account the stochastic properties of each of the datasets such as their varying spatial distributions and error factors.

As illustrated in Figure 3.4, for example there may be many airborne observations (green dots) within a bin, but only a small number of terrestrial observations (purple dots). Thus using the simple gridding method, the average value of grid will be heavily influenced by the values of the airborne observations simply because there are more of them in the bin.

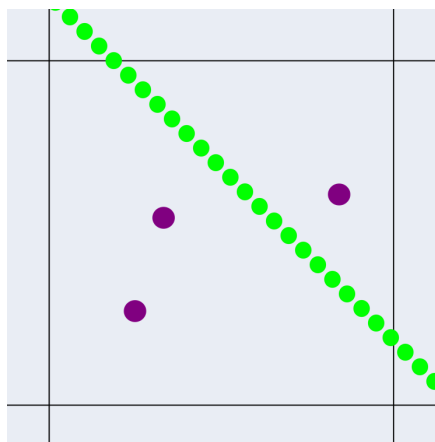


Figure 3.4: Illustration of multiple datasets combined using the natural neighbour method
Example airborne data (green) and terrestrial data (purple)

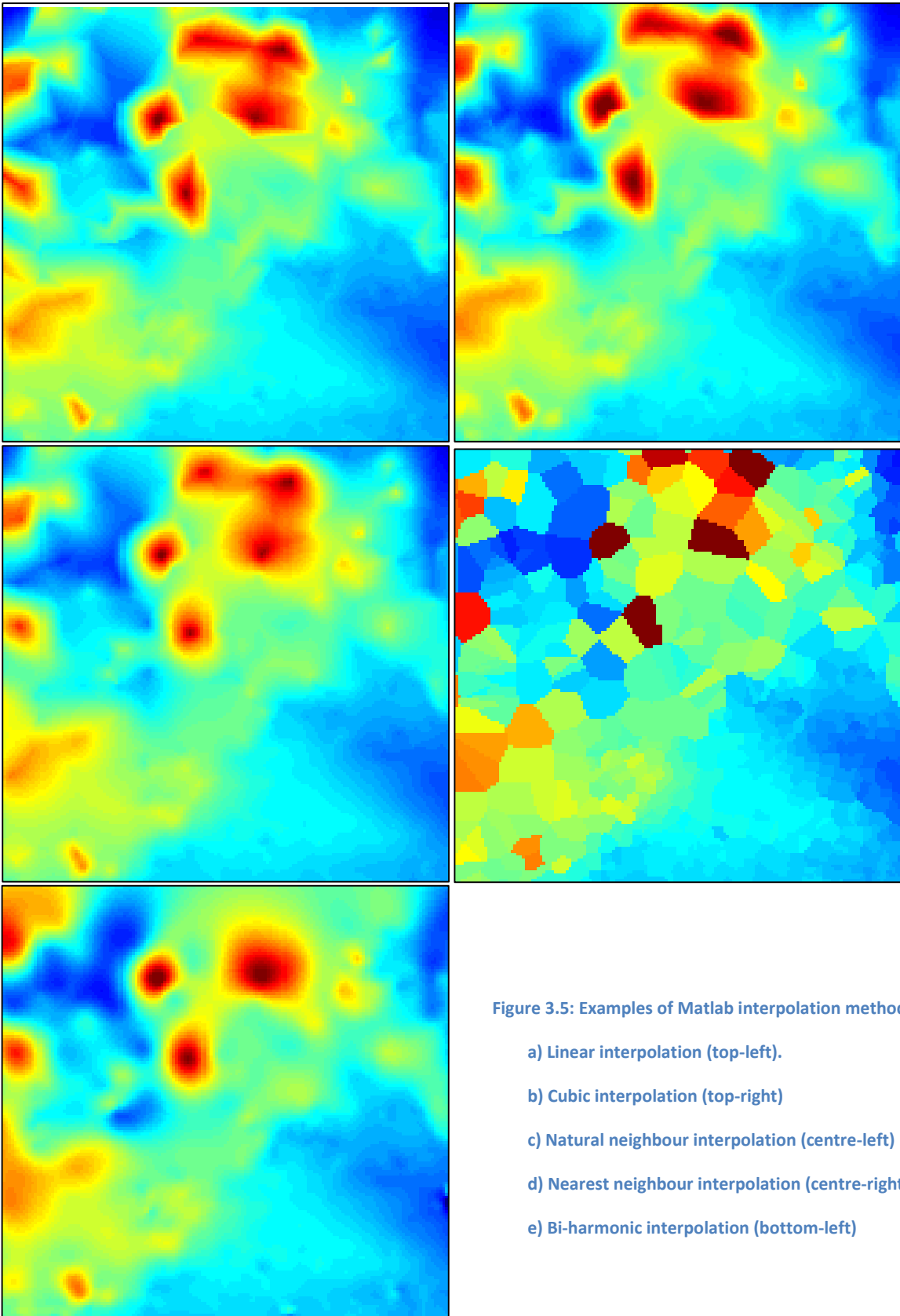


Figure 3.5: Examples of Matlab interpolation methods:

- a) Linear interpolation (top-left).
- b) Cubic interpolation (top-right)
- c) Natural neighbour interpolation (centre-left)
- d) Nearest neighbour interpolation (centre-right)
- e) Bi-harmonic interpolation (bottom-left)

In addition, the natural neighbour gridding method considers observations on a two-dimensional surface. This means that this method assumes that all the input data have been observed on, or reduced to a common, vertical reference surface.

3.4.2. Kriging

This method is used for the interpolation of observations (variables), which have a high degree of spatial correlation. The kriging approach requires a valid semi-variogram, a function which describes spatial correlation (dissimilarity between the points) model for the spatial process. The semi-variogram is described by Figure 3.6.

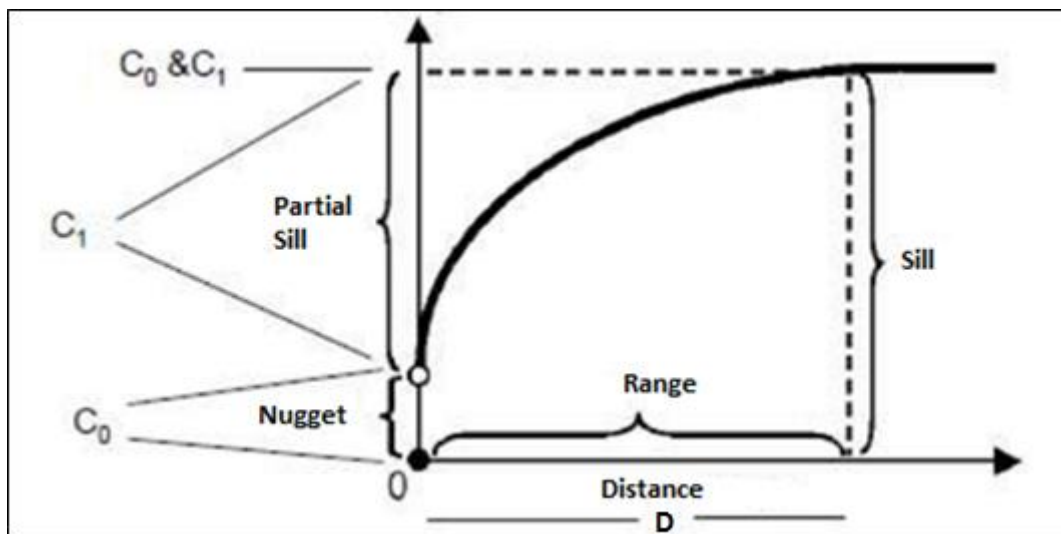


Figure 3.6: Illustration describing the components of the semi-variogram

where:

C_0 is the Nugget. This section represents the measurement error,
 D is the range. This is the distance at which the semi-variance level off. The range represents the spatially correlated portion of the semi-variogram, and
 C_0+C_1 is the sill: The portion over which levelling of the data takes place.

Kriging is exact interpolation method, meaning that the input data is preserved in the final model (Goovaerts, 1997), as long as the nugget value is zero.

The goal of which is to form a semi-variogram with minimal variance. Hence Ilie (2014) states that modelling the semi-variogram as the most difficult stage in kriging technique. This is because one must first select the appropriate theoretical model that will describe the variability of the observations with distance.

The outputs of the kriging method are the expected value and variance, computed for every point within a region. The variance provides an indication of the possible realisations which would agree with that data, based on the probabilistic behaviour of the field being observed.

Depending on the properties of the datasets being integrated, there are many different variations of the kriging method that can be used. For example, some common methods mentioned in literature (for example Ilie, 2014; Goovaerts, 1998; and Reguzzoni *et al*, 2005) are :

- **Simple Kriging** – This is the most mathematically straightforward form of kriging. However, it relies on the user knowing the *a priori* errors of the field being determined.
- **Ordinary Kriging** – forces primary data weights to a sum of ‘one’, which is an optimal predictor if the mean (over the entire area) is assumed constant.
- **Co-Kriging** – This is a variant of ordinary kriging. It calculates estimates for a poorly sampled variable, by comparing it directly with a highly correlated well sampled variable.
- **General Kriging** – Unification of least squares collocation and kriging, forcing a zero mean. Does not use point values, but rather values of linear functions of the unknown random field.

The alternative variations of the kriging method are summarised in Table 3.1. Ordinary kriging will be chosen for this study as there is only one variable to evaluate, the *a priori* errors are unknown so it is desirable to use a force mean and our data are point values, not linear functions. In addition, ordinary kriging is the most robust method and best preserves in the input data, by using an, unknown but constant mean.

	Simple Kriging	Ordinary Kriging	Co-Kriging	General Kriging
Forced Mean		✓	✓	✓
Single Variable	✓	✓		✓
Point Values	✓	✓	✓	

Table 3.1: Comparison of Kriging methods

3.4.2.1. Ordinary Kriging

Ordinary kriging is derived from geostatistics for surface modelling applications; as such it is the most commonly used variation of the kriging method (Webster & Oliver, 2007).

Ordinary Kriging uses an estimation algorithm (Equation 3.1), to predicted value of location ‘P’, where no observations have been made.

$$Z_p = \sum_{i=1}^n \lambda_i Z_i$$

Equation 3.1

where:

- Z_p is the predicted value at point P,
- Z_i are known values from in certain spatial locations, and
- λ_i are the corresponding weights for Z_i values.

Figure 3.7 demonstrates how the values of the surrounding points are used to predict the value of ‘P’.

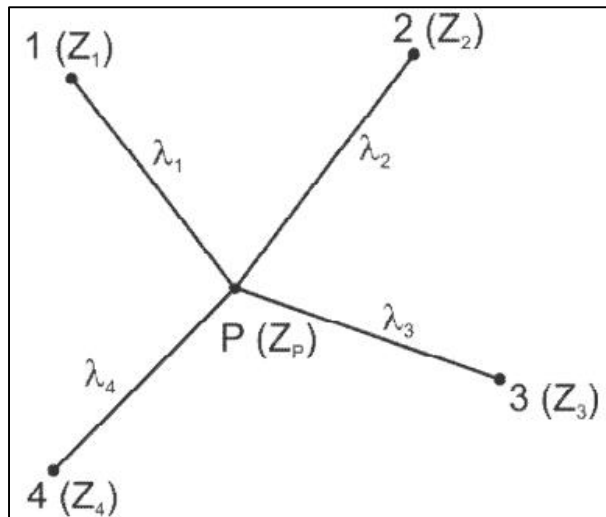


Figure 3.7: Conceptual diagram of the ordinary kriging process

Ordinary kriging uses an estimation algorithm to determine a value for Z_p using the weights from the observation points ($Z_1 Z_2 Z_3 Z_4 \dots$)

The benefit of the ordinary kriging method is that it uses the spatial correlation or dissimilarity between the points in order to derive a value. This value is able to be weighted according to the measurement method.

However, the limitation of the ordinary kriging method is that it preserves the values of the observation points. In addition, values are combined on a two-dimensional surface and this method is unable to be applied to observations which are at different reference elevations (Wackernagel 2003).

3.4.3. Least Squares

The concept behind least squares is to minimise the sum of the squared residuals between the data values. One of the components of the adjustment is a covariance model which describes similarity between the points. As shown in Figure 3.8 the covariance model used by least squares is the opposite the semi-variogram model used by the kriging method.

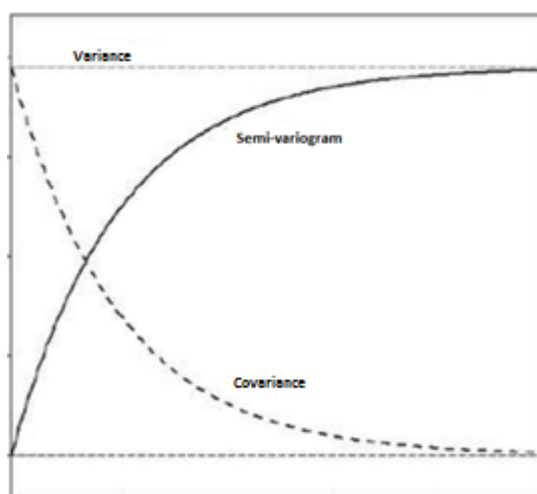


Figure 3.8: Illustration of the semi-variogram (kriging) and covariance (least squares) models

One of the features of the least squares method is that the modelled surface need not traverse all the sample points (kriging which must preserve the observation values or use the nugget values for the modelling of measurement errors, see Figure 3.6). However, this requires a balance between the interpolation accuracy and smoothness of the surface.

Depending on the properties of the datasets being integrated, there are two major variations of the Least Squares method that can be used. These are:

- **Least Squares Collocation** (Moritz, 1978; Krarup, 1969) - The method of least squares collocation may be used for the determination of approximations to the anomaly's gravity potential, and associated parameters such as biases or tilts. The method was developed in the 1960s based on the theoretical advancements of Kraup and Moritz (Tscherning, 2015).
- **Least Squares Spectral Combination** (Kern *et al*, 2003) - This is identified as an alternative method to classic least square collocation. This technique is applied in order to reduce long-wavelength distortions which may result from the use of Stokes formula, when combining terrestrial and global gravity data.

The Stokes formula is used in geodesy for geoid computations. One of the limitations of use of the Stokes formula in this study, is that it requires knowledge of Δg at every point on the geoid (Hofmann-Wellenhof & Moritz, 2006)

The advantage of least squares collocation is that it is able to combine observation data from a variety of sources. While, least squares spectral combination methods use the spherical harmonic part of the gravity field to provide, very accurate approximations for smooth solutions with relatively few degrees of freedom. The gravity datasets are observation based, therefore, least squares collocation will be chosen for this study.

3.4.3.1. Least Squares Collocation

Least squares collocation is an interpolation method derived within the geodetic sciences, for determining the Earth's shape (including gravitational field). Least squares collocation is a data processing method which simultaneously performs regression (determining a trended surface), filtering and spatial prediction (Hofmann-Wellenhof & Moritz, 2006).

The fundamental equation of least squares collocation is given in Equation 3.2. The signal \hat{s} is estimated by the three-dimensional position of the observations x .

$$\hat{s} = C_{sx}(C_{xx} + N_{co})^{-1}x$$

Equation 3.2

where:

- C_{sx} is the covariance matrix of the signal s and observations x ,
- C_{xx} is the covariance matrix of the observations, and
- N_{co} is the covariance matrix of the observation noise.

As shown in Figure 3.9, the least squares collocation method assumes that measurements consist of two components: a systematic component (trend surface) and a random component composed of *signal* (determined by local factors) and *noise* (caused by measurement errors).

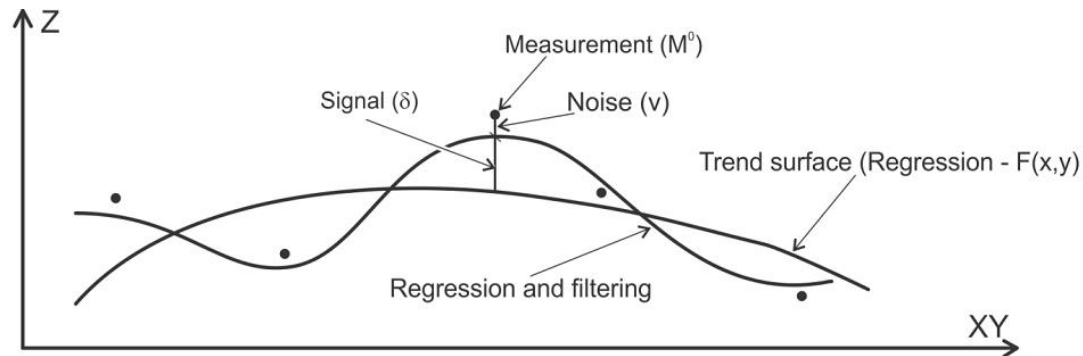


Figure 3.9: Graphical representation of the least squares collocation method (Ilie, 2014)

The major advantage of least squares collocation is that surface points do not have to pass through the observation values. This means that input observations do not need to be on the same vertical reference surface.

The principal drawback of least squares collocation is that in the observation spectra non-stationary noise leads to an approximate solution for the noise (Kern *et al*, 2003).

3.5. Step Four: Assessment

Once a favoured technique has been identified it will be assessed to ensure that it provides the outcomes identified in step one of this process. This means ensuring that the final model provides the best method to combine gravity data to create a single gravity map, which could be used for geoid modelling.

The final model will be assessed using two methods. The first method is to compare the output model to existing gravity models and/or models created using the other two observation techniques. This demonstrates where there are changes between the datasets. These differences are then able to be evaluated and confirmed as either variations or errors in the final model.

The second method is to test the fit of the final model i.e. that it is not biased by outlying data points. As the model uses all the available data in its computation, this will be tested using cross validation, a method where by a sample of the dataset is removed and the model recomputed – this process being repeated numerous times. The values of the missing points and those from the model are then compared to compute a residual for the final model.

For example, cross validation method was used by Featherstone & Sproule (2006) in order to model the separation between the Australian Height Datum (AHD) and Geodetic Reference System 1980 (GRS80) ellipsoid. Each point was individually removed from the model and the combined model was assessed. This was repeated for all 254 points in the dataset and provided useful error estimate of the data.

3.6. Summary

This Chapter has introduced the four-step integration process: Purpose, Data, Combination and Assessment. Each of these steps is required to ensure that an optional integration method is selected.

This study has identified three integration methods to be assessed: natural neighbour gridding, ordinary kriging and least squares collocation. A brief summary of these methods is illustrated by Table 3.2.

	Natural Neighbour Gridding	Ordinary Kriging	Least Squares Collocation
Multiple datasets	✓	✓	✓
<i>a priori</i> weights		✓	✓
Exact interpolation method	✓	✓	
3-D observations			✓

Table 3.2: Summary of integration techniques

Each of the three methods is able to be used to combine multiple datasets.

Natural neighbour gridding is the least computationally intensive method, merging datasets on a two-dimensional surface, with little regard to error weights.

The limitation here is that ordinary kriging points must then be represented on the same elevation surface. When combining airborne heights from flight altitude they must be first downward continued to a common surface.

However, the other two techniques least squares collocation and ordinary kriging, are better suited and weighted datasets. Simply speaking, the difference between the two methods is that Kriging interpolation passes through all the points in the dataset, while the least squares collocation method does not have to. This results in the least squares collocation surface being smoother.

4. CASE STUDY: Canterbury, New Zealand

4.1. Introduction

In this Chapter the four-step integration process: Purpose, Data, Combination and Assessment (identified in Chapter 3), will be used to combine the gravity datasets across Canterbury, New Zealand.

4.2. The Canterbury Test Area

The Canterbury region was chosen for this case study due to the availability of existing gravity datasets, including a local airborne gravity dataset (Winefield et al, 2014). This will allow the examination of the integration process, using authentic gravity datasets.

The Canterbury test area covers a region of approximately 30,000 km², located in the central South Island of New Zealand and includes the city of Christchurch (New Zealand's third largest city). The extent of the test area is defined in Table 4.1 and is represented by the area within the white box shown in Figure 4.1.

Northing	5,090,000 m	5,260,000 m
Easting	1,490,000 m	1,655,000 m

Table 4.1: Extent of the Canterbury Test Area
Projection: New Zealand Transverse Mercator 2000 (NZTM2000)



Figure 4.1: Location of the Canterbury test area, New Zealand
Indicated by area within the white box

This area contains a number of features of interest including the Canterbury Plains and foothills of the Southern Alps, Lake Ellesmere, the Banks Peninsular, shallow coastal areas and deeper areas offshore. The large part of the area (the Canterbury Plains), is formed by abandoned braided river and flood plains. This means it has vast resources of alluvial greywacke-aggregate, formed in the Southern Alps (Forsyth *et al*, 2008).

While most of the area is low and flat (less than 100 m above sea-level), the Banks Peninsular is more mountainous. It was formed by two large overlapping extinct volcanoes (Akaroa and Lyttelton), creating two natural harbours. This area's highest point is Mt Herbert (919 m) with several other peaks reaching higher than 800 m.

Winefield *et al* (2014) explain that the selection of this region for the local airborne gravity survey was due to the dense coverage terrestrial gravity and GPS-levelling networks in this area. This would provide ground truthing for the airborne gravity survey, which then could be used to test the proof of concept prior to a national airborne gravity campaign.

It is noted that the Canterbury region has been subject to a number of significant earthquakes since 2010 (Bannister & Gledhill, 2012). In areas close to waterways, height changes in the order of 1 metre have occurred, due to the effects of slumping and liquefaction. This means that the terrestrial gravity data; collected before the earthquakes and airborne gravity data; collected after the earthquakes are not measured in terms of the same ground surface. While acknowledged as a source of potential uncertainty, this study does not attempt to restore the terrestrial height for the earthquake effects.

However, this study notes that the case study area covers a region which is far from typical in terms of the density of the existing terrestrial gravity infrastructure across New Zealand in general. Much of the country is covered in much sparser networks, particularly across Fiordland; in the south of the South Island, and other hard to access regions. Therefore the conclusions from this case study may not be considered an optimal scenario for a national airborne gravity campaign the remainder of the country.

4.3. Integration Step One: Purpose

Determining the use of the model; which properties we wish our model to display.

As discussed in Chapter 2, there is no one gravity observation method which is able to capture the entire spectrum of the Earth's gravity field, in a manner that is uniform and of a resolution high enough for the regional modelling of the geoid.

For example, global gravity models provide a uniform long wavelength determination of the entire Earth's gravity field. However, due to the attenuation of the gravity signal with altitude, short wavelength features are best resolved at surface level. This means that for geological features in excess of 20 km to be resolvable, terrestrial gravity observations would be required at a global spacing of 5-10 km (Seigel, 1995).

The practical limitations of creating a uniform global short wavelength gravity dataset are prohibitive. This is because, some countries do not maintain their own terrestrial gravity networks or their gravity data are protected by commercial or military purposes. There also remain large gaps in coastal or estuarial regions.

Therefore, it is desirable to combine all the available datasets in order to obtain the best approximation of the entire gravity signal and form a map of the gravity field. However, as each of the gravity datasets possesses a degree of dissimilarity to the others, the simple combination of the datasets may not be straightforward. Therefore, this case study will evaluate integration methods, identified in Chapter 3, in order to determine an optimal method of integrating the heterogeneous gravity datasets.

The final product will be a single combined Bouguer gravity map of the case study area, produced using the method identified as the best method to integrate the datasets.

4.4. Integration Step Two: Data

Understand the datasets characteristics, remove gross errors and estimate the remaining uncertainties.

The data used in this case study includes five gravity datasets: terrestrial, ship-borne, airborne, satellite altimetry and a GGM. Plots of these datasets are available in Appendix A. This section describes each of these datasets, outlining their selection and measures taken to reduce and/or estimate their errors. This includes checking the metadata to ensure that the datasets are similar (i.e. are of the same scale and reference surface) and are therefore able to be combined.

All data used in this case study are existing data sets, either freely-available or used under-licence; no additional data were collected.

4.4.1. Terrestrial Gravity

From the New Zealand terrestrial gravity database (Chapter 2.3.1) 2,574 of the stations are contained within the Canterbury test area. The locations of these stations are shown in Figure 4.2.

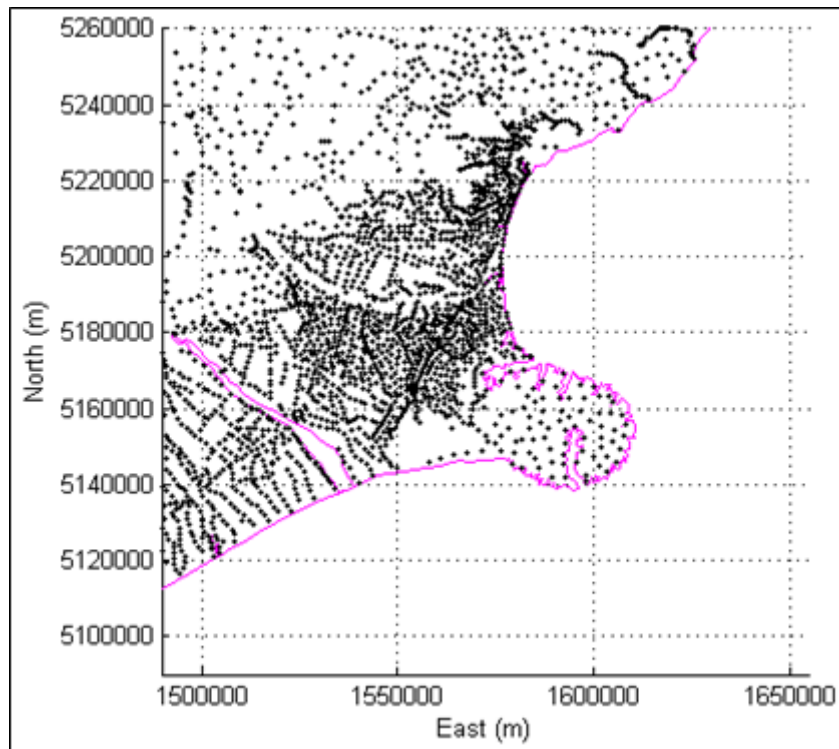


Figure 4.2: Location of terrestrial gravity stations within the Canterbury test area

The metadata for this dataset are provided in Stagpoole (2012) and summarised in Table 4.2. However, as discussed in more detail below, the supplied latitude and longitude metadata have been recorded incorrectly and should read New Zealand Geodetic Datum 1949 (NZGD1949).

Spreadsheet	Metadata
NZMG (X,Y)	New Zealand Map Grid
Latitude, Longitude	(WGS84) in decimal degrees
NZTM (E,N)	New Zealand Transverse Mercator

Table 4.2: Metadata for terrestrial gravity database, as supplied (Stagpoole, 2012)

4.4.1.1. Metadata Assessment - Horizontal

On receipt of the terrestrial gravity database, the data were imported to a GIS, for visualisation. As an exercise, the data was imported for the two projections and one set of geodetic coordinates in terms of the WGS84 ellipsoid, listed in Table 4.2.

Figure 4.3 shows the output coordinate position for terrestrial gravity Station 39/ Sheet 21, located in Riccarton, Christchurch. However, as illustrated there is an inconsistency with the coordinate information. The NZTM2000 and New Zealand Map Grid (NZMG) coordinates are coincident and are represented by the cyan circle, while the reportedly World Geodetic System 1984 (WGS84) coordinate, shown by the yellow circle, has been located approximately 200 m to the south.



Figure 4.3: Visualisation of the coordinates for the terrestrial gravity mark: Station 39/Sheet 21 NZTM/NZMG: cyan circle and the incorrectly identified projection: yellow circle

The WGS84 reference ellipsoid is essentially the same as the GRS80 ellipsoid used by NZGD2000. As shown in Table 4.3 the only variations between the two are due to a small difference between the flattening terms that is insignificant at the Earth's surface, and a different origin at the centre of the Earth's mass. This means that for most practical purposes (Grant *et al*, 1999) NZGD2000 and WGS84 coordinates can be considered the same and no transformation is required.

Ellipsoid	Semi-major Axis (m)	Inverse Flattening
GRS80	6,378,137	298.257 222 101
WGS84	6,378,137	298.257 223 563
International 1924	6 378 388	297

Table 4.3: Parameters of ellipsoids most commonly used in New Zealand

However, NZGD1949 was based on the International 1924 ellipsoid. As seen in Table 4.3 the parameters of this ellipsoid are significantly different to those of GRS80. As a consequence the NZGD1949 latitudes and longitudes are offset approximately 200 m south from the equivalent NZGD2000 coordinates.

It is concluded the latitude and longitude values contained in the terrestrial gravity database, are not WGS84, but NZGD1949 geodetic coordinates. Therefore Table 4.2 should be replaced by Table 4.4 below.

Spreadsheet	Metadata
NZMG (X,Y)	New Zealand Map Grid
Latitude, Longitude	New Zealand Geodetic Datum 1949
NZTM (E,N)	New Zealand Transverse Mercator 2000

Table 4.4: Metadata for terrestrial gravity database, corrected

4.4.1.2. Metadata Assessment - Vertical

Terrestrial gravity heights have varying degrees of uncertainty and ambiguity. To begin, the metadata for the terrestrial gravity database provided heights, recorded in metres to the nearest 0.1 m. However, the datum of these observations is not stated.

The metadata provide limited information as to how the height was determined, and three measurement methods (shown in Table 4.5) have been distinguished.

Database Code	Height Type
0	Benchmark, survey point, DGPS
1	Spot height, GPS
2	Barometric levelling

Table 4.5: Terrestrial gravity database height determination methods

On inspection of the data we find that, for example, Station 35/Sheet 27, positioned on the coastline has a recorded height of 0.6m (Database Code: 1 height). According to LINZ (2005), the coastline on a LINZ topo50 map represents the line of mean high water level (MHW). Contours represent the heights above mean sea level (MSL).

The observation of 0.6 m is indicative that this observation is a spot height, and is orthometric (in terms of the local vertical datum). Therefore it is assumed that all heights in the database are orthometric.

4.4.1.3. Positional uncertainties

One of the data integrity checks suggested by Stagpoole (2012) is to compare the recorded height of a gravity station in the database with the derived height of its coordinate computed from the DEM. Heights with a significant difference (plus or minus 10 m as this is the error margin of the vertical component of the DEM) indicate some level of uncertainty with the three-dimensional position of the observation. This analysis is unable to identify if these uncertainties are due to an error of station heighting, horizontal positioning or an incorrect height reading from the DEM. However, as an uncertainty in the vertical component of ~ 10 m, equates to an uncertainty in the gravity anomaly of ~ 3 mGal it is desirable to identify the stations beyond this limit.

Figure 4.4 shows the results of comparison between the full terrestrial gravity database (40667 observations) and DEM heights using a cumulative distribution function (CDF) plot. This plot demonstrates the dataset is leptokurtic beyond the 95% confidence intervals.

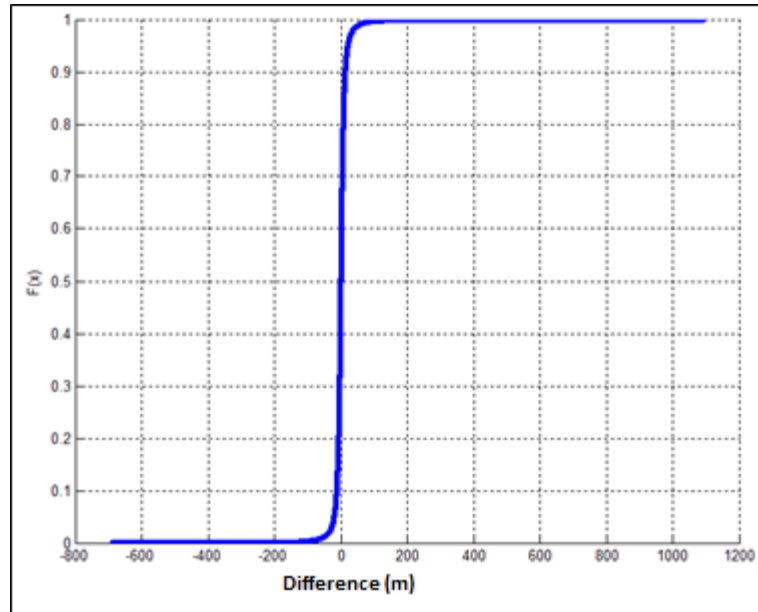


Figure 4.4: CDF plot of differences between terrestrial database and DEM heights

Of the 2,574 stations in the Canterbury test area, the 66 gravity stations identified as being beyond the 95% confidence interval are now weighted to zero, (effectively removing them from the dataset). The locations of these stations are shown by a red 'x' in Figure 4.5. While the remaining 2,508 observation from the Canterbury test area, have been assigned a weighting of one. The locations of these stations are shown by a blue '+' in Figure 4.6.

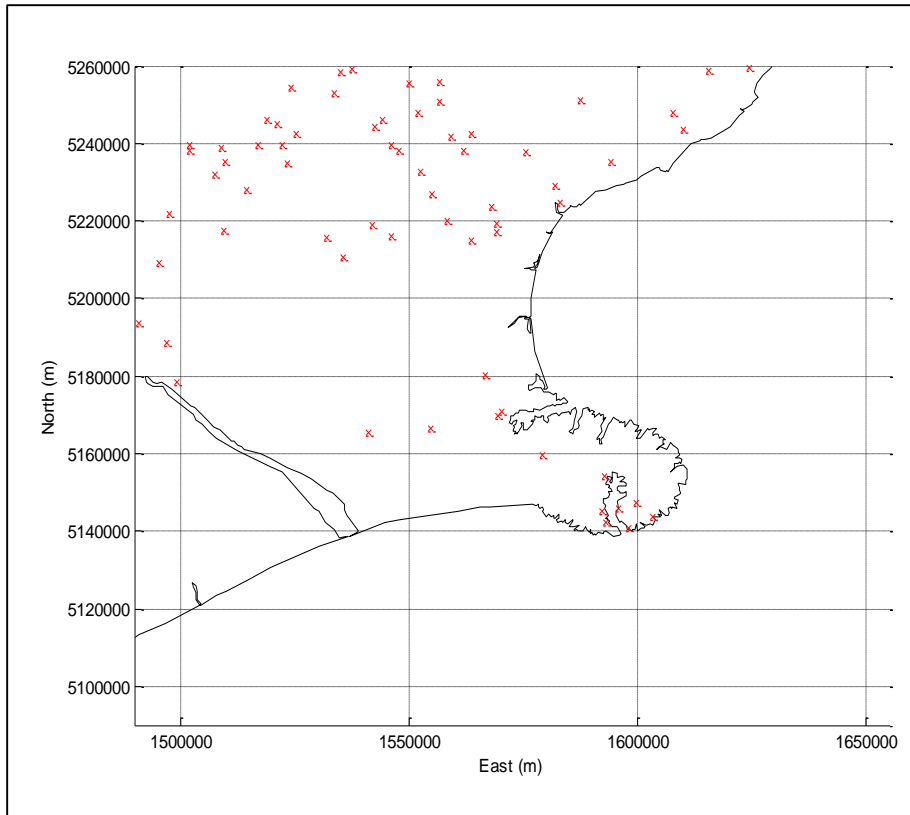


Figure 4.6: Terrestrial gravity stations identified beyond the 95% confidence interval (66)

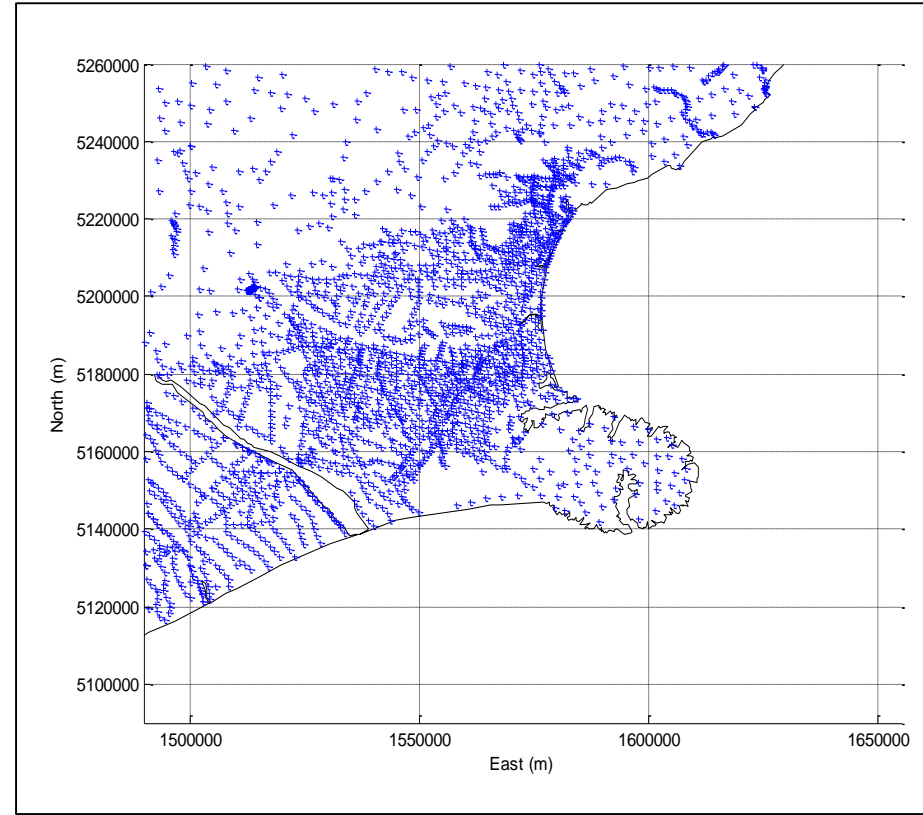


Figure 4.5: Terrestrial gravity stations identified within the 95% confidence interval 2508)

While this method of weighting reduces the density of the dataset, for the purposes of geoid modelling we wish to retain a station distribution of marks of ~5km is adequate. Within the Canterbury test area there is a sufficient density of marks that stations with height uncertainty beyond the 95% confidence interval can be excluded from the dataset, without significantly degrading the desired distribution target.

As a check, a surface constructed from the 95% terrestrial database was removed from a surface constructed from the airborne free air data. The resulting plot, Figure 4.7 identified three individual observations, listed in Table 4.6, which do not agree with the values of the surrounding stations.

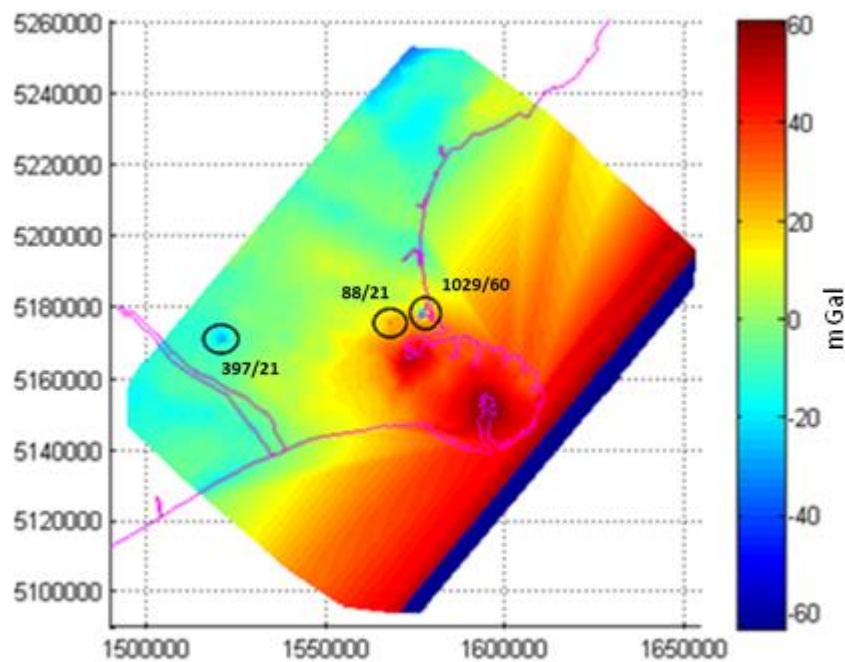


Figure 4.7: Plot showing the locations of the resulting three irregularities
Terrestrial Bouguer anomaly surface subtracted from the Airborne Free-air anomaly surface

It is assumed that observation 1029/60 has an incorrect sign (recorded as -28 mGal while the surrounding values are positive), while observations 397/21 and 88/21 disagree by a factor of 10 when compared to neighbouring observations (suggesting decimal point may be missing).

Station	Map Sheet	Assumed Error
1029	60	incorrect sign
397	21	disagree by a factor of 10
88	21	disagree by a factor of 10

Table 4.6: List of the resulting three irregularities
Terrestrial Bouguer anomaly surface subtracted from the Airborne Free-air anomaly surface

However, in lack of any additional evidence to confirm, or otherwise, that the above assumption are correct, these three observations shown in Table 4.6 were weighed zero. This leaves 2,505 observations in the terrestrial gravity dataset.

4.4.1.4. Estimating Uncertainties

In the sections above, a diagnostic test was used to identify outliers which were more than ± 10 m vertically and/or where the coordinate of the mark was insufficiently accurate to plot the true position. Those within the 95% confidence interval were weighted, while those beyond the confidence level were weighted zero, for all practical purposes removing their effects from any integration. This means that the remaining data have an uncertainty of up to ± 10 m vertically, equating to an uncertainty of 3 mGal in the gravity anomaly.

As described in Chapter 2.3.1 the majority of the New Zealand terrestrial database was collected using LaCoste and Romberg instruments such as the G-meter, which has an expected accuracy of 0.015 mGal.

Based on these two factors and allowance for systematic error throughout the observation, all remaining observations have been assigned an uncertainty of ± 3 mGal.

4.4.2. Ship-borne Gravity

There are 5,391 ship-track points contained within the Canterbury test area, as shown in Figure 4.8.

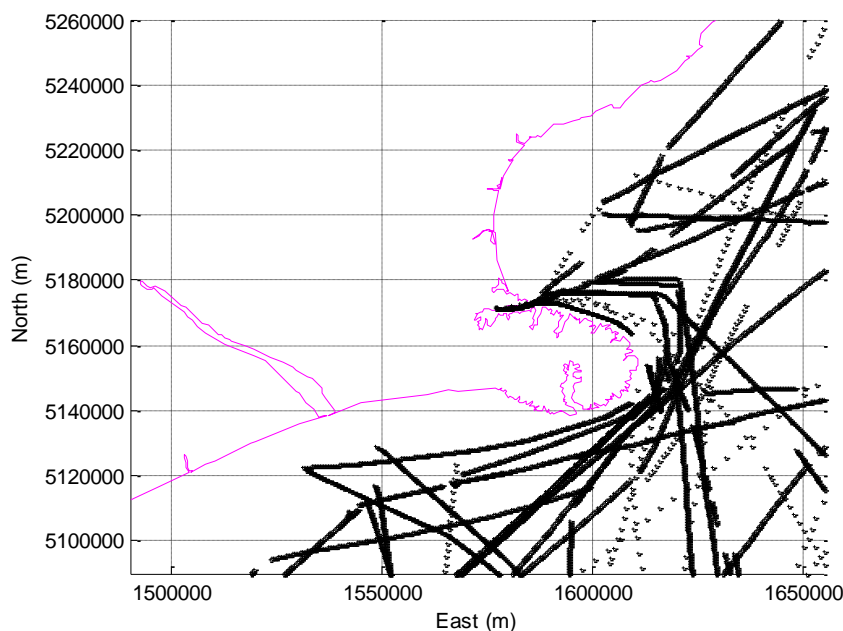


Figure 4.8: Location plot of the Canterbury test area ship-borne data tracks

These data were crossover-adjusted in 2003 (Brent, 2004) and as discussed in Chapter 2.3.2, this has resulted in a consistent dataset. No additional processing of the raw observations will therefore be required by this study.

4.4.2.1. Estimating Uncertainties

Ship-borne gravity data is prone to inconsistencies in positioning. In Chapter 2.3.2 it is identified that using a LaCoste and Romberg 'S' dynamic relativity gravity meter, and using GNSS positioning, that accuracies of ± 1 mGal are obtainable. However, much of the gravity survey data were collected prior to the advent of GPS, so the accuracy of the ship's positioning is harder to determine, as it is impacted by the measuring system and sea conditions. The most reliable technique for accessing the accuracy of the ship-borne data is by the analysis of the values at the crossover points (Wessel & Watts, 1998). As discussed, prior to the crossover adjustment, the standard deviation of the crossover error was ~ 2 mGal and this was reduced to ~ 0.3 mGal by the crossover adjustment.

However, while the crossover adjustment improved the consistency of the dataset, the adjustment was poorly constrained and therefore standard deviation after the adjustment does not necessarily reflect the accuracy of the data. The ship-borne dataset has therefore been assigned an uncertainty of ± 3 mGal to account for this.

4.4.3. Airborne Gravity

The Canterbury airborne gravity survey was completed over seven days, from 14-23 April 2012 (Winefield *et al*, 2014). The extent of the survey area is shown in Figure 4.9. The survey included twelve 150 km flight-lines (10 kilometres apart).

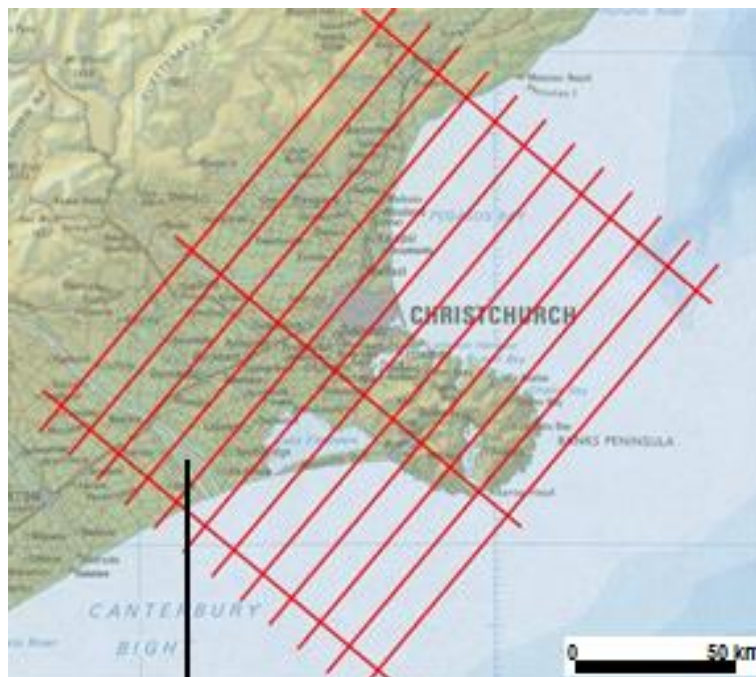
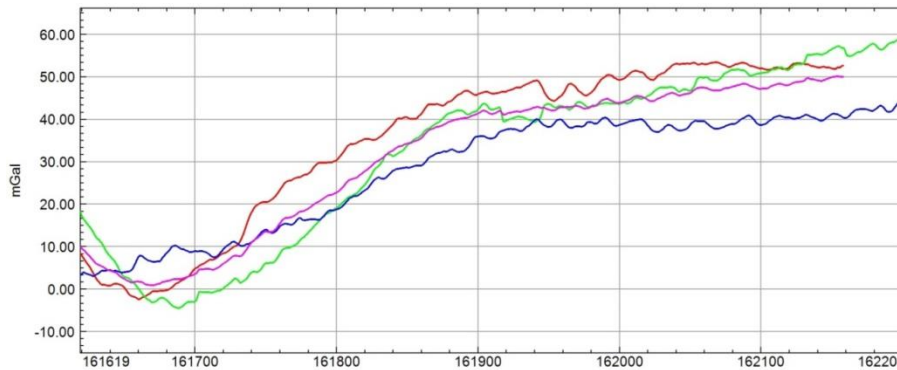


Figure 4.9: Extent of Canterbury airborne gravity survey, April 2012.
12 flight lines and 3 cross-ties are shown in red and a north-south calibration line is shown in black.
Projection: NZTM2000

To allow for the evaluation of the internal error estimate, two additional lines types were observed: three 100 km cross-ties and a north-south calibration line of 70 km. Figure 4.10 compares the free-air anomalies for the four times that the north-south calibration line was flown.



**Figure 4.10: Comparison of north-south calibration lines
Showing repeatability of 5 mGal with RTK GPS**

Using only the Real Time Kinematic (RTK) GPS data, a repeatability of ± 5 mGal was achieved. This was improved to better than 3 mGal with the introduction of post-processed GPS data.

The airborne gravity database is made up of 33,846 measurements. However, some observations were determined to have been taken prior to the stabilisation of the platform. Therefore, only 33,627 observations are usable for this study.

4.4.3.1. Aircraft Positioning

All flights within the Canterbury test area survey were flown using a Cessna 402B, Figure 4.11.



**Figure 4.11: Cessna 402B, used in airborne gravity survey
(Provided under contract by New Zealand Aerial Mapping)**

Each flight was prescribed to be flown at an altitude of 3,600 feet (~1,100 m), at a ground speed of 150 knots and to remain at a constant heading along each line. However, under normal operating

conditions these parameters are only approximate. Actual speed, altitude and direction of the aircraft vary due to wind gusts and flight movements: roll, pitch and yaw (demonstrated in Figure 4.12). The gravity meter is set up in the centre of the aircraft in an attempt to minimise the effects of the aircraft movement on the survey observations.

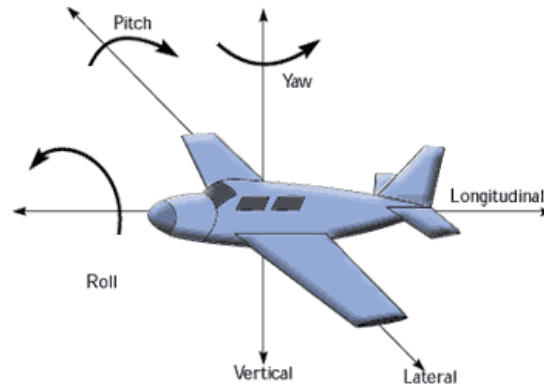


Figure 4.12: Aircraft rotations
Roll, pitch and yaw (source: www.novatel.com)

The aircraft altitude during the flight is established by using barometric pressure. The initial height is, therefore, only approximate and will be influenced as weather conditions change along the flight line. Throughout the flight the aircraft is subject to pitch, similar to the effect of waves on a ship, causing up to ± 10 m variation in altitude. Down or up-drafts can also influence the flight altitude by ± 20 m. In addition, the Civil Aviation Authority (CAA) requested flights directly over the international airport be flown at 7200ft (~ 2200 m). These flight and operational conditions result in different altitudes between observation points.

The actual position and altitude of the aircraft is tracked by GNSS. These coordinates are post-processed, using a method known as DGPS (Differential Global Positioning System) where the aircraft coordinates are reprocessed against known sites: the New Zealand CORS (Continuously Operating Reference Stations) PositionZ stations (<http://www.linz.govt.nz/data/geodetic-services/positionz>). Post-processing provides a recomputed the path of the aircraft during the flight, using carrier phase (C/A) data and expected accuracy of better than 1m.

4.4.3.2. Data Improvement

It is not the intention of this study to reprocess the airborne gravity data. However, the purpose of this section is to evaluate the airborne gravity, and identify where the observation quality could be improved and remove any gross errors.

Recovery of Bouguer Anomalies

The database as supplied by GNS Science does not provide Bouguer Anomalies, so these are computed using the complete Bouguer model as described in Chapter 2.4.6. A DEM is used to provide heights for the terrain beneath the survey, so that terrain corrections can be calculated (see Chapter 2.4.5. However, unlike the terrestrial data (h_{ground}) which is on the Earth's surface and is

influenced by the surrounding topography (which may be higher or lower than the gravity station), flight altitude is constantly above the topography (h_{air}), see Figure 4.13. This means that the terrain correction can be calculated in one step, without the need to compute the Bouguer slab corrections separately (McCubbine, 2016).

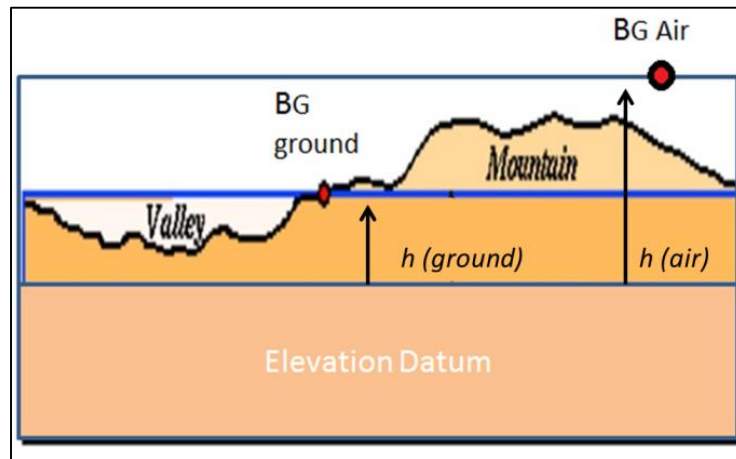


Figure 4.13: Flight altitude is constantly above the topography

Dipole Events

McCubbine (2016) identifies that at times during the national airborne gravity survey the meter is subjected to an acceleration which forces the spring to its maximum extent, and corrupts the signal as the meter over-compensates while it recovers. These events appear in the airborne Bouguer gravity signal as a dipole; the blue signal in Figure 4.14, as opposed to the smooth EGM2008 Bouguer gravity signal; shown in black .

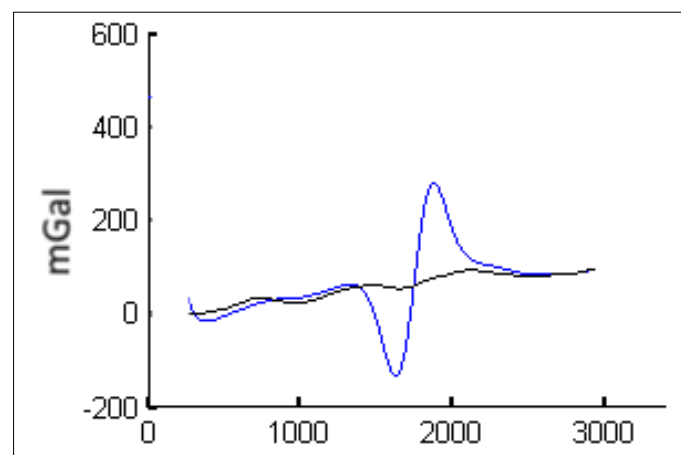


Figure 4.14: Example of a dipole in the airborne gravity signal
Blue: airborne gravity signal, Black: EGM2008 gravity signal

In the Bouguer gravity maps these are seen as gravity low, between two high spots (or *vice versa*).
On the western extent of

Figure 4.15 we see a feature which is a potential dipole, with a high-low-high-low in the signal.

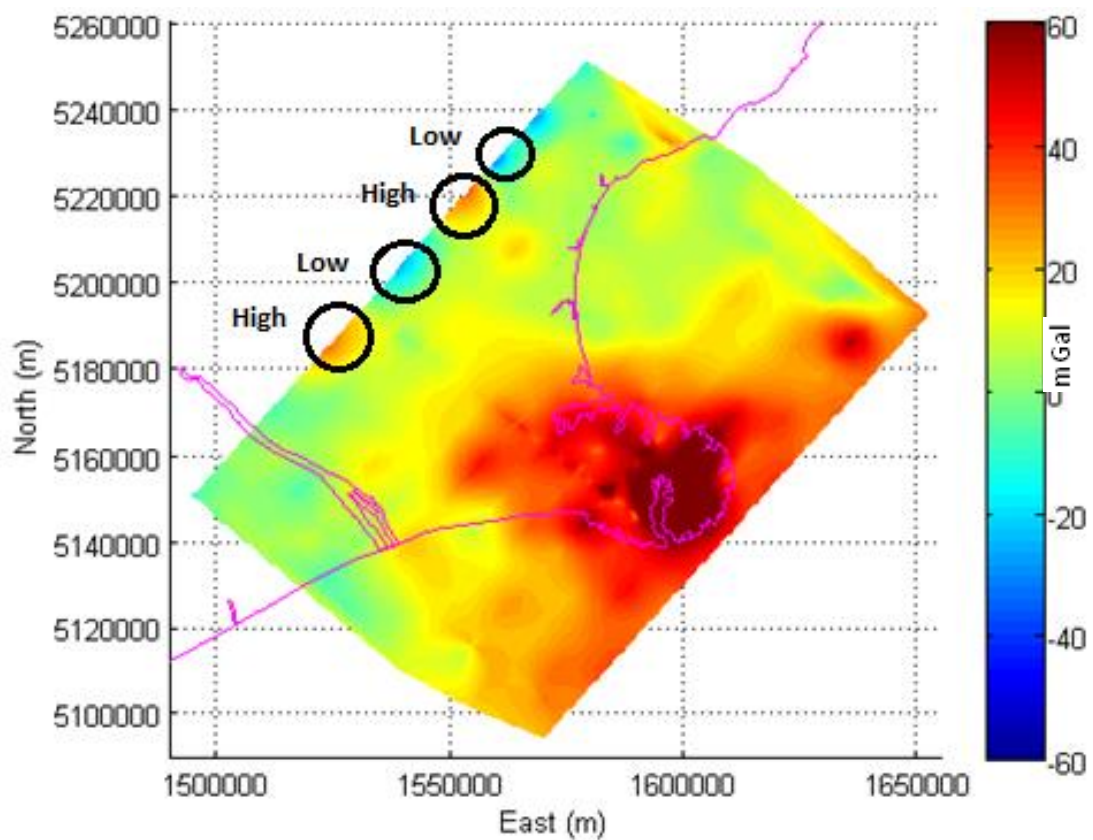


Figure 4.15: Airborne Bouguer anomaly map, with dipole event present

If 'repairing' flight lines for use in geoid modelling, one could set up procedures to splice out sections of the suspect data and replace it with track from the GGM (McCubbine, 2016). However, as this

event influences just one flight (line one), the entire flight-line was removed from the airborne gravity dataset for analysis (Figure 4.16).

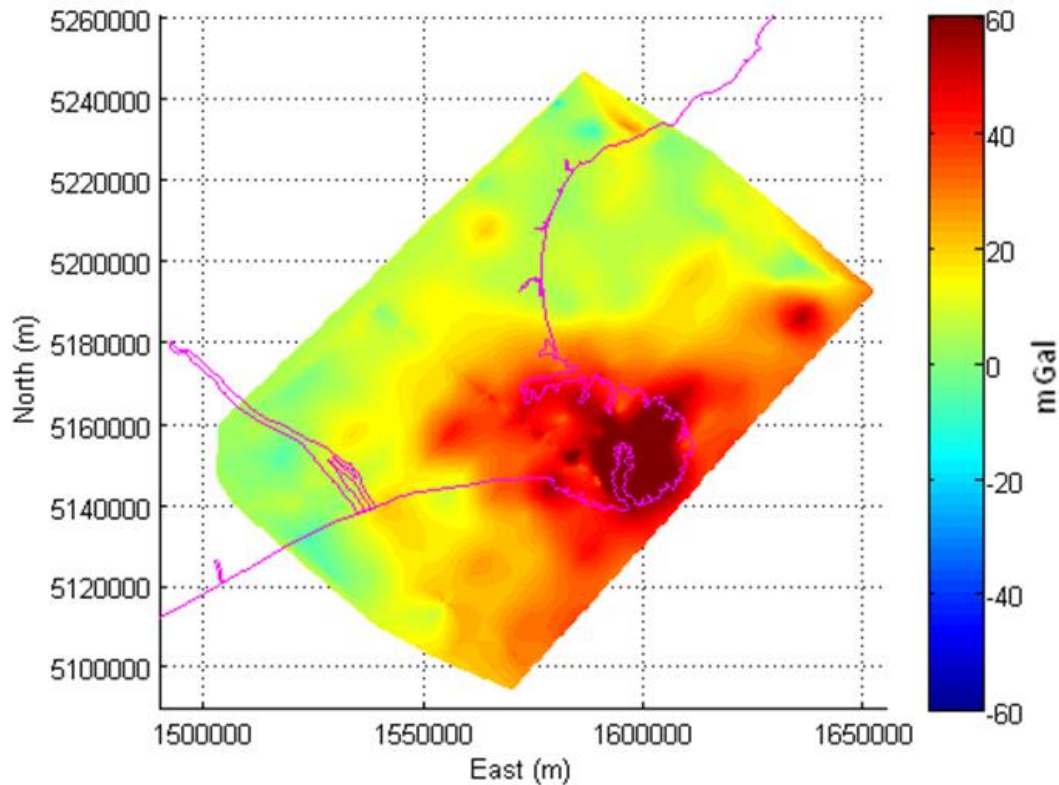


Figure 4.16: Airborne Bouguer anomaly map, flight-line with dipole event removed

Down-sampling the dataset

Airborne gravity observations are observed every second. However, during the data processing (McCubbine, 2016) a 90 second filter is applied. This means that our observation points are over sampled and biased by the filtering. In addition the dataset is too large to manipulate easily. The practical solution is to down-sample the data (i.e. to only use every nth point in the dataset) this leaves one observation every 4 km. A 50 point sampling rate was considered to be appropriate for use on this dataset, a total of 440 observations in the dataset

4.4.3.3. Estimating Uncertainties

The gravity meter used in this survey was a Lacoste and Romberg S-80 marine gravimeter which had recently been upgraded for use on an airborne platform. While this particular meter has been deployed on ship-borne campaigns for over 25 years e.g. Davy & Caldwell (1998), this trial airborne campaign required the instrument be installed on an aeroplane. Therefore its performance on an airborne platform was hitherto untested.

As the repeatability on the calibration line was approximately 3 mGal, the airborne dataset has been assigned an uncertainty of ± 3 mGal.

4.4.4. Satellite Altimetry

The satellite altimetry model has been taken from Sandwell & Smith version 23.1, Figure 2.1) The v23.1 grid is based on data from two new satellites: CryoSat-2 and Jason-1, which were augmented with older data from (contributing over 70 months of data) which have been augmented with older altimeter data from Geosat and ERS-1. The altimeter derived gravity field is estimated to be accurate to around 2 mGal (Sandwell *et al*, 2014).

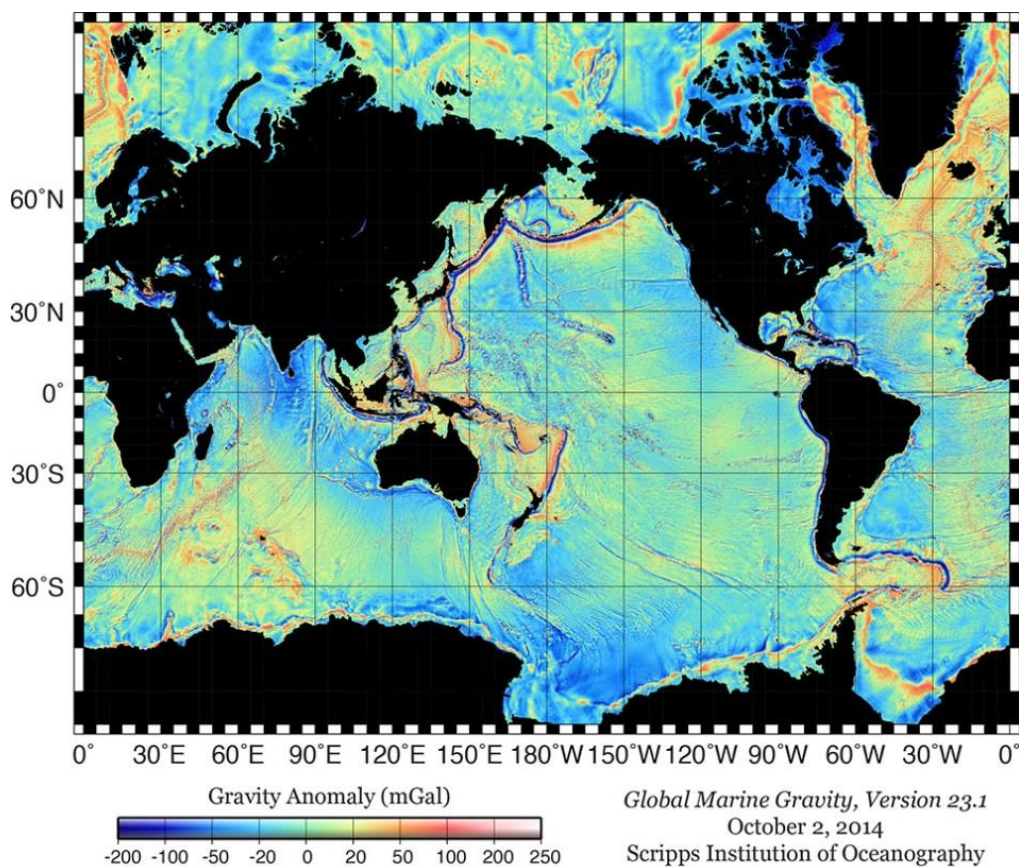


Figure 4.17: Sandwell & Smith satellite altimetry model, Version 23.1

Shun *et al* (1997) suggest that observations with depths less than 200 m should be masked. However, as shown by Figure 4.18, this would exclude most of the altimetry data in the test area, leaving only the bathymetry shown in red, deeper than 200m.

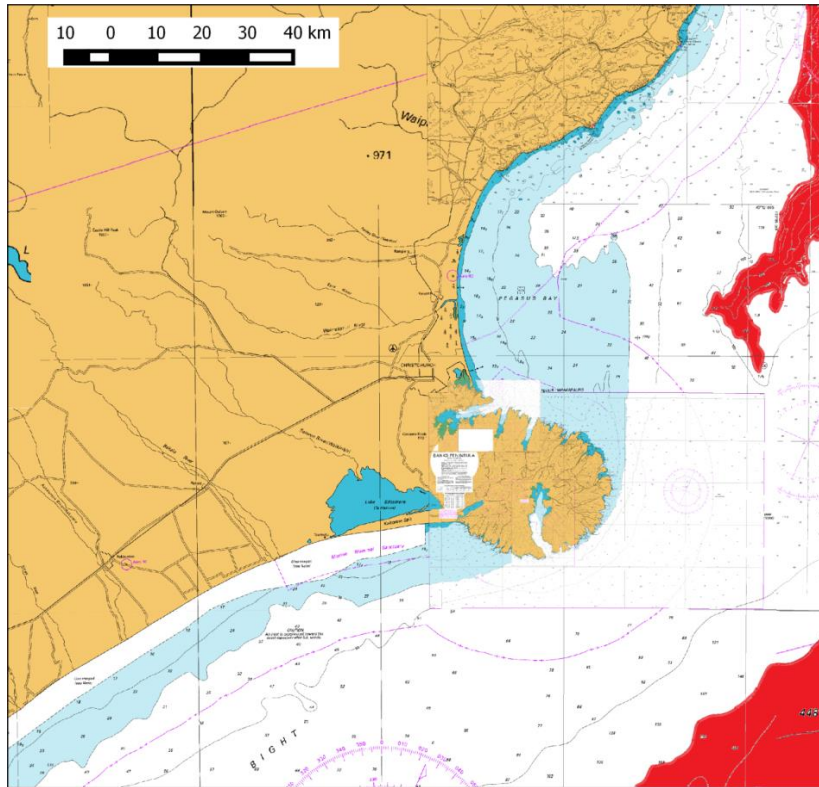


Figure 4.18: Bathymetry of the Canterbury test area
 Depths greater than 200 m shown in red. Projection is NZTM2000

The Sandwell & Smith v23.1 satellite altimetry dataset provides a corresponding global error model, with their marine gravity model. An extract of the Canterbury test area from the global error model is shown in Figure 4.19.

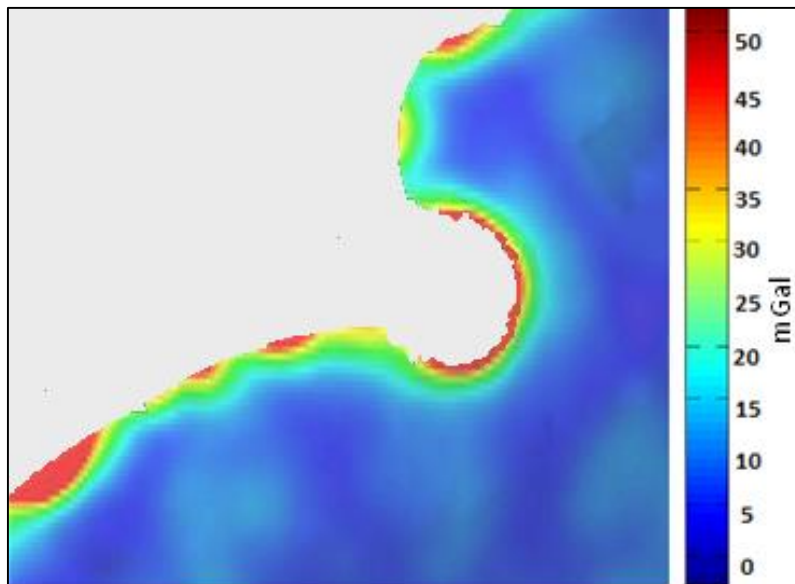


Figure 4.19: Expected errors from Sandwell & Smith satellite altimetry model v23.1
 Terrain shown in grey

The Sandwell & Smith v23.1 error model demonstrates that while there are significant uncertainties (up to more than 50 mGal) close to the coast, the dataset is much more reliable than predicted by Shum *et al* (1997).

Therefore the satellite altimetry dataset was not masked, resulting in 5,487 observations within the Canterbury test area (Figure 4.20). The uncertainties for this dataset will be set with the values shown in the error model.

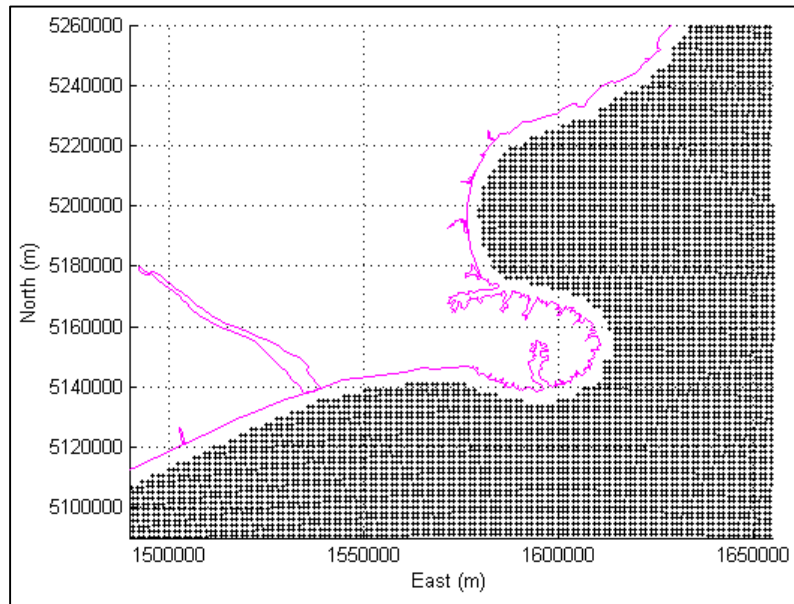


Figure 4.20: Location of Sandwell & Smith v23.1 satellite altimetry data points within the Canterbury test area (5487)

4.4.5. Global Gravity Model

Since the 1960s global and regional models have relied on satellite gravity observations to provide accurate long wavelength measurements for the Earth's gravity field (Featherstone, 2010). Satellite gravity recovers wavelengths greater than 100 km (Sandwell *et al*, 2001), but cannot recover the shorter wavelengths because of the survey altitude. As gravity is measured at satellite altitude, the noise from shorter wavelengths is amplified during the downward continuation process (see Chapter 2.4.5).

McCubbine (2016) finds that of the most recent seven satellite only models available on the International Centre for Global Earth Models website (<http://icgem.gfz-potsdam.de/ICGEM/>) the model GO_CONS_GCF_2_DIR_R5 (for now on referred to as: DIR_R5) fits best both the New Zealand levelling/GPS dataset and the terrestrial gravity data. Of the nine combined global gravity anomaly models, EGM2008 fits the terrestrial gravity the best and Eigen-6C4 fits the levelling and GPS derived geoid undulations the best.

DIR_R5 is a satellite only model. It was produced using the direct approach and is calculated to a maximum degree of 300. It was computed using GOCE, half GRACE, and NASA's Laser Geodynamic satellite 1 (LAGEO – 1) and the Italian Space Agency's LAGEO -2. LAGEO – 1, launched 1976 and LAGEO -2, launched 1992, orbit at 5800 and 5600 km (compared with GOCEs altitude of 283.2 km at injection and 259.6 km at decommission), contribute to the very low degree coefficient of the gravity

field. More information regarding the processing details of DIR_05 can be found in Pail *et al* (2011) and Brunisma *et al* (2014).

4.4.5.1. DIR_R5 vs EGM2008

EGM2008 is a commonly used GGM, for example, it was used in the realisation of NZVD2009 (Claessens, 2009). For this study, however, a satellite only approach is preferred as it is less likely to result in computational biases caused by the same data point being introduced as an adjustment multiple times.

The global geoid height differences between DIR_R5 and EGM2008 are shown in Figure 4.21, with a spatial grid resolution of $0.75^\circ \times 0.75^\circ$ and a maximum degree/order 240 (Brunisma *et al*, 2014).

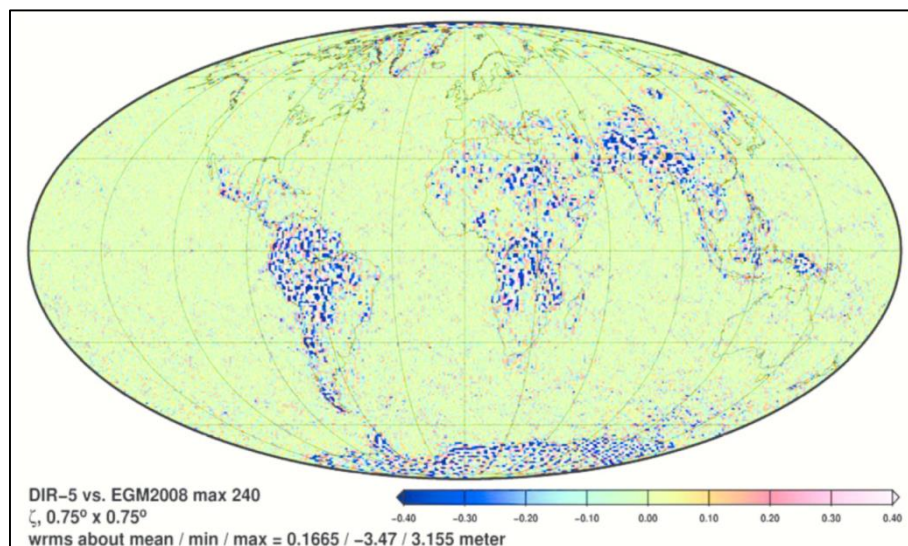


Figure 4.21: Global geoid height difference between EGM2008 and DIR-R5 (Brunisma *et al*, 2014)

4.4.5.2. Estimating Uncertainties

As a demonstrative statistical comparison, the GOCE mission (the major component of DIR_5) is expected to provide a cumulated geoid accuracy of 1-2 cm at degree 200 (Pail *et al*, 2011). While Pavlis *et al* (2008) find that EGM2008 provides a cumulated geoid accuracy of 7 cm at degree 200.

4.5. Integration Step Three: Combination

Identify the range of combination methodologies available, including their strengths, limitations and suitability in relation to the datasets.

Chapter 3.4 identified three interpolation methods: natural neighbour, ordinary kriging and least squares collocation. This step of the integration process uses each of these interpolation methods to assess:

1. their ability to combine multiple datasets,
2. the use of *a priori* weights,
3. if they are an exact interpolation method, and
4. their ability to combine data in a three-dimensional space.

This section evaluates each of these four tests, using the gravity data from the Canterbury test area. Finally, identifying which best combines these datasets.

4.5.1. Test One – Combines Multiple Datasets

This first test evaluates the ability of each of the integration methods to combine more than two gravity datasets. The data used for this trial are the Canterbury test area terrestrial, ship-borne and airborne Bouguer anomaly datasets.

Test one is evaluated by combining the terrestrial, ship-borne and airborne Bouguer anomaly datasets from the Canterbury test area, to form a single grid.

The result is three plots (one for each integration method) demonstrated by Figure 4.22, Figure 4.23 and Figure 4.24. This confirms that all three interpolation methods (natural neighbour, ordinary kriging and least squares collocation) are able to combine multiple gravity datasets.

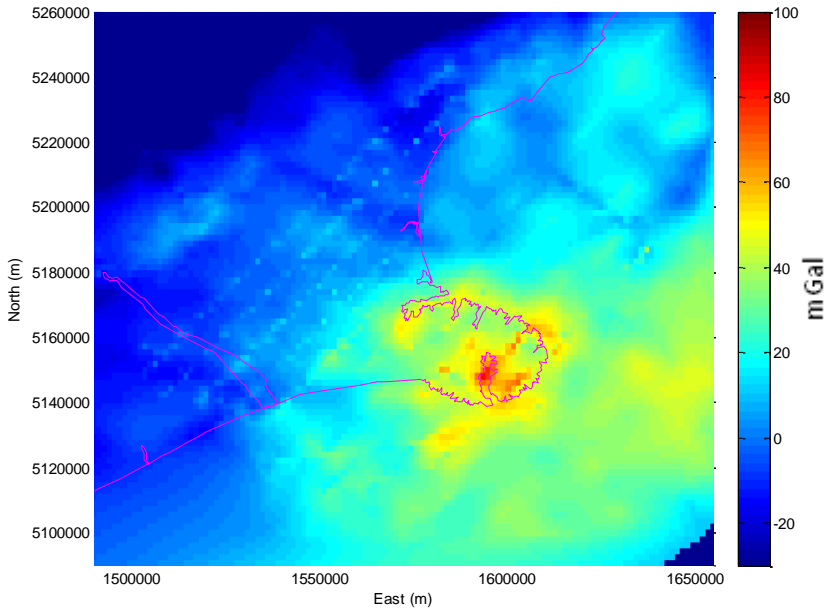


Figure 4.22: Natural neighbour method - displaying terrestrial, airborne and ship-borne gravity datasets

Figure 4.23: Ordinary kriging method: displaying - terrestrial, airborne and ship-borne gravity datasets

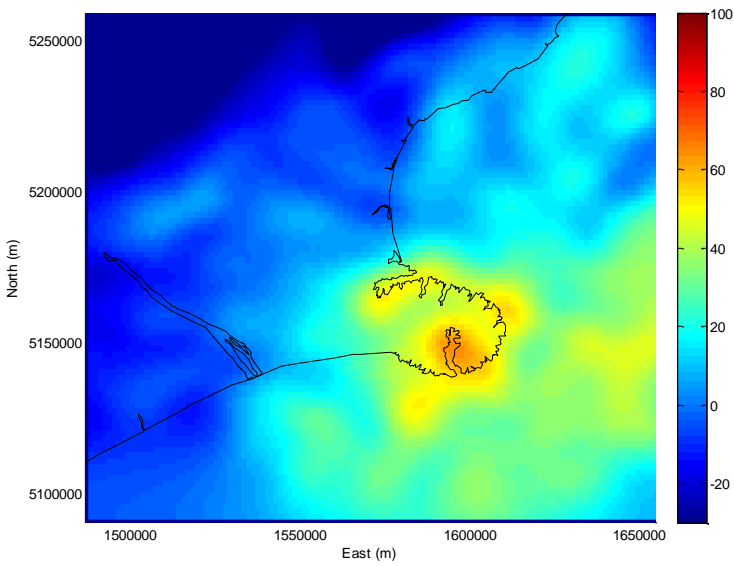
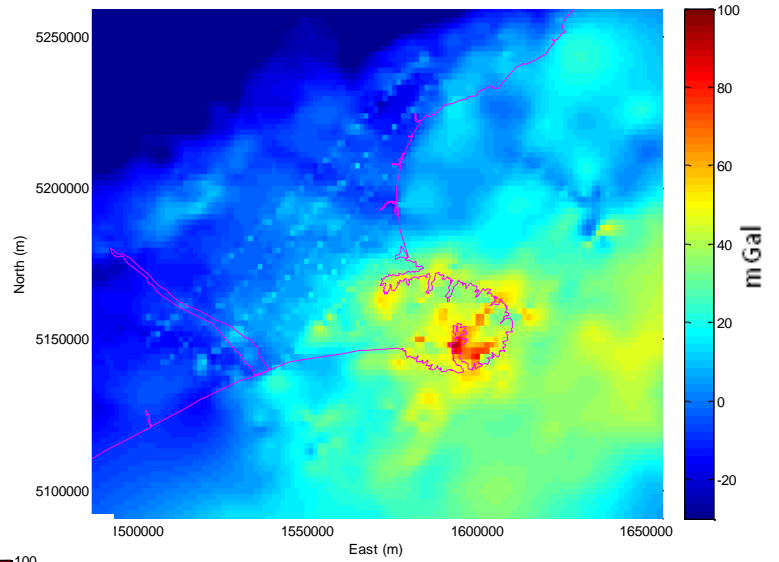


Figure 4.24: Least squares collocation method - displaying terrestrial, airborne and ship-borne gravity datasets

4.5.2. Test Two – Uses *a priori* Weights

The second test investigates the ability to apply *a priori* weights as part of the integration process. The data used for this trial are from the Canterbury test area terrestrial Bouguer anomaly dataset.

For this test the terrestrial gravity dataset from the Canterbury test area is combined using each of the interpolation methods with a weighing of 'zero', to produce a plot of the area. This test is then repeated to produce a second plot of the area, with a weighting of 'three'. The two plots are then presented on the same page to be compared.

The results are that the natural neighbour method is unable to be weighted, so has not been provided as a plot.

The ordinary kriging method is able to be weighted, and is shown by Figure 4.25 with a zero weight and Figure 4.26, with a weight of three.

The least squares collocation method is able to be weighted, and is shown by Figure 4.27 with a zero weight and Figure 4.28, with a weight of three.

These four plots demonstrate that change of weighting from zero to three suppressions of the low frequency gravity signal.

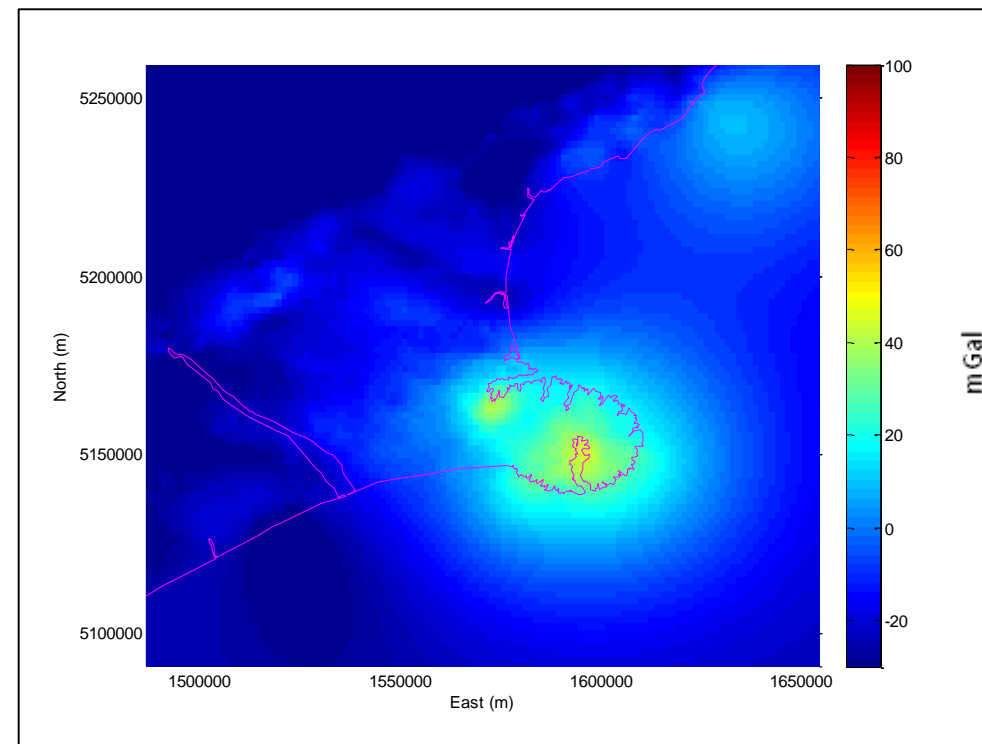
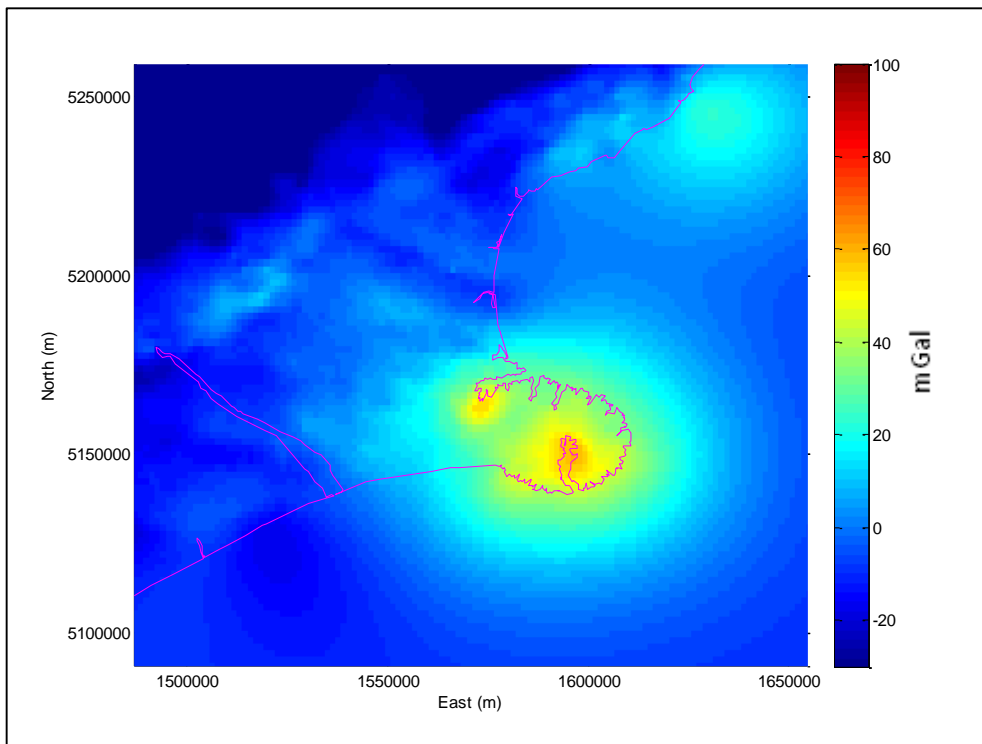


Figure 4.25: Ordinary kriging method, terrestrial dataset additional weight set to 'zero'

Figure 4.26: Ordinary kriging method, terrestrial dataset additional weight set to 'three'

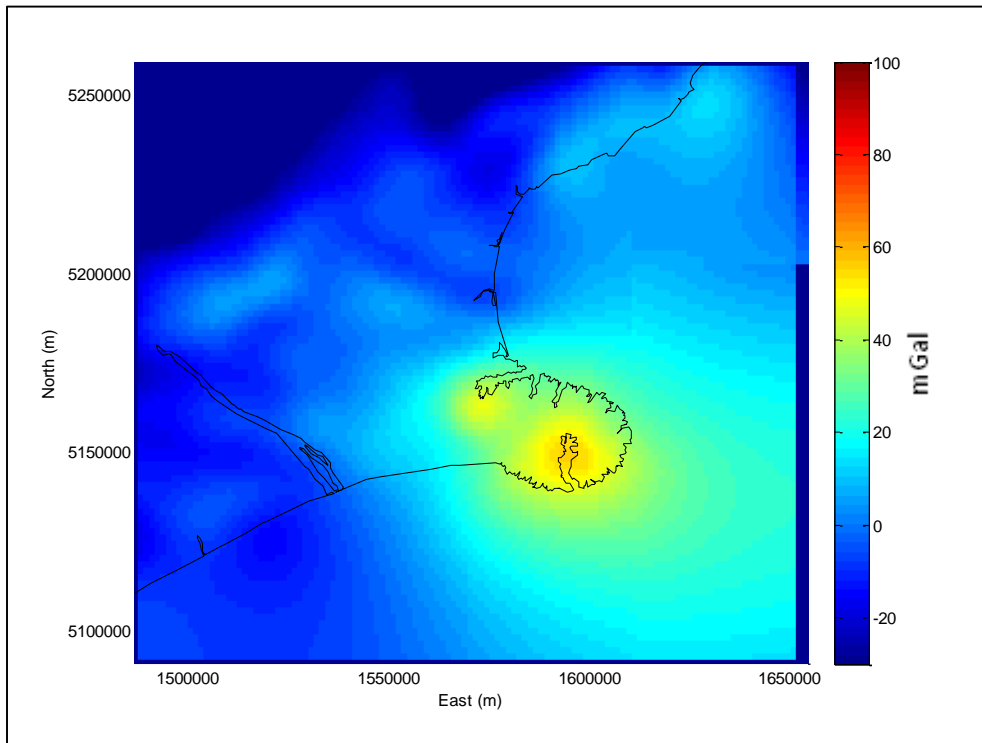


Figure 4.27: Least squares collocation method, terrestrial dataset additional weight set to 'zero'

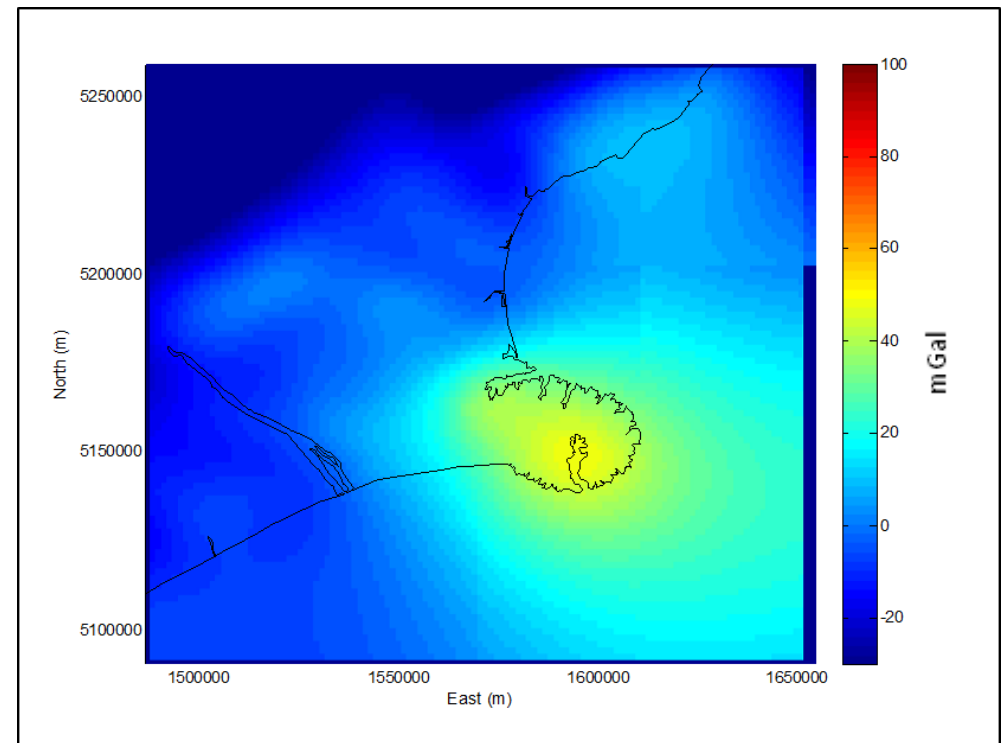


Figure 4.28: Least squares collocation method, terrestrial dataset additional weight set to 'three'

4.5.3. Test Three – Is an Exact Interpolation Method

Test three checks if the interpolation method forces the modelled surface through the input observation points (exact interpolation method) or if the model fits the points with some degree of uncertainty. The data used for this trial are from the Canterbury test area terrestrial Bouguer anomaly dataset.

This test is conducted by first determining the Bouguer anomaly value for each of the gravity stations within the Canterbury test area. The location of the gravity stations are shown in Figure 4.29.

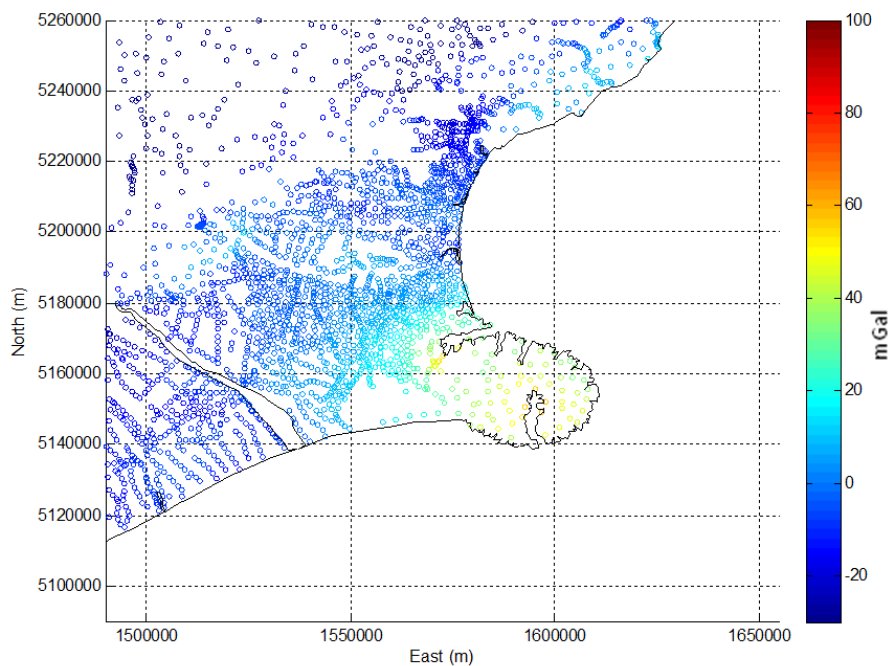


Figure 4.29: Location of terrestrial gravity data points used in Test Three

Each of the three interpolation methods (natural neighbour, ordinary kriging and least squares collocation) are used to produce a surface of Bouguer anomalies in the Canterbury test area.

The Bouguer values from the gravity dataset are then compared to the modelled values at the same locations. The result is a CDF plot showing the difference between the observations and the three models.

As shown for the natural neighbour (Figure 4.30) and ordinary kriging methods (Figure 4.31) the two CDF plot show a difference of zero (the long tails are a feature of the edge effects). This means that models were produced using an exact interpolation method.

In contrast the least squares collocation method (Figure 4.32), produces an ‘S’ shaped curve, about a mean of zero. This indicates that Least Squares Collocation is not an exact interpolation method. The standard deviation of this difference curve is ± 3 mGal. This value reflects the ± 3 mGal uncertainties value that has been applied to the terrestrial gravity dataset in the Canterbury Test area (c.f. Section 4.4.3.3).

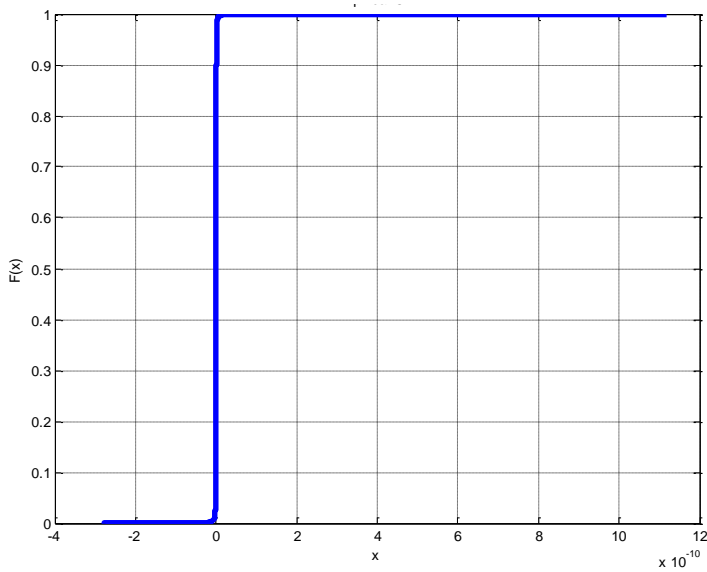


Figure 4.30: Natural neighbour method - CDF plot difference of terrestrial gravity values before and after integration

Figure 4.31: Ordinary kriging method - CDF plot difference of terrestrial gravity values before and after integration

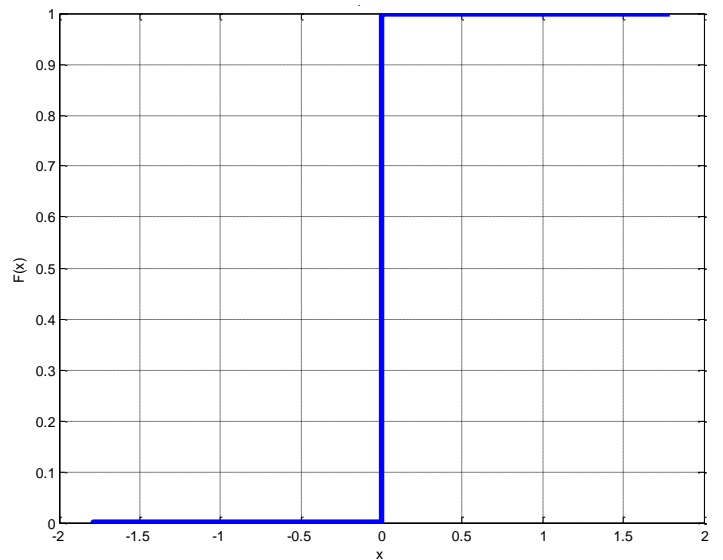
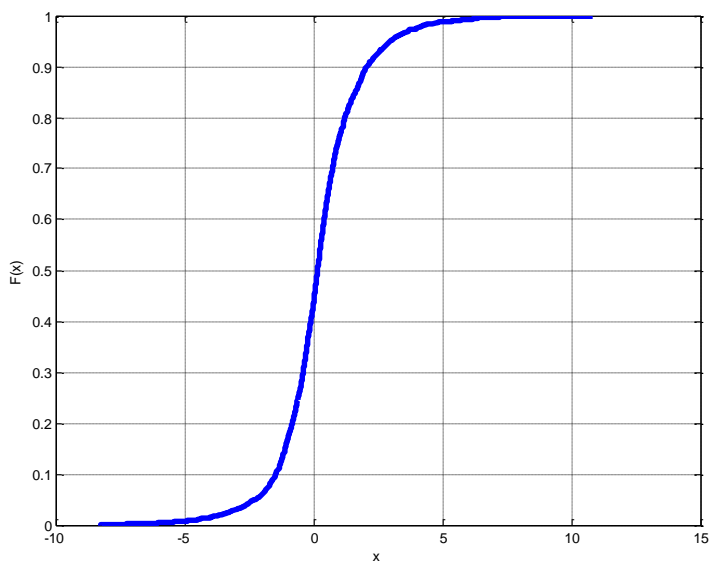


Figure 4.32: Least squares collocation method - CDF plot difference of terrestrial gravity values before and after integration

Standard Deviation = 2.904 mGal



4.5.4. Test Four – Supports Three-Dimensional Interpolation

This final test investigates the ability of each of the integration methods to combine datasets observed at different altitudes, with respect to the Earth's surface. The data used for this trial are from the Canterbury test area terrestrial and airborne Bouguer anomaly datasets. These two datasets were chosen for use in this trial as these two datasets intersect (unlike the terrestrial and ship-borne/satellite altimetry datasets which abut) and are the most disparate, in terms of observation height overlap.

When combining data it is desirable to maintain the data in a format which is as close to possible to its natural state. This means manipulating the data as little as possible, as transformations can result in data degradation, due to factors such as compounding rounding error or the use of unstable functions. Therefore, we wish to limit the use of functions such as the inverse Poisson method, used for downward continuation (as identified in Chapter 2.5.2), as it is inherently unstable and in effect it is a form of low pass filtering, removing the higher frequency signals.

As such, it is desirable to combine our datasets without first downward continuing the airborne dataset to the terrain surface. Therefore, in Test Four A, the airborne and terrestrial gravity dataset are combined using each of the three integration methods.

Subsequently, Test Four B, repeats the combination of the airborne and terrestrial gravity datasets using each of the three integration methods. However, in this trial the airborne gravity dataset has been downward continued by use of the inverse Poisson method prior to the integration.

4.5.4.1. Test Four A - Survey Altitude Airborne Dataset

In this first test the airborne and terrestrial gravity datasets are combined at their observation attitude. A plot is created for each of the integration methods: natural neighbour, ordinary kriging and least squares collocation.

Visible in the natural neighbour, Figure 4.34 and ordinary kriging, Figure 4.33 integration methods are the artefacts of the flight-line tracks (north-east/south-west striations)

However these parallel lines are not evident in Figure 4.35, when the least squares collection integration method was used, resulting in a smooth transition between the airborne and terrestrial datasets. This provides evidence that the Least Squares Collocation method is the most suitable method to combine datasets at various altitudes.

Further evidence can be found in Figure 4.36, Figure 4.37 and Figure 4.38, which display the differences between the models produced by the three methods. Significant differences are shown between Least Squares Collocation and both the Natural Neighbour and Ordinary Kriging models. While there are only slight difference between the Natural Neighbour and Ordinary Kriging models, indicating that these two models provide only a two-dimensional interpolation method.

Therefore, least squares collocation is the only one of the three integration methods which is able to support three-dimensional interpolation.

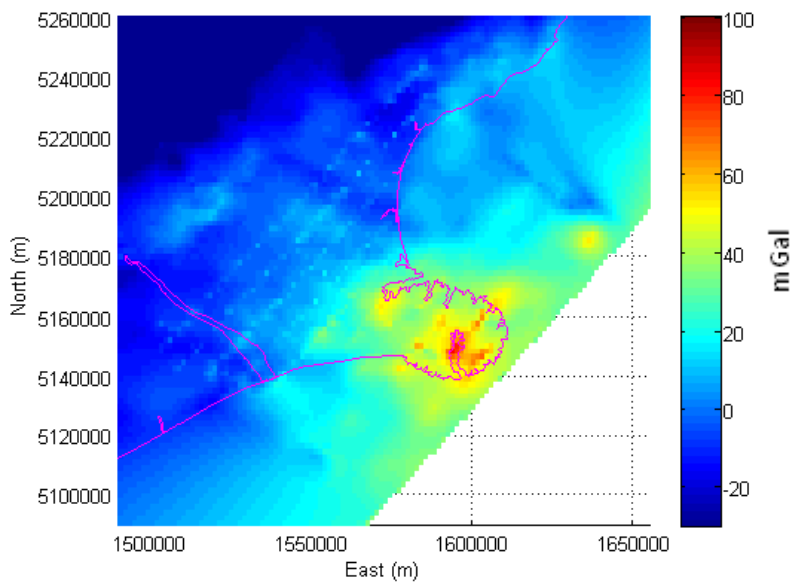


Figure 4.33: Natural neighbour method - combination of airborne and terrestrial datasets

Figure 4.34: Ordinary kriging method - combination of airborne and terrestrial datasets

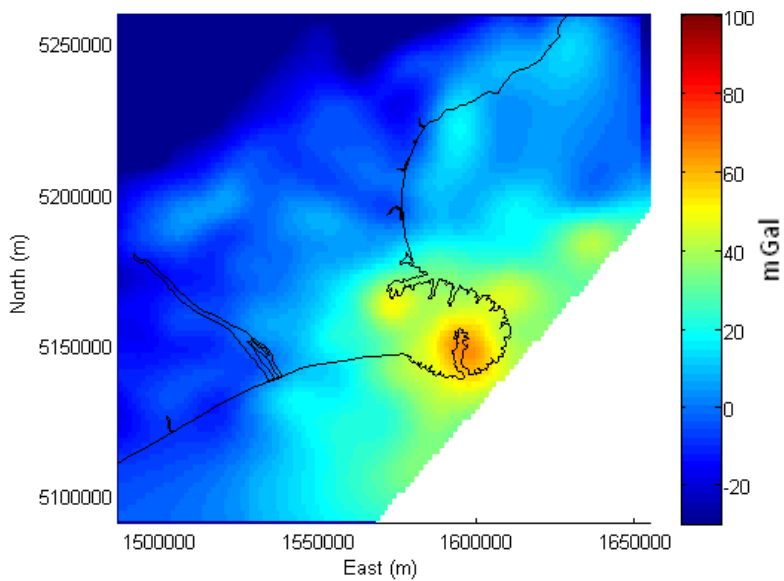
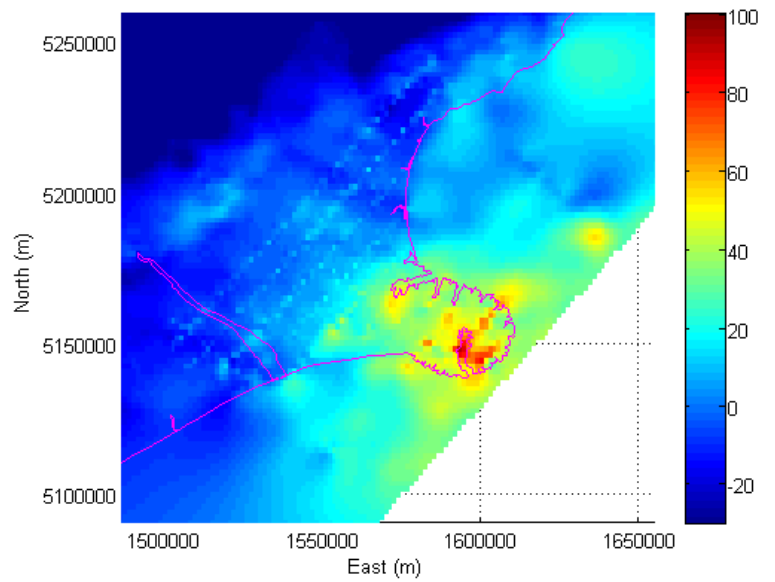


Figure 4.35: Least squares collocation method - combination of airborne and terrestrial datasets

Differences

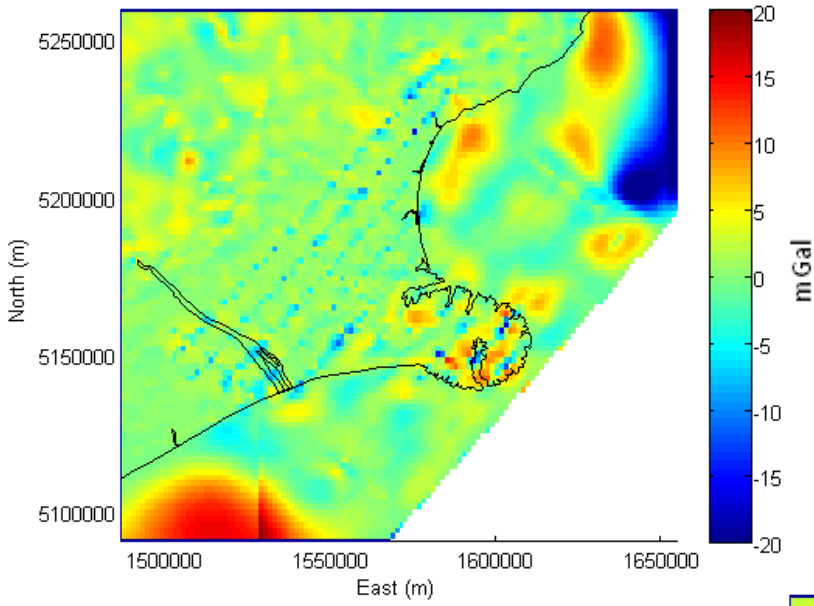


Figure 4.36: Combination of airborne and terrestrial datasets, difference between least squares collocation and natural neighbour methods

Figure 4.37: Combination of airborne and terrestrial datasets, difference between least squares collocation and ordinary kriging methods

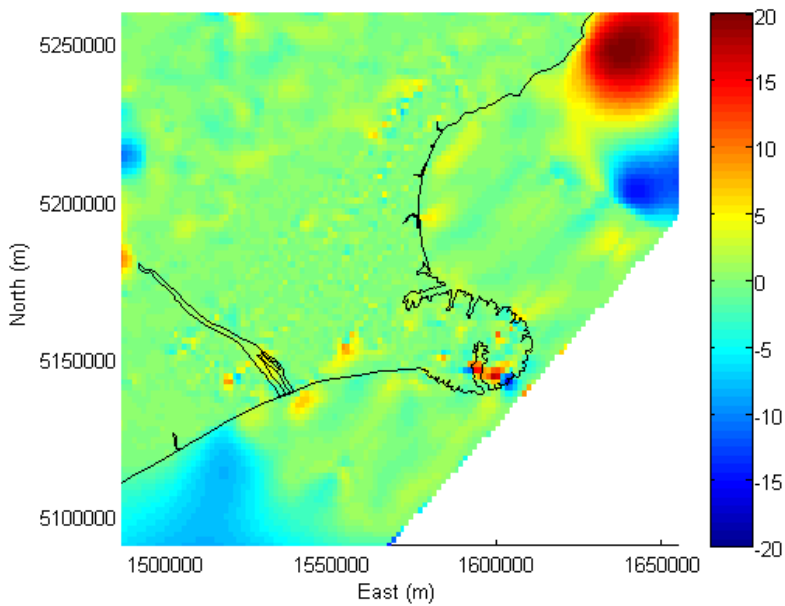
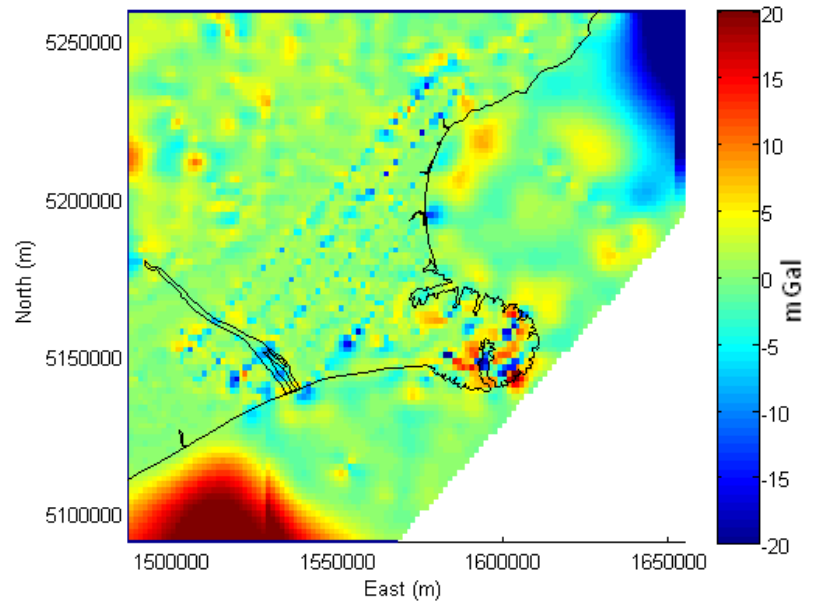


Figure 4.38: Combination of airborne and terrestrial datasets, difference between ordinary kriging and natural neighbour methods

4.5.4.2. Test Four B - Downward Continued Airborne Dataset

As the Natural Neighbour and Kriging methods require the input dataset to be on the same surface, in this second test the airborne dataset was first downward continued using the Inverse Poisson method.

The downward continuation process requires that that data is first upward continued (to 5,000 m), in order to dampen the high frequency signals, and then reduced to surface elevation.

The downward continuation process used in the study is limited as it evaluates a surface, rather than the observation points individually. As identified in Chapter 4.4.3, the altitude of the survey platform varies significantly (± 10 m or ~ 3 mGal) while in flight. In addition, the downward continuation process is sensitive to edge effects. This resulted in the application of a buffer at the extent of the surface, reducing the size of the observation area. Therefore, Test Two should be considered as an indicative assessment only of the inclusion of downward continued datasets to the integration process.

In this test the terrestrial gravity datasets are combined with the downward continued airborne data. A plot is created for each of the integration methods: Natural Neighbour, Ordinary Kriging and Least Squares Collocation. The output model is then compared to the corresponding model from test Four B, to form a different map for each method.

Figure 4.39 and Figure 4.40 show the test results for the natural neighbour interpolation method, while Figure 4.41 and Figure 4.42 show the test results for the ordinary kriging interpolation method. For both of these methods it is found that although the line artefacts from the airborne dataset have been slightly reduced, they still remain visible in the output models. This is largely expected as both of these methods are exact interpolation methods, and therefore there has been no allowance due to the uncertainties in the downward continued heights.

Figure 4.43 and Figure 4.44 show the results of the least squares collocation method.

In all three methods, we have seen the effects of the loss of the high frequency signals. This is particularly evident in the offshore regions where the airborne data is unconstrained by the effects of the terrestrial dataset.

It is acknowledged that the downward continuation method used in this case study was coarse. With additional re-processing accounting for the variation of the airborne platform, it may be possible to improve the altitude issue. However, this is at the expense of the high frequency signals and possible degradation of the model from the downward continuation process.

It is therefore suggested that the least squares collocation is the most optimal for the creation of a Bouguer gravity map, as it does not require prior downward continuation of the datasets to a constant elevation.

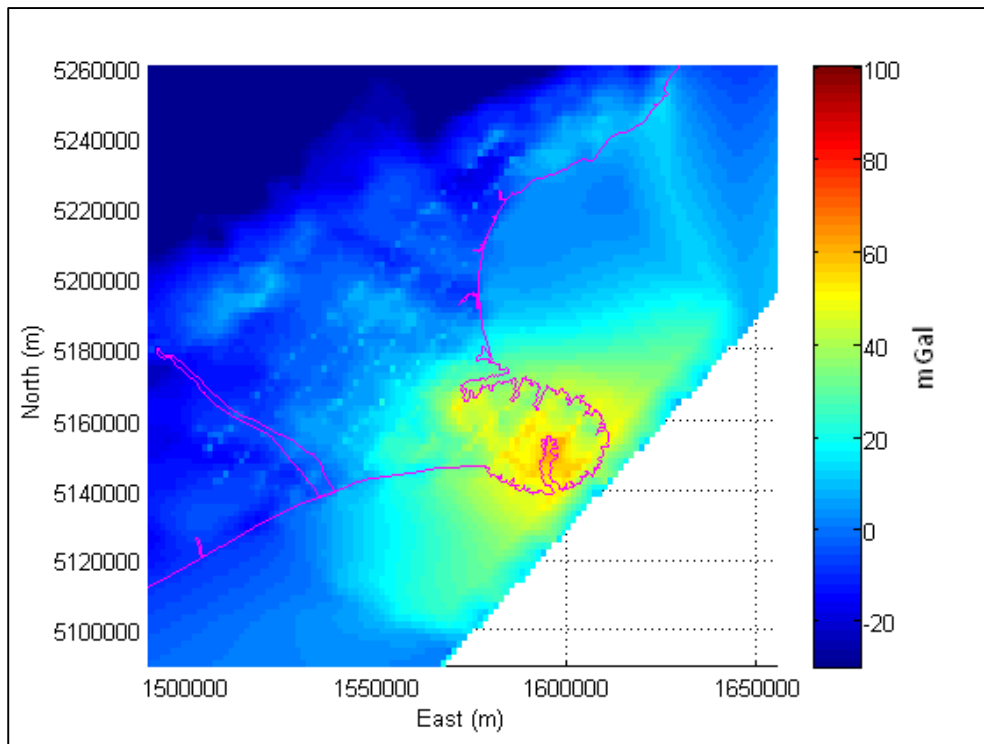


Figure 4.40: Natural neighbour method - combination of terrestrial and downward continued airborne datasets

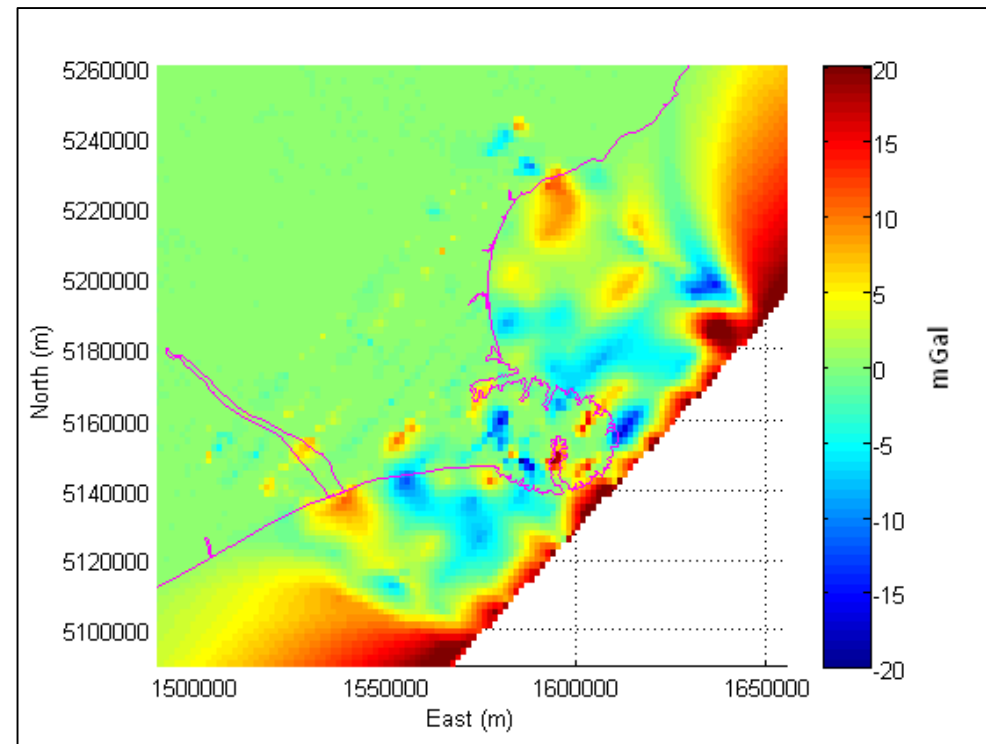


Figure 4.39: Natural neighbour method, difference map of integration result, without and with downward continued airborne data

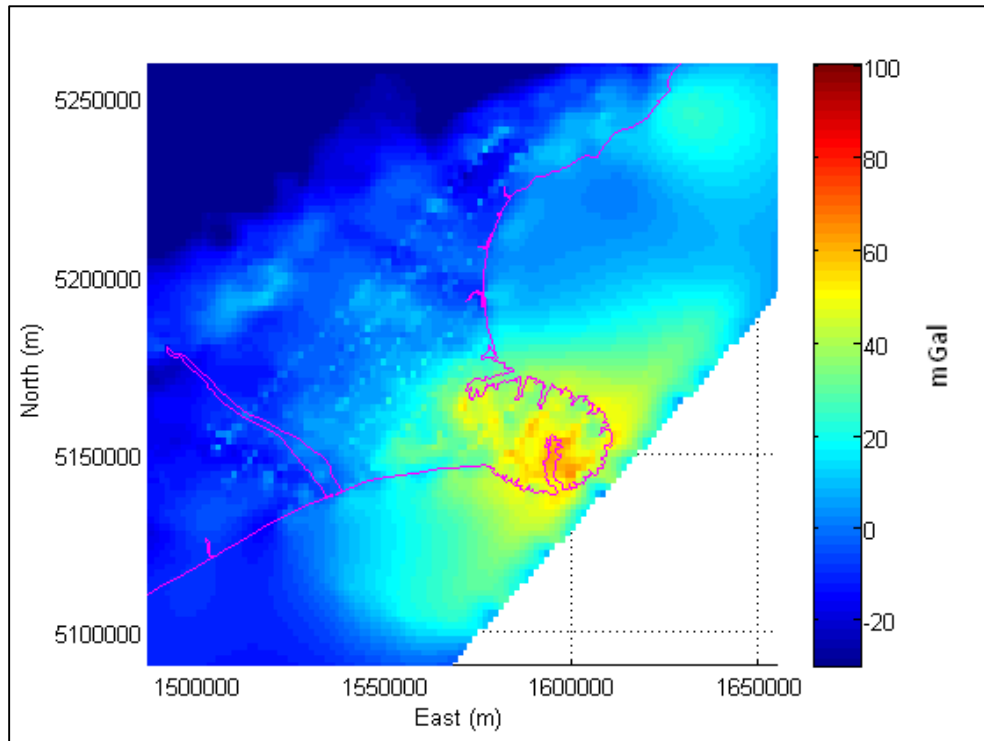


Figure 4.41: Ordinary kriging method, combination of terrestrial and downward continued airborne datasets

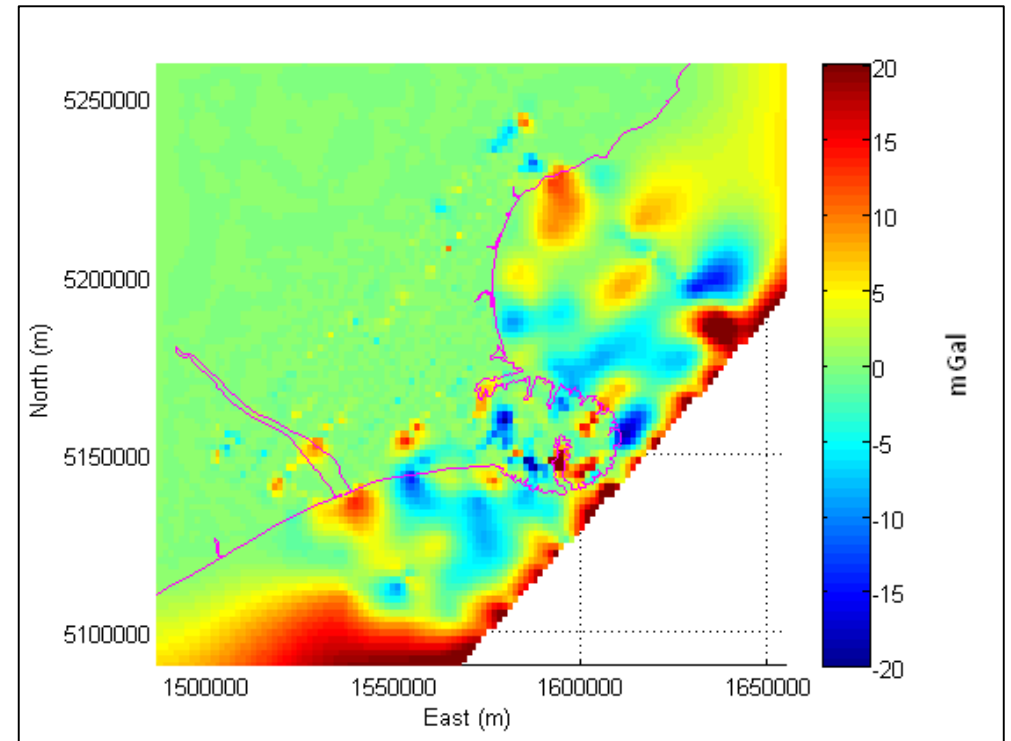


Figure 4.42: Ordinary kriging method, difference map of integration result, without and with downward continued airborne data

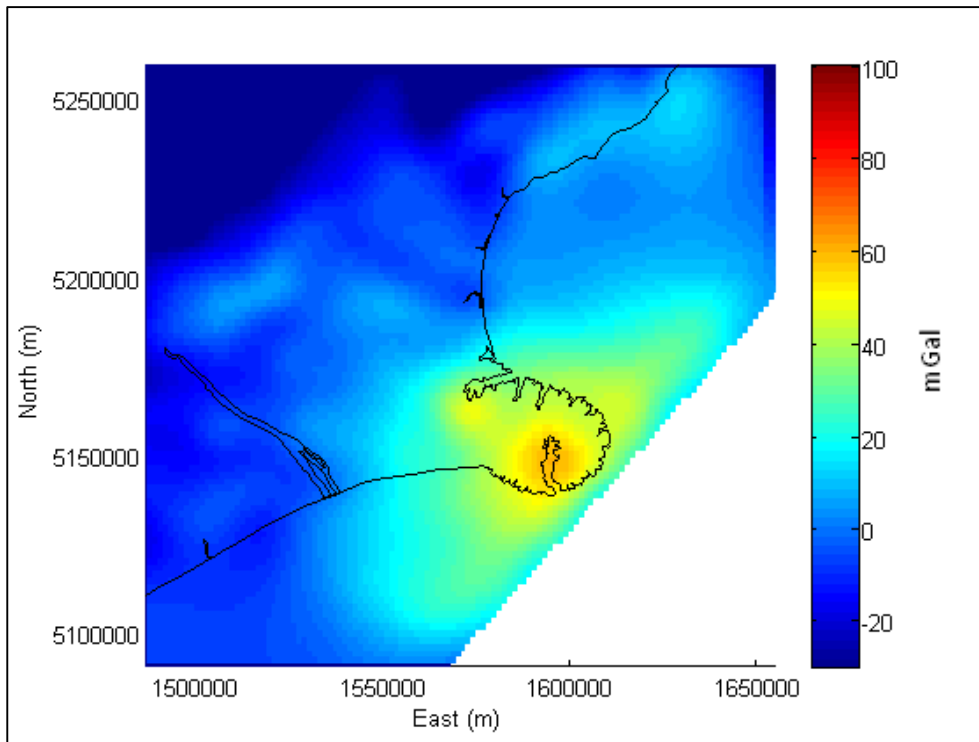


Figure 4.44: Least squares collocation method, combination of terrestrial and downward continued airborne datasets

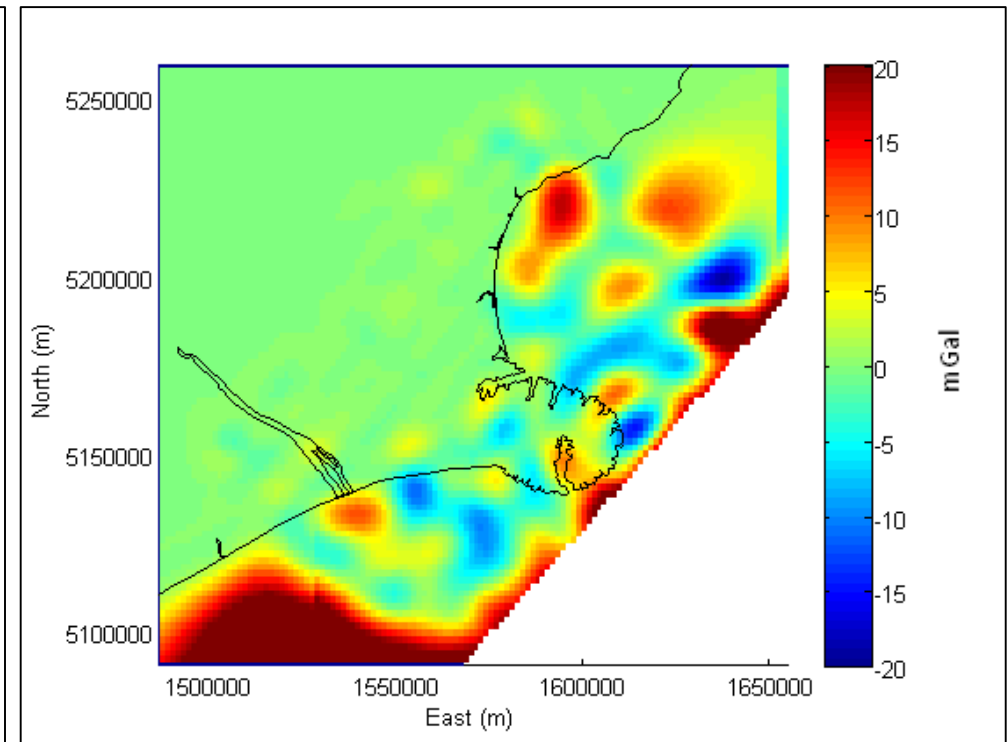


Figure 4.43: Least squares collocation method, difference map of integration result, without and with downward continued airborne data

4.6. Step Four: Assessment

Ensure that the final output model dataset has met the requirements.

In this final step we ensure that the integration model identified in step three: Least Squares Collocation is an optimal integration method for heterogeneous gravity datasets. At the assessment stage we wish to ensure that we have created a single well integrated gravity anomaly map.

This assessment is completed in two stages:

1. compare the output model to existing gravity models, and
2. test the fit of the final model.

4.6.1. Comparison of Models

In the comparison of models assessment the final case study gravity map is compared to other gravity models of the area. It is acknowledged that the models will have been created using different datasets, different methods, different resolutions and at different periods. Therefore it is not expected that the models are identical. However, it is expected that the anomalies are of the same magnitude, and same general trends between models and that any differences between the models are justifiable.

For this assessment the Case Study Bouguer anomaly map, Figure 4.45 , is compared to the EGM2008 derived Bouguer anomaly map of the Canterbury test area Figure 4.46. The differences between the two models are shown by Figure 4.47.

The best agreement is found in terrestrial areas which are flat and well sampled by terrestrial observations.

The largest variations occur in the coastal areas, particularly in the areas influence by the complex terrain of Lyttelton and Akaroa harbour. These differences are expected as they occur in a zone where satellite altimetry would be unable to acquire a reliable return signal due to the shallow waters and proximity of steep terrain, compounded with poorly sampled terrestrial measurements. Therefore, these areas would have been poorly modelled in EGM2008. In contrast, this area is well sampled by the airborne dataset in the Canterbury case study. This leads to a better approximation of the Bouguer anomaly in the Banks Peninsula area by the Case Study Bouguer anomaly map.

When comparing these two models we find that they are in general agreement and the major differences are mostly high frequency or as expected.

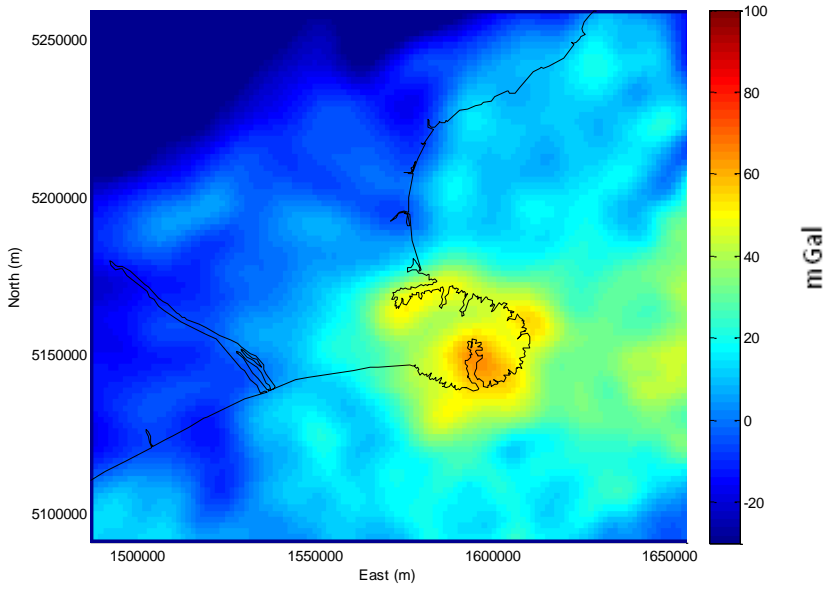


Figure 4.45: Case study Bouguer anomaly map

Figure 4.46: EGM2008 derived Bouguer anomaly map of the Canterbury test area

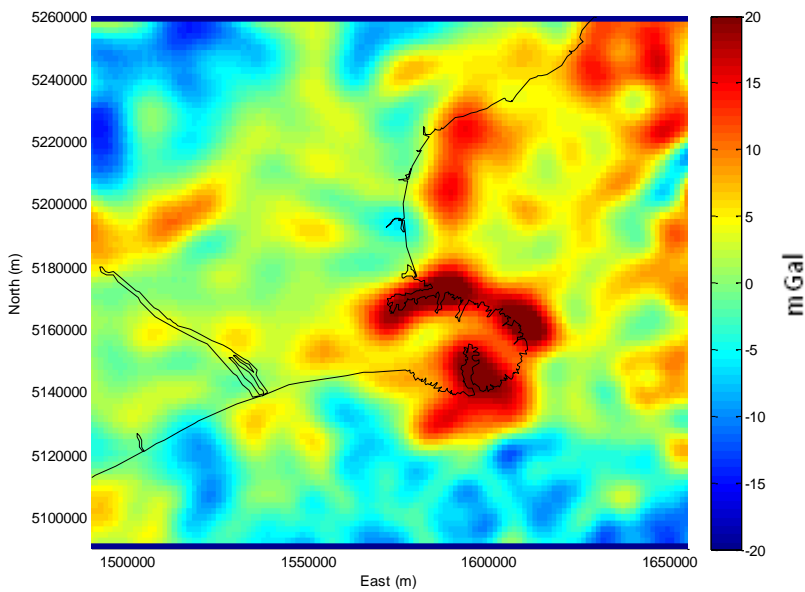
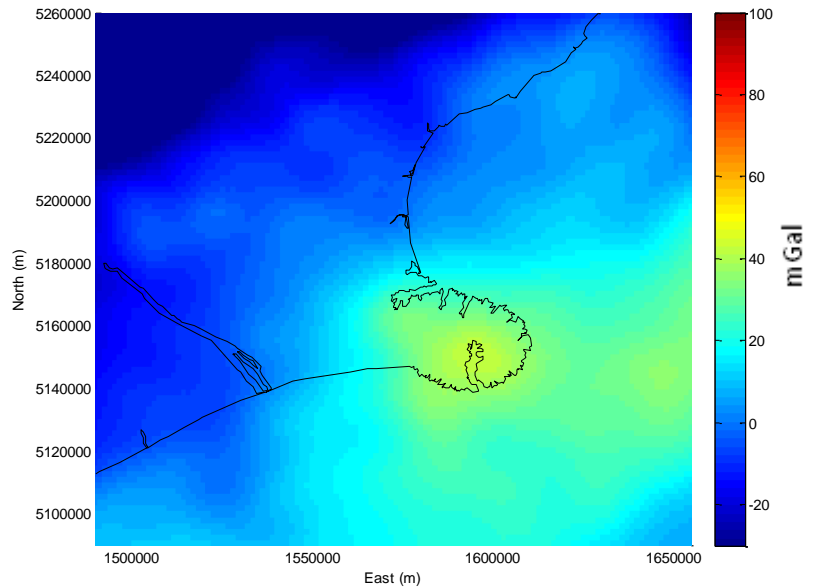


Figure 4.47: Differences map between the case study and EGM2008 Bouguer anomalies

4.6.2. Test of Fit

The second assessment is a test of the fit of the final model with the input data. This means ensuring that correctly integrated datasets and that the model produced accurately portrays the gravity field. As all available data has been used in the calculation of the final Bouguer anomaly map, this assessment will be completed using a method of cross-validation. The process of cross-validation involves:

- computing a model,
- removing an observation,
- re-computing the model,
- evaluating the modelled value at the removed point, and
- returning the observation to the model.

This process is completed multiple times, ideally until all the observations have been removed once. However, as the Least Square Collocation integration programme takes up to five minutes to determine a solution for the Canterbury test area, for this assessment only a subset, approximately five percent of the marks were tested. The observations chosen to be tested in this assessment were selected randomly by row number.

This process was completed for each of the terrestrial, airborne and ship-borne datasets. The GGM and satellite altimetry model are not assessed as they have been provided as gridded models and not observation points.

The results of this second assessment are shown in Table 4.7. This indicates that the final model and input data are a good fit.

Dataset	Observations in Case Study	Observations removed	Mean	Maximum	Minimum	Standard Deviation
Terrestrial	2,505	150	-0.050	1.065	-0.954	0.240
Airborne	440	25	0.322	2.505	-1.005	0.732
Ship-borne	5,391	250	0.019	0.353	-0.076	0.048

Table 4.7: Cross-validation result (mGal)

The cumulative results of these two assessments suggest that the final Case Study Bouguer anomaly map is a single well integrated gravity anomaly map of the Canterbury Test area.

4.7. Summary

This case study used the four step integration process to identify a combination method to produce a single Bouguer anomaly map of the Canterbury test area, shown in Figure 4.48.

The purpose of this investigation was to create a single gravity anomaly map which:

1. combines data from the entire spectral range,
2. uses an integration method which will minimise the inconsistencies between the datasets, and
3. is well-integrated.

This case study used five gravity datasets from the Canterbury test area: satellite, altimetry terrestrial, ship-borne, airborne and satellite gravimetry. In this chapter each of these datasets were defined, ensuring they would provide coverage of the spectral range and evaluated in order to determine the uncertainties in each of the datasets.

The datasets were then used to assess each of the three integration techniques: Natural Neighbour, Ordinary Kriging and Least Squares Collocation, on their ability to combine multiple datasets, incorporate *a priori* weights, determine if they are an exact interpolation method and if they would support the three-dimensional integration of datasets.

It was found that the Least Squares Collocation method is the only one of the three methods which is able to integrate data collected at different altitudes. Therefore an additional test was used to establish the impact of combining a downward continued airborne gravity dataset using the three integration methods. However, as the Natural Neighbour and Ordinary Kriging methods are exact interpolation methods and the downward continuation process reduces the high frequency signal, the downward continued process did not provide an improved model.

Finally the output model of the Canterbury case study region was assessed to ensure that it provided a good representation of the local Bouguer anomaly field and that it was a well-integrated model.

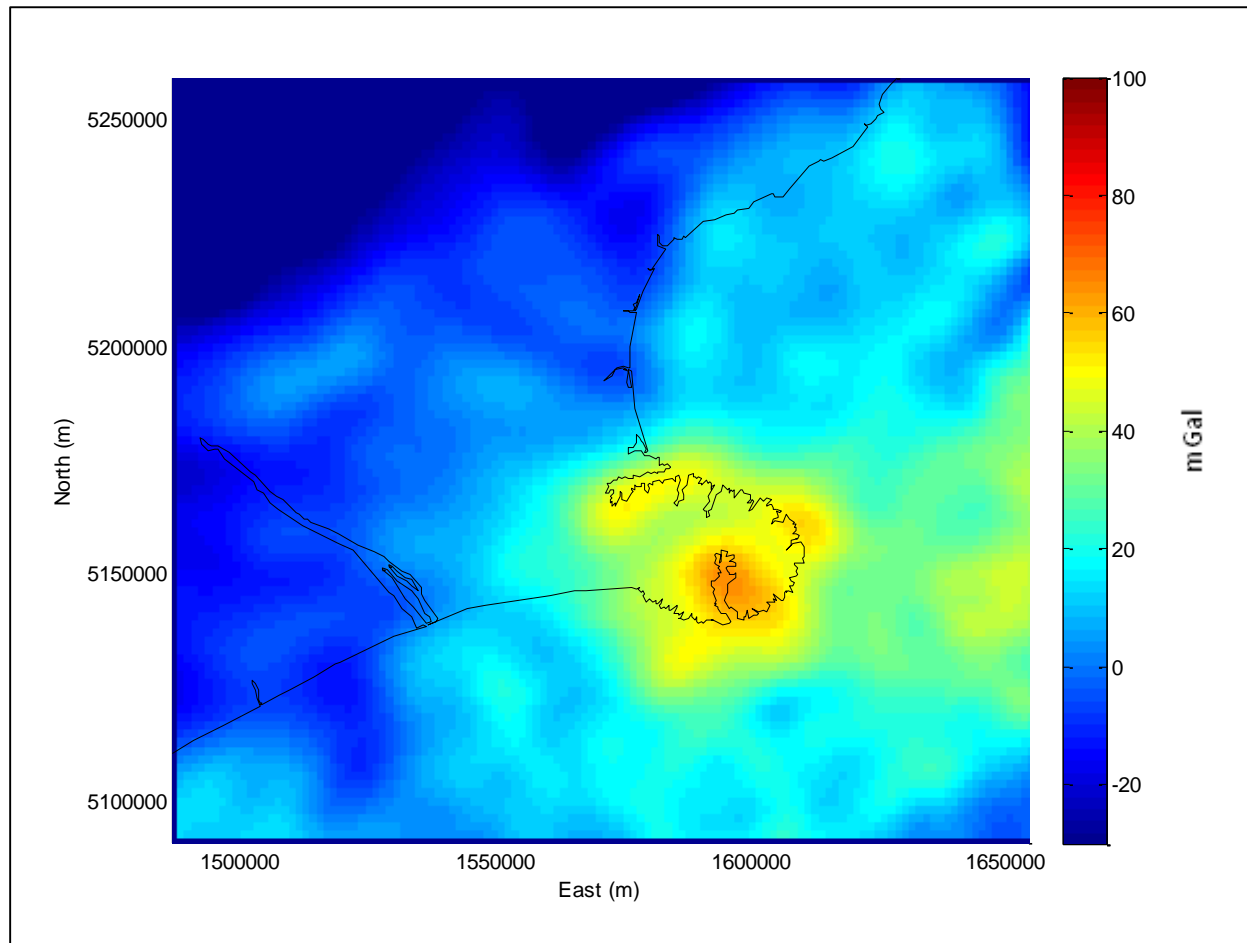


Figure 4.48: Final Bouguer anomaly map of the Canterbury case study region (Enlargement of Figure 4.45)

5. SUMMARY, CONCLUSIONS AND RECOMMENDATIONS

5.1. Project Summary

The principle aim of this study was to determine a method to produce a single gravity map of the Canterbury case study area, derived from multiple disparate gravity datasets and combined in an optimal manner for the purposes of geoid modelling.

This aim was realised through the identification and application of a four step integration process: purpose, data, combination and assessment. The resulting product was a Bouguer anomaly field map of the Canterbury case study area, both on and offshore, combining satellite altimetry and terrestrial, ship-borne, airborne, and satellite gravimetry using least squares co-location.

The Canterbury test area was chosen as the case study for this investigation as the area was unique to New Zealand in having five gravity datasets available, including recent airborne gravity data.

5.1.1. Purpose

Gravity is a force, which on the Earth's surface is observed as acceleration towards centre of the Earth. In geodesy, gravity observations are used to define the geoid, an equipotential surface that would coincide with sea level, if sea level were able to flow through the continents. A practical application of the geoid is that it can be used as a transformation surface, allowing heights measured by GNSS; in terms of an ellipsoid, to be transformed to orthometric heights; in terms of sea level.

One of the challenges in gravity field modelling is that each of the gravity observation methods: satellite altimetry and terrestrial, ship-borne, airborne, and satellite gravimetry, are suited to modelling different parts of the Earth's gravity spectrum. For example, terrestrial gravity observations are non-uniform, limited to easy-to-access land areas and best contributes to the shortwave length gravity signals (i.e. less than 25 km). In contrast, satellite gravimetry provides uniform, global coverage of the Earth's gravity field, but contributes the long wavelength gravity signals (i.e. more than 100 km).

To derive a full map of the Earth's gravity field it is necessary to combine, multiple heterogeneous datasets. However, the different error characteristics of the datasets and the combination method have an impact on the final solution.

It is for these reasons that the purpose of this investigation was determine the best method to determine a single, well integrated gravity map, suitable for use in the geoid modelling process.

5.1.2. Data

The second step of the integration process was to identify the data, determine the characteristics of each of the gravity datasets available, their limitations and contributions to defining the gravity field. This was done in two parts.

First, Chapter 2 introduced the five gravity data collection methods: satellite altimetry and terrestrial, ship-borne, airborne, and satellite gravimetry. This chapter identified that while each of

the observation methods observe different parts of the gravity field and/or in different ways the data are best combined when as homogeneous as possible.

This means reducing the gravity observations to Bouguer anomalies, using the complete Bouguer model (Chapter 2.4.6). This provides a smoothed surface, where the effects of the surround terrain and the mass between the observation station and geoid have been removed.

At this point it was noted that while the other methods have been observed on the surface of the Earth, the airborne data is at flight altitude i.e. observed on different surfaces and therefore this needs to be addressed either as part of the integration technique or as separate transformation prior to combination.

The most appropriate method of downward continuation outside of the integration process uses an Inverse Poisson function. However this is known to be an inherently unstable function, which amplifies spurious high frequency noise.

Secondly, Chapter 4.4 identified each of the datasets which were used for the case study. In particular, the terrestrial and airborne gravity data involved additional error analysis and metadata checks to ensure that they would be consistent, and in terms of the same scale and projection. This means ensuring that the coordinate reference frame, ellipsoid (datum) and projection are consistent between datasets. Finally, each case study dataset was evaluated and from the differences in the data uncertainties were assigned.

5.1.3. Combination

This study identified three methods that could be used to combine two or more gravity datasets. As detailed in Chapter 3.4, these methods are: natural neighbour, ordinary kriging and least squares collocation. Much like the datasets being combined, each of the methods has its own strengths and limitations.

The natural neighbour method is quick to run, but requires the airborne dataset to be downward continued prior to integration. It is an exact interpolation method and does not take into account the uncertainties assigned to each dataset or observation.

The ordinary kriging method is also an exact interpolation method and requires the airborne dataset to be downward continued prior to integration. However, it more robust than the natural neighbour method and the datasets can be weighed.

Least squares collocation is not an exact interpolation method, it allows data weighting and is able to complete the downward reduction of the airborne dataset as part of the integration process. i.e. it allows the gravity signal to be estimated anywhere in a three dimensional space.

As demonstrated in the three dimensional reduction tests, Chapter 4.5.4, completing the downward continuation process as part of the least squares collocation method preserves the high frequency signal from the airborne dataset and reduces the introduction of rounding and/or transformation errors.

Therefore least squares collocation has been identified as the best integration method. As it combines data from the entire spectral range and uses an integration method which will minimise the inconsistencies between the datasets.

5.1.4. Assessment

The final step of the integration process was to ensure that the integration method identified has resulted in a well-integrated gravity anomaly map. This was completed using two tests: a comparison of models and a test of fit.

For the comparison of models check, the case study Bouguer anomaly map was compared to a Bouguer anomaly map derived from EGM2008. As the two models were at different resolutions (0.5 km and 10 km respectively), and created using different datasets, this is a high level assessment to identify that those differences between the models are at expected locations. The assessment suggests a good agreement between the models as the differences are features such as the improved resolution of the volcanic craters on Banks Peninsular and the differences closer to the coast where the case study map includes airborne data and re-tracked satellite altimetry data which was not available in EGM2008.

The second test assesses the fit of the final model to the datasets. Ideally there would be an independent dataset that could be used for this evaluation. However, all the available data went in to producing the case study Bouguer anomaly map. Therefore, a cross validation method was used, where an observation is removed from the least squares collocation integration and the values at that station before and after are compared. The assessment evaluated 5 percent of the data points from the terrestrial, airborne and ship-borne datasets, finding standard deviations of 0.24, 0.73 and 0.05 mGal respectively. This indicates that the case study Bouguer anomaly map provides a good fit to the underlying datasets.

This final step in the integration process: Assessment concludes that the least squares collocation integration method should be used to produce a Bouguer anomaly map of the Canterbury case study area.

5.2. Conclusions and Recommendations

As geoid modelling requires the combination of heteronomous datasets, it is beneficial to be able to combine the dataset using an integration method which operates in a three-dimensional space. Of the three methods assessed in this study least squares collocation is the only integration method which is able to perform this type of reduction.

It is therefore recommend that when combining airborne gravity with other gravity datasets that the least squares collocation method is used.

5.3. Future Work

The following are recommendations for future work:

1. Integration of data across other locations - The Canterbury case study area was chosen due to the availability of an airborne gravity dataset. However, the terrain of Canterbury area is generally smooth and contains a greater density of terrestrial gravity marks than other areas in New Zealand. Therefore, the results of this study may not reflect the fit of datasets from other regions of New Zealand.
2. Increased airborne survey area –The airborne survey area should be greater than the study area. As processes such as downward continuation are susceptible to edge effects buffers and filters were used to ensure that these effects were negligible, but further limiting the area.
3. Enhancement of the downward continuation process – The ability to downward continue the airborne gravity dataset using the inverse Poisson function was limited by the vertical positioning of aircraft. While an average altitude was used for the reduction, the variation in altitude throughout the flight due to pitch is in the order of ± 10 m (which equates to ± 3 mGal).
4. Further analysis of the airborne gravity dataset – There were a number of features of the airborne gravity dataset which were included for further investigation or remediation. This includes the analysis of the cross over points and along line error detection. It is recommended that such analysis should be conducted on future surveys to ensure the quality of the airborne data.
5. Airborne survey to be completed at a constant altitude – comparing and merging the airborne gravity data was complicated by the flight lines being flown at different altitudes. It is recommended that all flights in an airborne gravity survey be flown at the same altitude, whenever possible.

References

- Abbasi, M., Barriot, J. P. & Verdun, J. (2007). *Airborne LaCoste & Romberg gravimetry: a space domain approach*. *Journal of Geodesy*. 81(4), 269-283.
- Albertella, A., Migliaccio, F. & Sansó, F. (2002). *GOCE: The Earth gravity field by space gradiometry*. *Celestial mechanics and dynamical astronomy*. 83(1-4), pp 1-15.
- Alberts, B. A. (2009). *Regional gravity field modeling using airborne gravity data* (Doctoral dissertation). TU Delft, Delft University of Technology.
- Allaby, A. & Allaby, M. (eds). (2008). *A Dictionary of Earth Sciences*. 3rd edition. Oxford: Oxford University Press. pp 197.
- Amos, M. J. (2007). *Quasigeoid modelling in New Zealand to unify multiple local vertical datums* (Doctoral dissertation). Curtin University of Technology.
- Amos, M. & Featherstone, W. (2003). *Preparations for a new gravimetric geoid model of New Zealand, and some preliminary results*. *New Zealand Surveyor*. 293, pp 9-20.
- Amos, M. & Featherstone, W. (2004) *A comparison of gridding techniques for terrestrial gravity observations in New Zealand*. *Gravity, Geoid and Space Missions 2004 proceedings*. Porto, Portugal.
- Amos, M. J., Featherstone, W. E. & Brett, J. (2005). *Crossover adjustment of New Zealand marine gravity data, and comparisons with satellite altimetry and global geopotential models*. *Gravity, Geoid and Space Missions*. 125, pp 266-271.
- Andersen, O. B., Knudsen, P. & Trimmer, R. (2005). *Improved high resolution altimetric gravity field mapping (KMS2002 global marine gravity field)*. In *A Window on the Future of Geodesy*. Springer Berlin Heidelberg. 128, pp 326-331.
- Andersen, O. B. & Knudsen, P. (2009). *DNSS08 mean sea surface and mean dynamic topography models*. *Journal of Geophysical Research: Oceans* (1978–2012), 114.
- Andersen, O. B., Knudsen, P. & Berry, P. A. (2010). *The DNSS08GRA global marine gravity field from double retracked satellite altimetry*. *Journal of Geodesy*. 84(3), pp 191-199.
- Andersen, O. B., Knudsen, P., Berry, P., Pavlis, N. & Kenyon, S. (2008). *The DNSS08 ocean-wide altimetry-derived gravity anomaly field*. *European Geosciences Union General Assembly 2008* Vienna, Austria.
- Bannister, S. & Gledhill, K. (2012). *Evolution of the 2010–2012 Canterbury earthquake sequence*. *New Zealand Journal of Geology and Geophysics*. 55(3), pp 295-304.
- Barzaghi, R., Borghi, A., Keller, K., Forsberg, R., Giori, I., Loretti, I., ... & Stenseng, L. (2009). *Airborne gravity tests in the Italian area to improve the geoid model of Italy*. *Geophysical Prospecting* 57(4), pp 625-632.

- Bayoud, F. A. & Sideris, M. G. (2003). *Two different methodologies for geoid determination from ground and airborne gravity data*. *Geophysical Journal International*. 155(3), pp 914-922.
- Brett, J. (2004). *Marine gravity crossover adjustment for New Zealand, Report to Land Information New Zealand*. Intrepid Geophysics, Melbourne, Australia.
- Brozena, J. M. (1992). *The Greenland Aerogeophysics Project: Airborne gravity, topographic and magnetic mapping of an entire continent*. In *From Mars to Greenland: Charting Gravity with Space and Airborne Instruments*. Springer New York. pp 203-214.
- Bruinsma, S. L., Förste, C., Abrikosov, O., Lemoine, J. M., Marty, J. C., Mulet, S., ... & Bonvalot, S. (2014). *ESA's satellite-only gravity field model via the direct approach based on all GOCE data*. *Geophysical Research Letters*. 41(21), pp 7508-7514.
- Cardarelli, F. (2006). *Encyclopedia of Scientific Units, Weights, and Measures*. Electronic Version. Springer-Verlag London.
- Catalão, J. & Sevilla, M. J. (2009). *Mapping the geoid for Iberia and the Macaronesian Islands using multi-sensor gravity data and the GRACE geopotential model*. *Journal of Geodynamics*. 48(1), pp 6-15.
- Claessens, S., Hirt, H., Featherstone, W. & Kirby, J. (2009). *Computation of a new gravimetric quasigeoid model for New Zealand*. Contract report for LINZ. Curtin University of Technology, Perth. pp 39.
- Custodio, S., Page, M. T. & Archuleta, R. J. (2007). *A New Approach for Combining GPS and Seismic Data in Kinematic Inversions*. In *AGU Fall Meeting Abstracts*. 1, pp 5.
- Dahl, O. C. & Forsberg, R. (1999). *Different ways to handle topography in practical geoid determination*. *Physics and Chemistry of the Earth, Part A: Solid Earth and Geodesy*, 24(1), pp 41-46.
- Davy, B.W. Caldwell, T.G. (1998) *Gravity, magnetic and seismic surveys of the caldera complex, Lake Taupo, North Island, New Zealand*. *Journal of Volcanology and Geothermal Research*. 81(1/2), pp 69-89
- Dehlinger, P. (1978). *Marine gravity*. 1st Edition. Elsevier Scientific Publishing Company, Amsterdam. pp 149.
- Deng, X., Featherstone, W. E., Hwang, C. & Berry, P. A. M. (2002). *Estimation of contamination of ERS-2 and POSEIDON satellite radar altimetry close to the coasts of Australia*. *Marine Geodesy*, 25(4), pp 249-271.
- DoSLI. (1989). *Geodetic Survey Branch Manual of Instruction*. Department of Survey and Land Information, Wellington. pp 117.
- Drinkwater, M. R., Floberghagen, R., Haagmans, R., Muzi, D. & Popescu, A. (2003). *GOCE: ESA's first Earth Explorer Core mission*. In *Earth gravity field from space—From sensors to earth sciences* Springer Netherlands. pp. 419-432.

- Dumrongchai, P., Wichienchareon, C. & Promtong, C. (2012). *Local geoid modeling for Thailand*. International Journal of Geoinformatics. 8(4).
- Ellmann, A. (2011). *Downward continuation of airborne gravity data using high-resolution global geopotential models*. In Selected papers of the 8th international conference on environmental engineering. pp. 19-20.
- Farr, T. G. & Kobrick, M. (2000). *Shuttle Radar Topography Mission produces a wealth of data*. Eos, Transactions American Geophysical Union. 81(48), pp 583-585.
- Featherstone, W. E. (2010). *Satellite and airborne gravimetry: their role in geoid determination and some suggestions*. Airborne gravity 2010.
- Featherstone, W. E. & Kirby, J. F. (2000). *The reduction of aliasing in gravity anomalies and geoid heights using digital terrain data*. Geophysical Journal International. 141(1), pp 204-212.
- Featherstone, W. E. & Sproule, D. M. (2006). *Fitting AusGeoid98 to the Australian height datum using GPS-levelling and least squares collocation: application of a cross-validation technique*. Survey Review. 38(301), pp 573-582.
- Featherstone, W. E., Evans, J. D. & Olliver, J. G. (1998). *A Meissl-modified Vaníček and Kleusberg kernel to reduce the truncation error in gravimetric geoid computations*. Journal of Geodesy. 72(3), pp 154-160.
- Filmer, M. S., Featherstone, W. E. & Claessens, S. J. (2014). *Variance component estimation uncertainty for unbalanced data: application to a continent-wide vertical datum*. Journal of Geodesy. 88(11), pp 1081-1093.
- Forsberg, R., Olesen, A., Bastos, L., Gidskehaug, A., Meyer, U. & Timmen, L. (2000). *Airborne geoid determination*. Earth Planets and Space. 52(10), pp 863-866.
- Forsberg, R., Olesen, A., Munkhtsetseg, D. & Amarzaya, B. (2007). *Downward continuation and geoid determination in Mongolia from airborne and surface gravimetry and SRTM topography*. In Strategic Technology, 2007. IFOST 2007, International Forum. pp. 470-475.
- Forsberg, R. & Tscherning, C. C. (1981). *The use of height data in gravity field approximation by collocation*. Journal of Geophysical Research: Solid Earth (1978–2012), 86(B9), pp 7843-7854.
- Forsyth, P. J., Jongens, R. & Barrell, D. J. A. (2008). *Geology of the Christchurch area*. Lower Hutt: GNS Science.
- Garcia, E. S., Sandwell, D. T. & Smith, W. H. (2014). *Retracking CryoSat-2, Envisat and Jason-1 radar altimetry waveforms for improved gravity field recovery*. Geophysical Journal International, 196(3), pp 1402-1422.
- Gomez, M. E., Bagu, D. R., Del Cogliano, D. & Perdomo, R. A. (2013). *Evaluation of terrain corrections through FFT and classical integration in two selected areas of the Andes and their impact on geoidal heights*. Boletim de Ciências Geodésicas. 19(3), pp 407-419.

- Goodkind, J. M. (1999). *The superconducting gravimeter*. Review of scientific instruments. 70(11), pp 4131-4152.
- Goovaerts, P. (1997). *Geostatistics for natural resources evaluation*. 1st Edition. Oxford University Press on Demand.
- Goovaerts, P. (1998). *Ordinary cokriging revisited*. Mathematical Geology. 30(1), pp 21-42.
- GRACE. (1998). *GRACE science and mission requirements document*. Revision A. JPLD-15928
- Grant, D. B., Blick, G. H., Pearse, M. B., Beavan, R. J. & Morgan, P. J. (1999). *The development and implementation of New Zealand Geodetic Datum 2000*. IUGG 99 General Assembly, Birmingham, UK, July 1999.
- Hackney, R. I. & Featherstone, W. E. (2003). *Geodetic versus geophysical perspectives of the 'gravity anomaly'*. Geophysical Journal International. 154(1), pp35-43.
- Hammer, S. (1939). *Terrain corrections for gravimeter stations*. Geophysics. 4(3), pp 184-194.
- Hannah, J. (2001). *An assessment of New Zealand's height systems and options for a future height datum*. Report prepared for Land Information New Zealand.
- Harms, J. (2015). *Terrestrial Gravity Fluctuations*. Living Reviews in Relativity. 18(3).
- Haxby, W. F., Karner, G. D., LaBrecque, J. L. & Weissel, J. K. (1983). *Digital images of combined oceanic and continental data sets and their use in tectonic studies*. Eos, Transactions American Geophysical Union. 64(52), pp 995-1004.
- Heiskanen, W. A. & Moritz, H. (1981). *Physical geodesy*. Reprint. Institute of Physical Geodesy, Technical University.
- Herring, T. (2007). *Geodesy*. 1st Edition. Treatise on Geophysics. 3, pp 1-11.
- Higgins, M. B., Pearse, M. B. & Kearsley, A. H. W. (1996). *Using digital elevation models in the computation of geoid heights*. Geomatics Research Australasia. pp 59-74.
- Hinderer, J., Crossley, D. & Warburton, R. (2007). *Gravimetric Methods—Superconducting Gravity Meters*. *Treatise on Geophysics*. pp 65-122.
- Hinze, W. J. (2003). *Bouguer reduction density, why 2.67?*. Geophysics. 68(5), pp 1559-1560.
- Hofmann-Wellenhof, B. & Moritz, H. (2006). *Physical geodesy*. 2nd edition. Springer Science & Business Media.
- Holom, D. I. & Oldow, J. S. (2007). *Gravity reduction spreadsheet to calculate the Bouguer anomaly using standardized methods and constants*. Geosphere. 3(2), pp 86-90.
- Hsiao, Y. S. & Hwang, C. (2010). *Topography-assisted downward continuation of airborne gravity: an application for geoid determination in Taiwan*. Terrestrial, Atmospheric and Oceanic Sciences. 21(4), pp 627-637.

- Huang, J. & Véronneau, M. (2015). *Assessments of Recent GRACE and GOCE Release 5 Global Geopotential Models in Canada*. Newton's Bulletin, Issue n.5
- Hunt, T. M. (1970). *Gravity changes associated with the 1968 Inangahua earthquake*. New Zealand Journal of Geology and Geophysics. 13(4), pp 1050-1051.
- Hwang, C., Hsu, H. J., Chang, E. T., Featherstone, W. E., Tenzer, R., Lien, T., ... & Jai, P. H. (2014). *New free-air and Bouguer gravity fields of Taiwan from multiple platforms and sensors*. Tectonophysics. 611, pp 83-93.
- Ilie, A.S. (2014). *Geostatistics Kriging Method as a Special Case of Geodetic Least-Squares Collocation*. RevCAD Journal of Geodesy and Cadastre. 16, pp 127-134
- Jackson, J. E. (1961). *The Cambridge pendulum apparatus*. Geophysical Journal International. 4, pp 375-388.
- Jekeli, C. & Kwon, J. H. (1999). *Results of airborne vector (3-d) gravimetry*. Geophysical Research Letters. 26(23), pp 3533-3536.
- Kater, H. (1818). *An account of experiments for determining the length of the pendulum vibrating seconds in the latitude of London*. Philosophical Transactions of the Royal Society of London. 108, 33-102.
- Kern, M., Schwarz, K.P. & Sneeuw, N. (2003). *A study on the combination of satellite, airborne, and terrestrial gravity data*. Journal of geodesy. 77(3-4), pp 217-225.
- Kirby, J. F. & Featherstone, W. E. (1999). *Terrain correcting Australian gravity observations using the national digital elevation model and the fast Fourier transform*. Australian Journal of Earth Sciences. 46(4), pp 555-562.
- Kirby, J. F. & Featherstone, W. E. (2001). *Anomalously large gradients in Version 1 of the "GEODATA 9 SECOND" Digital Elevation Model of Australia, and their effects on gravimetric terrain corrections*. Cartography. 30(1), pp 1-10.
- Kirby, J.F. & Featherstone, W.E. (2002). *High resolution grids of gravimetric terrain corrections and complete Bouguer gravity reductions over Australia 2002*. Exploration Geophysics. 3(3-4), pp 161-165.
- Klees, R., Ditmar, P. & Broersen, P. (2003). *How to handle colored observation noise in large least-squares problems*. Journal of Geodesy. 76(11-12), pp 629-640.
- Knudsen, P., Bingham, R., Andersen, O. & Rio, M. H. (2011). *A global mean dynamic topography and ocean circulation estimation using a preliminary GOCE gravity model*. Journal of Geodesy, 85(11), pp 861-879.
- Krarup, T. (1969). *A contribution to the mathematical foundation of physical geodesy*. Meddelelse no. 44, Geodætisk Institut, København.
- LaCoste & Romberg. (1998). *Lacoste and Romberg model "S" air-sea dynamic gravity meter*. Austin, TX.

- LaFehr, T.R. (1991). *An exact solution for the gravity curvature (Bullard B) correction*. Geophysics. 56(8), pp 1179-1184.
- Li, Z., Zhu, C. & Gold, C. (2004). *Digital terrain modeling: principles and methodology*. English Edition. CRC press.
- Ligas, M. & Kulczycki, M. (2010). *Simple spatial prediction-least squares prediction, simple kriging, and conditional expectation of normal vector*. Geodesy and Cartography. 59(2), pp 69-81.
- LINZ. (2005). *Topo50 Map Reading Guide*. First Edition. Land Information New Zealand
- LINZ. (2009). *Standard for the New Zealand Vertical Datum 2009*. LINZS25004. Land Information New Zealand, Wellington.
- LINZ. (2011). *Airborne gravity for an improved vertical datum: options for the development of New Zealand's vertical datum*. Internal report, Land Information New Zealand.
- Longman, I. M. (1959). Formulas for computing the tidal accelerations due to the moon and the sun. *Journal of Geophysical Research*. 64(12), pp 2351-2355.
- Lyatsky, H.V. & Pana, D.I., 2003. *Catalogue of Selected Regional Gravity and Magnetic Maps of Northern Alberta*. EUB/Alberta Geological Survey, Special Publication 56, pp 40.
- Marson, I. (2012). *A short walk along the gravimeters path*. *International Journal of Geophysics*.
- Matsuo, K. & Otsubo, T. (2013). *Temporal variations in the Earth's gravity field from multiple SLR satellites: Toward the investigation of polar ice sheet mass balance*. In *The 18th ILRS Workshop proceedings*. Fujiyoshida, Japan.
- McCubbine, J. (2016). *Airborne Gravity Across New Zealand - For An Improved Vertical Datum* (Doctoral dissertation). Victoria University of Wellington. Chapters 6-7.
- Merlet, S., Bodart, Q., Malossi, N., Landragin, A., Dos Santos, F. P., Gitlein, O. & Timmen, L. (2010). *Comparison between two mobile absolute gravimeters: optical versus atomic interferometers*. *Metrologia*, 47(4), pp 9.
- Micro-g Solutions. (1999). *Operator's manual, FG5 absolute gravimeter*. Micro-g Solutions Incorporated, Erie.
- Monahan, D. (2008) *A Look To The Future; Ocean Mapping In The Twenty First Century*. Charting the Secret World of the Ocean Floor. The GEBCO Project 1903-2003.
- Moritz, H. (1978). *Least-squares collocation*. *Reviews of geophysics*. 16(3), pp 421-430.
- Moritz, H. (1980). Geodetic reference system 1980. *Journal of Geodesy*. 54(3), pp 395-405.
- Nagy, D. (1966). *The gravitational attraction of a right angular prism*. *Geophysics*. 1(2), pp 362-371.
- NGS. (1986). *Geodetic Glossary*. National Geodetic Survey, Rockville, MD.

- Niebauer, T. (2007). *Gravimetric methods-absolute gravimeter: instruments concepts and implementation*. Treatise on Geophysics. 3, pp 43-64.
- Niebauer, T. M., Sasagawa, G. S., Faller, J. E., Hilt, R. & Klopping, F. (1995). *A new generation of absolute gravimeters*. Metrologia. 32(3), pp 159.
- NOAA. (2010.) *Introduction to Hydrography*. University Corporation for Atmospheric Research.
- Nowell, D.A.G. (1999) *Gravity terrain corrections an overview*. 1999. Journal of Applied Geophysics. 42(2), pp 117-134.
- NRCan. (2014). *Height Reference System Modernisation*. Natural Resources Canada. <http://webapp.geoid.nrcan.gc.ca> (Date Modified: 2014-01-14).
- Olesen, A. V. (2002). Improved airborne scalar gravimetry for regional gravity field mapping and geoid determination (Doctoral dissertation), Faculty of Science, University of Copenhagen.
- Omar, K., Mohamed, A. & Ses, S. (2005). *Enhancement of Height System For Malaysia Using Space Technology: The Study of the Datum Bias Inconsistencies in Peninsular Malaysia*. Faculty of Geoinformation Science and Engineering.
- Omang, O. C. D. & Forsberg, R. (2000). *How to handle topography in practical geoid determination: three examples*. Journal of Geodesy. 74(6), pp 458-466.
- Osborne, J. W. & Overbay, A. (2004). *The power of outliers (and why researchers should always check for them)*. Practical assessment, research & evaluation. 9(6), pp 1-12.
- Othman, A. H., Omar, K., ZA, M. S. & Opaluwa, Y. D. (2014). *Unification of Vertical Datum in Sabah and Sarawak*. Jurnal Teknologi. 71(4).
- Pail, R., Bruinsma, S., Migliaccio, F., Förste, C., Goiginger, H., Schuh, W. D., ... & Veicherts, M. (2011). *First GOCE gravity field models derived by three different approaches*. Journal of Geodesy. 85(11), pp 819-843.
- Pavlis, N. K., Holmes, S. A., Kenyon, S. C. & Factor, J. K. (2008). *An earth gravitational model to degree 2160: EGM2008*. EGU General Assembly. pp 13-18.
- Pavlis, N. K., Holmes, S. A., Kenyon, S. C. & Factor, J. K. (2012). *The development and evaluation of the Earth Gravitational Model 2008 (EGM2008)*. Journal of Geophysical Research: Solid Earth (1978–2012). pp 117.
- Payne, L. E. & Schaefer, P. W. (1989). *Duality theorems in some over-determined boundary value problems*. Mathematical Methods in the Applied Sciences. 11(6), pp 805-819.
- Rapp, R. H. & Rummel, R. (1975). *Methods for the computation of detailed geoids and their accuracy*. Rep. 233Dep. of Geod. Sci., Ohio State Univ., Columbus.
- Reguzzoni, M., Sanso, F. & Venuti, G. (2005). *The theory of general kriging, with applications to the determination of a local geoid*. Geophysical Journal International. 162(2), pp 303-314.

- Reigber, C., Balmino, G., Schwintzer, P., Biancale, R., Bode, A., Lemoine, J. M., ... & Barthelmes, F. (2002). *A high-quality global gravity field model from CHAMP GPS tracking data and accelerometry (EIGEN-1S)*. *Geophysical Research Letters*. 29(14), pp 37-41.
- Reilly, W. I. (1972). *New Zealand gravity map series*. *New Zealand journal of geology and geophysics*. 15(1), pp 3-15.
- Reynolds, J. M. (2011). *An introduction to applied and environmental geophysics*. 2nd Edition. John Wiley & Sons. Chapter 3.
- Robertson, H. W. & Garrick, R. A. (1960). *Gravity measurements in New Zealand with the Cambridge pendulum apparatus*. *New Zealand Journal of Geology and Geophysics*. 3(4), pp 626-642.
- Rummel, R. (1986). *Satellite gradiometry*. *Mathematical and numerical techniques in physical geodesy*. pp 317-363.
- Rummel, R., Balmino, G., Johannessen, J., Visser, P. N. A. M. & Woodworth, P. (2002). *Dedicated gravity field missions—principles and aims*. *Journal of Geodynamics*. 33(1), pp 3-20.
- Sacerdote, F. & Sanso, F. (1984). *The overdetermined boundary value problems of physical geodesy*. Università di Pisa. Dipartimento di Matematica.
- Sandwell, D. T., Mller R. D., Smith W. H., Garcia E. & R. Francis R. (2014). *New global marine gravity model from CryoSat-2 and Jason-1 reveals buried tectonic structure*. *Science*. 346(6205), pp 65-67.
- Sandwell, D. T., Smith, W. H., Gille, S., Jayne, S., Soofi, K. & Coakley, B. (2001). *Bathymetry from space*. Report of the High-resolution Ocean topography Science working Group Meeting. pp 2001-4.
- Sandwell, D., Garcia, E., Soofi, K., Wessel, P., Chandler, M. & Smith, W. H. (2013). *Toward 1-mGal accuracy in global marine gravity from CryoSat-2, Envisat, and Jason-1*. *The Leading Edge*. 32(8), pp 892-899.
- Schaffrin, B. & Iz, H. B. (2002). *Integrating heterogeneous data sets with partial inconsistencies*. In *Gravity, Geoid and Geodynamics 2000*. Springer Berlin Heidelberg. pp. 49-54.
- Schwintzer, P., Kang, Z. & Perosanz, F. (2000). *Accelerometry aboard CHAMP*. In *Towards an Integrated Global Geodetic Observing System (IGGOS)*. Springer Berlin Heidelberg. pp 197-200.
- Seigel, H. O. (1995). *A guide to high precision land gravimeter surveys*. First Edition. Scintrex LTD, Concord, Ontraio.
- Serra, E. M. T., Delouis, B., Emolo, A. & Zollo, A. (2013). *Combining strong-motion, InSAR and GPS data to refine the fault geometry and source kinematics of the 2011, Mw 6.2, Christchurch earthquake (New Zealand)*. *Geophysical Journal International*. 194(3), pp 1760-1777.
- Sharma, P. V. (1997). *Environmental and engineering geophysics*. Cambridge University Press.

- Shum, C. K., Woodworth, P. L., Andersen, O. B., Egbert, G. D., Francis, O., King, C., ... & Parke, M. E. (1997). *Accuracy assessment of recent ocean tide models*. *Journal of Geophysical Research: Oceans*. 102(C11), pp 25173-25194.
- Sideris, M. G. (1985). *A fast Fourier transform method for computing terrain corrections*. *Manuscripta geodaetica*. 10(1), pp 66-73.
- Sjöberg, L. E. (2011). *Geoid determination by spectral combination of an Earth gravitational model with airborne and terrestrial gravimetry—a theoretical study*. *Studia Geophysica et Geodaetica*. 55(4), pp 579-588.
- Stagpoole, V. (2012). *Description of the data in the GNS Science gravity database*. GNS Science internal report.
- Stagpoole, V.M., Caratori-Tontini, F., Amos, M., Dando, N. and Black, J. (2015) *Absolute Gravity Observations at principal New Zealand stations 2015*. GNS Science Report 2015/46.
- Szűcs, E., Papp, G. & Benedek, J. (2014). *A study of different wavelength spectral components of the gravity field derived from various terrestrial data sets*. *Acta Geodaetica et Geophysica*. 49(3), pp 327-342.
- Tapley, B. D., Bettadpur, S., Watkins, M. & Reigber, C. (2004). *The gravity recovery and climate experiment: Mission overview and early results*. *Geophysical Research Letters*. 31(9).
- Tarback, E. J. L., Tarback, F. K. E. J. & Lutgens, F. K. (2002). *Earth: an introduction to physical geology*. 7th Edition. Chapter 5.
- Thompson, L. G. D. and LaCoste, L. J. B. (1960). *Aerial gravity measurements*. *Journal of Geophysical Research*. 65(1), pp 305–32.
- Torge, W. & Müller, J. (2012). *Geodesy*. 4th Edition. Walter de Gruyter.
- Triarahmadhana, B. & Heliani, L. (2014). *Evaluation of GOCE's Global Geopotential Model to the Accuration of Local Geoid (Case Study: Java Island, Indonesia)*. FIG Congress 2014. Kuala Lumpur, Malaysia 16 – 21 June 2014.
- Tscherning, C. C. (2015). *Developments in the implementation and use of Least-Squares Collocation*. International Association of Geodesy Symposia. Springer Berlin Heidelberg.
- Tscherning, C. C., Rubek, F. & Forsberg, R. (1998). *Combining airborne and ground gravity using collocation*. *Geodesy on the Move*. Springer Berlin Heidelberg. pp 18-23.
- Tseng, K. H., Shum, C. K., Yi, Y., Emery, W. J., Kuo, C. Y., Lee, H. & Wang, H. (2014). *The improved retrieval of coastal sea surface heights by retracking modified radar altimetry waveforms*. *Geoscience and Remote Sensing*. IEEE Transactions. 52(2), pp 991-1001.
- van Loon, J. P. & Kusche, J. (2007). *Towards an optimal combination of satellite data and prior information*. In *Dynamic Planet*. Springer Berlin Heidelberg. pp 345-353.

- Wackernagel, H. (2003). *Multivariate Geostatistics: an Introduction with Applications*. 3rd Edition. Springer, Berlin.
- Wang, Y. M. (1988). *Downward Continuation of the Free-Air Gravity Anomalies to the Ellipsoid Using the Gradient Solution, Poisson's Integral and Terrain Correction-Numerical Comparison and Computations (No. OSU/DGSS-393)*. Ohio State Univ Columbus Dept of Geodetic Science and Surveying.
- Wang, X. T., Xia, Z. R., Shi, P. & Sun, Z. M. (2004). *A comparison of different downward continuation methods for airborne gravity data*. Chinese Journal of Geophysics. 47(6), pp 1143-1149.
- Wang, J., Wang, J. & Roberts, C. (2009). *Investigations into a Dynamic Geocentric Datum*. Observing our Changing Earth. Springer Berlin Heidelberg. pp 11-19.
- Wang, Y. M., Preaux, S., Diehl, T., Childers, V., Roman, D. & Smith, D. (2013). *Accuracy assessment of test flights using the Turnkey Airborne Gravity System over Alabama in 2008*. Journal of Geodetic Science. 3(2), pp 136-142.
- Warf, B. (Ed.) (2006). *Encyclopaedia of human geography*. 1st Edition. Sage Publications.
- Webster, R. & Oliver, M. A. (2007). *Geostatistics for environmental scientists*. 2nd Edition. John Wiley & Sons. Chapter 8.2
- Wessel, P. & Chandler, M. T. (2011). *The spatial and temporal distribution of marine geophysical surveys*. Acta Geophysica. 59(1), pp 55-71.
- Wessel, P. & Watts, A. B. (1988). *On the accuracy of marine gravity measurements*. Journal of Geophysical Research. 93, pp 393-413.
- Wessel, P., Smith, W. H., Scharroo, R., Luis, J. & Wobbe, F. (2013). *Generic mapping tools: improved version released*. Eos, Transactions American Geophysical Union. 94(45), pp 409-410.
- Wilson, C. R., Scanlon, B., Sharp, J., Longuevergne, L. & Wu, H. (2012). *Field test of the superconducting gravimeter as a hydrologic sensor*. Ground water, 50(3), pp 442-449.
- Winefield, R., Amos, M. & Caratori Tontini, F. (2014). *Airborne Gravity Trial for an improved National Geoid*. New Zealand Surveyor.303, pp 26-31
- Wingham, D. J., Francis, C. R., Baker, S., Bouzinac, C., Brockley, D., Cullen, R. & Wallis, D. W. (2006). *CryoSat: A mission to determine the fluctuations in Earth's land and marine ice fields*. Advances in Space Research. 37(4), pp 841-871.
- Wonnacott, R. & Merry, C. (2011). *A New Vertical Datum for South Africa?* Conference Proceedings of the AfricaGEO.
- Yale, M. M., Sandwell, D. T. & Herring, A. T. (1998). *What are the limitations of satellite altimetry? The leading edge*. 17(1), pp 73-76.

A. Appendix

A.1. Gravity Datasets

The following are the Bouguer anomaly maps over the Canterbury case study area, for each of the five gravity observation methods: terrestrial, ship-borne, airborne, satellite altimetry and satellite only GGM. The maps were modelled using the natural neighbour method.

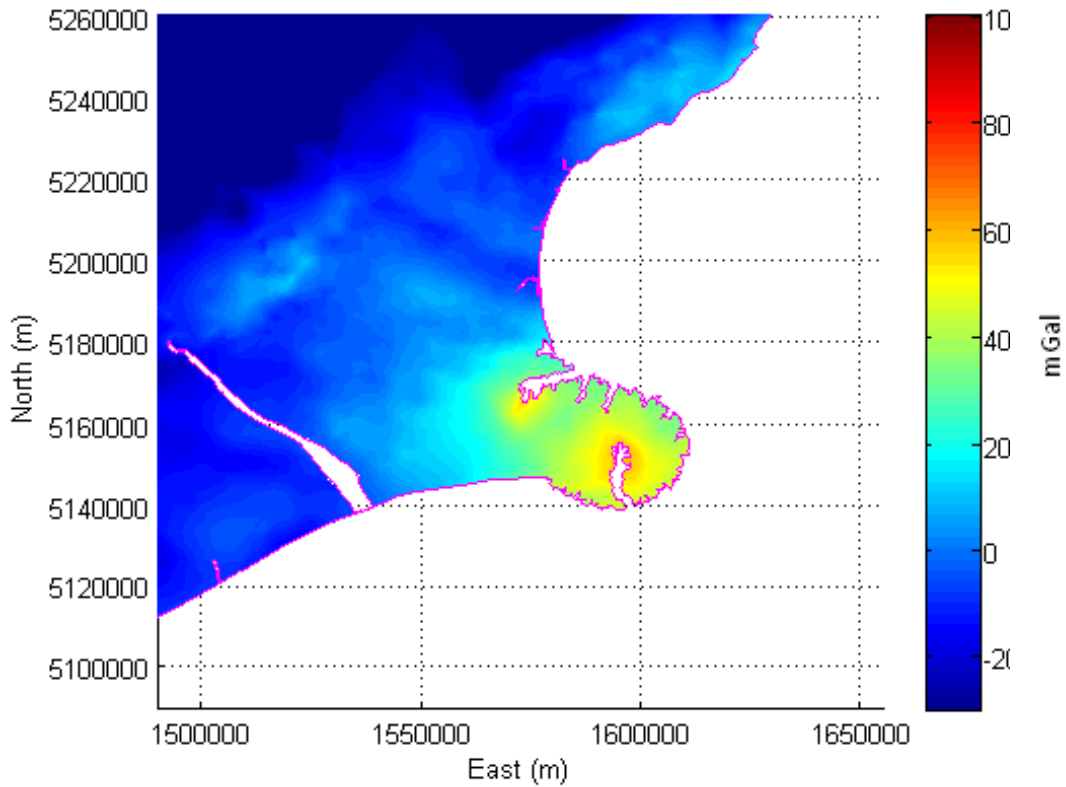


Figure A.1: Canterbury test area terrestrial gravity dataset

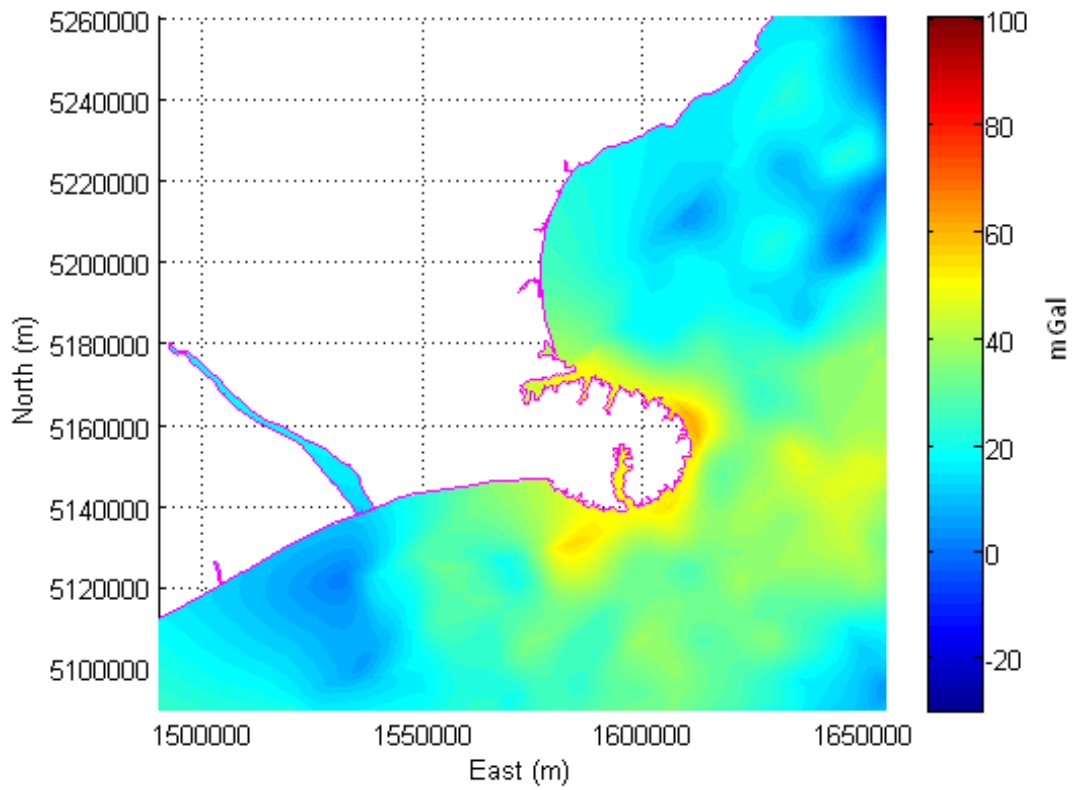


Figure A.2: Canterbury test area ship-borne gravity dataset

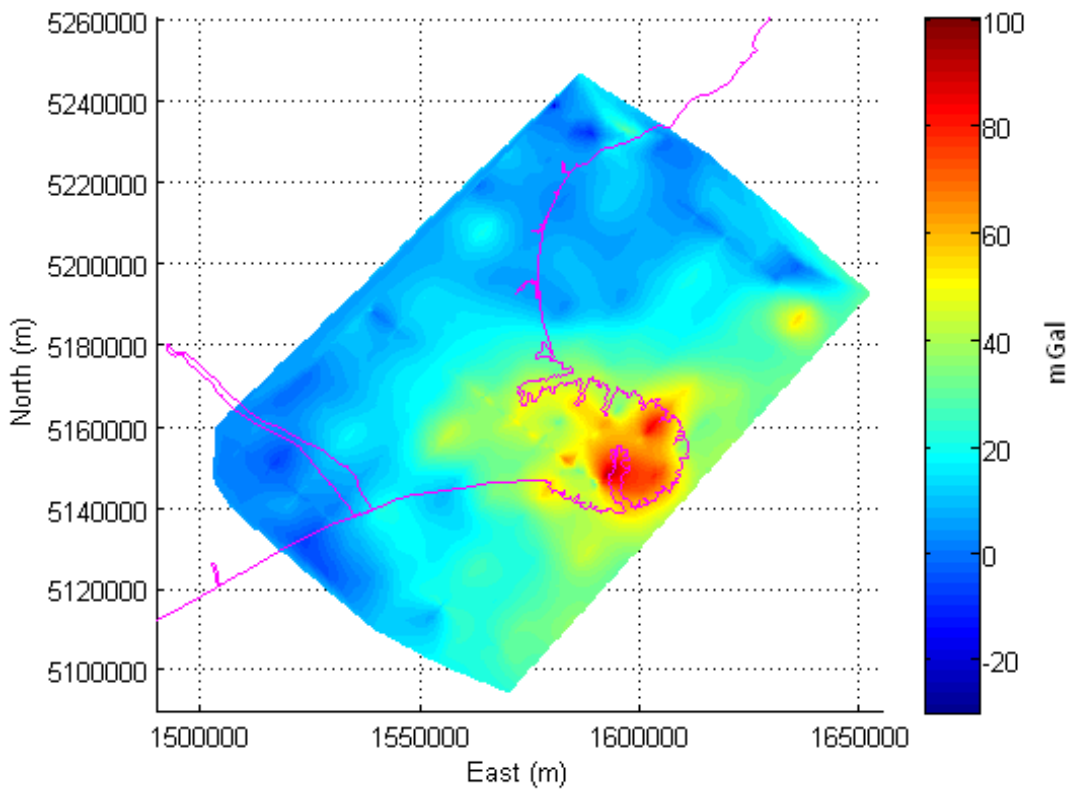


Figure A.3 Canterbury test area airborne gravity dataset

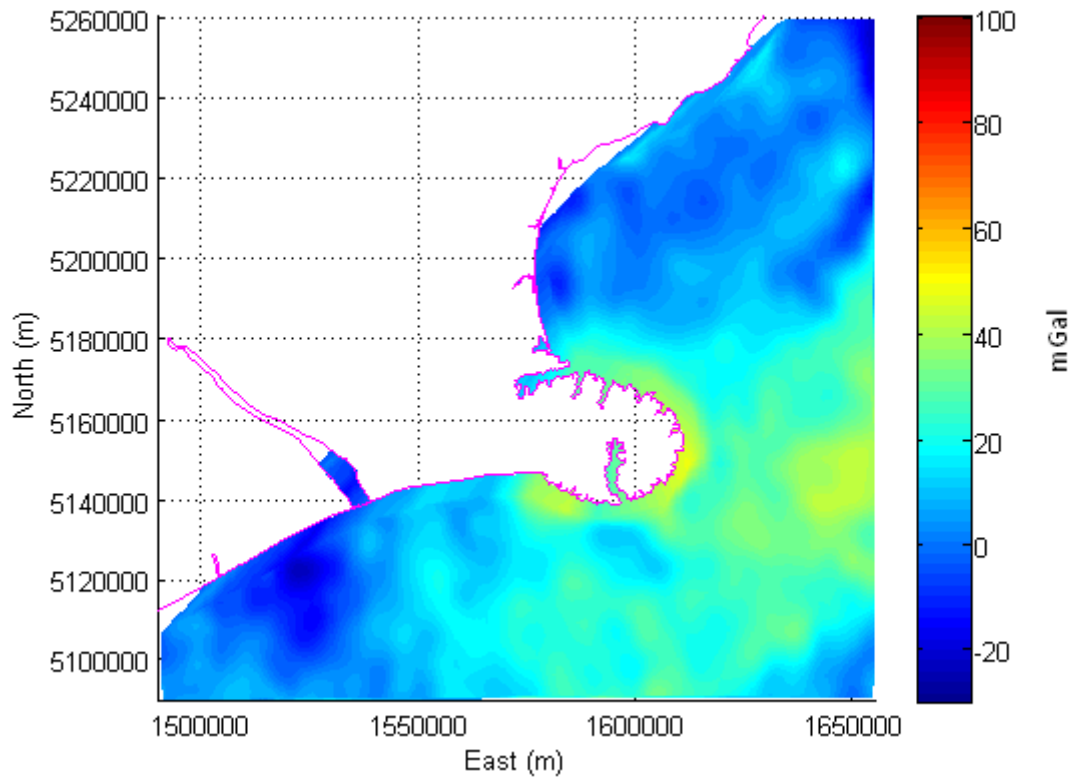


Figure A.4: Canterbury test area satellite altimetry dataset

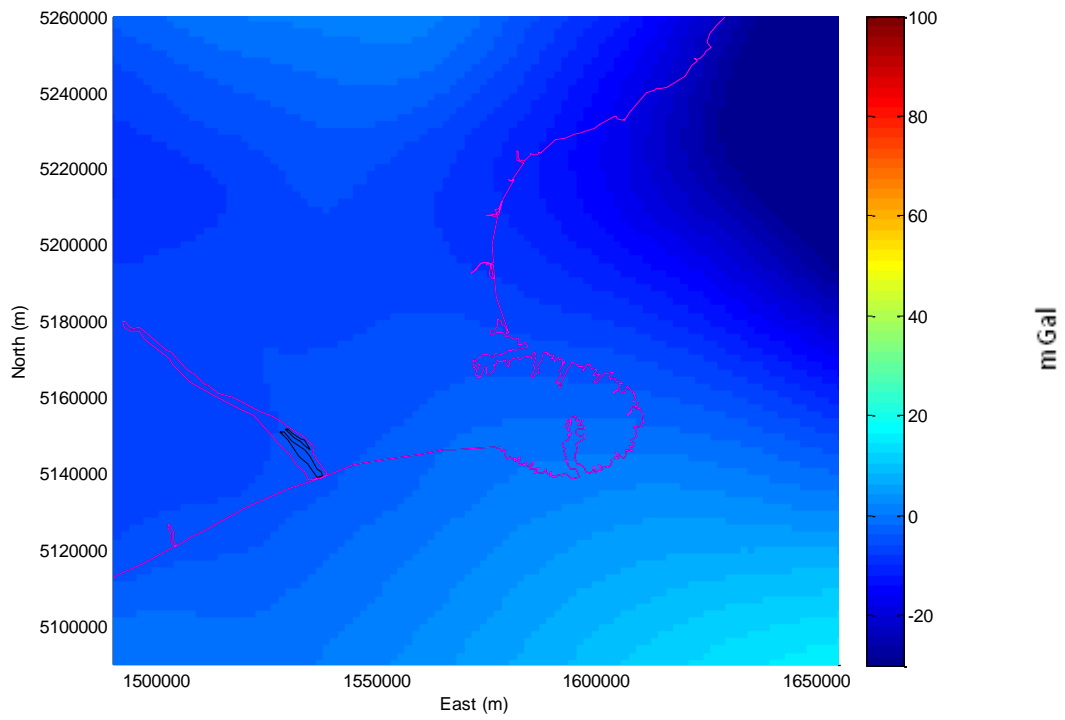


Figure A.5: Canterbury test area satellite gravity data, GGM DIR_5